Local signal processing in mouse horizontal cell dendrites

Dissertation

Zur Erlangung des Grades eines

Doktors der Naturwissenschaften

der Mathematisch-Naturwissenschaftlichen Fakultät

und

der Medizinischen Fakultät

der Eberhard-Karls-Universität Tübingen

vorgelegt

von

Camille Chapot

Aus Gouvieux, Frankreich

September 2017

Tag der mündlichen Prüfung: 28 November 2017

Dekan der Math.-Nat. Fakultät: Prof. Dr. W. Rosenstiel

Dekan der Medizinischen Fakultät: Prof. Dr. I. B. Autenrieth

1. Berichterstatter: Prof. Dr. Thomas Euler

2. Berichterstatter: Prof. Dr. Cornelius Schwarz

Prüfungskommission: Prof. Dr. Frank Schaeffel

Prof. Dr. Aristides Arrenberg

Erklärung / Declaration:

Ich erkläre, dass ich die zur Promotion eingereichte Arbeit mit dem Titel: "**Local signal processing in mouse horizontal cell dendrites**" selbständig verfasst, nur die angegebenen Quellen und Hilfsmittel benutzt und wörtlich oder inhaltlich übernommene Stellen als solche gekennzeichnet habe. Ich versichere an Eides statt, dass diese Angaben wahr sind und dass ich nichts verschwiegen habe. Mir ist bekannt, dass die falsche Abgabe einer Versicherung an Eides statt mit Freiheitsstrafe bis zu drei Jahren oder mit Geldstrafe bestraft wird.

*I hereby declare that I have produced the work entitled "***Local signal processing in mouse horizontal cell dendrites***", submitted for the award of a doctorate, on my own (without external help), have used only the sources and aids indicated and have marked passages included from other works, whether verbatim or in content, as such. I swear upon oath that these statements are true and that I have not concealed anything. I am aware that making a false declaration under oath is punishable by a term of imprisonment of up to three years or by a fine.*

Tübingen, den …….. ……

Datum / Date Unterschrift / Signature

Table of contents

Table of figures

Tables

Abbreviations

AC	amacrine cell
A_{LRF}	maximum kernel amplitude
AMPA	α-amino-3-hydroxy-5-methyl-4-isoxazolepropionic acid
ATP	adenosine triphosphate
A-type	axon-less horizontal cell type
a.u.	arbitrary unit
BC	bipolar cell
BK channel	large conductance calcium-activated potassium channel
BP	band pass
B-type	axon-bearing horizontal cell type
Ca^{2+}	calcium ion
CaM	calmodulin
CaMKII	calmodulin dependent kinase type II
C_i	consistency index
CICR	calcium induced calcium release
Cl^-	chloride ion
cone	cone photoreceptor
cpGFP	circularly permutated green fluorescent protein
CTZ	cyclothiazide
Cx	connexin
d_{base}	distance to cone axon terminal base
DLi	dark-light index
DMSO	dimethyl sulfoxide
eCFP	enhanced cyan fluorescent protein
F_0	baseline level
FRET	Förster resonance energy transfer
GABA	gamma-aminobutyric acid

GC	ganglion cell
GFP	green fluorescent protein
GTP	guanosine triphosphate
H^+	hydrogen ion
HC	horizontal cell
I_{BKG}	background intensity
I_{MAX}	maximum intensity
I_{MIN}	minimum intensity
IPL	inner plexiform layer
IR	infrared
IS	inner segment
K^+	potassium ion
KA	kainate
KCC	K-Cl co-transporter
LED	light-emitting diode
L-opsin	long wavelength opsin
MAD	median absolute deviation
mGluR1	metabotropic glutamate receptor 1
mGluR6	metabotropic glutamate receptor 6
M-opsin	medium wavelength opsin
musc	muscimol
Na^+	sodium ion
NBQX	6,7-dinitroquinoxaline-2,3-dione
NKCC	Na-K-Cl co-transporter
OGB1	Oregon Green 488 BAPTA-1
OPL	outer plexiform layer
OS	outer segment
P*	photoisomerisation
PBS	phosphate-buffered saline

PFA	paraformaldehyde
PMT	photomultiplier
Q_i	quality index
rod	rod photoreceptor
ROI	region-of-interest
SARFIA	semi-automated routines for functional image analysis
SC	spectral contrast
s.d.	standard deviation
SEM	standard error of the mean
SERCA	sarco-endoplasmic reticulum calcium-ATPase
S-opsin	short wavelength opsin
SR101	sulforhodamine 101
thap	thapsigargin
TRPM1	transient receptor potential cation channel subfamily M member
UV	ultra violet
vera	verapamil
VGCC	voltage gated calcium channel
ΔF	response amplitude
λ_{max}	maximum absorbance wavelength

Abstract

Most neurons in the central nervous system have elaborate dendritic arbours which come in a large variety of sizes and morphologies (Lefebvre et al., 2015). For many decades, dendrites have been thought to simply relay presynaptic signals to the soma and to the axon terminal system by acting as “passive cables”. However, it has become clear that dendrites are capable of much more than passively integrating synaptic input, they can also act independently and modulate presynaptic signals (reviewed by Branco and Häusser, 2010). Dendritic signal processing has been reported to support sophisticated functions in the cortex, hippocampus, and cerebellum as well as in the retina. In the latter case, multiple processing within one dendrite is essential to process considerable amounts of information from the outside world but, at the same time to use space efficiently: The retina needs to be thin and transparent to reduce light scattering within the tissue. Dendritic processing has already been described in inner retinal neurons (Euler et al., 2002; Grimes et al., 2010; Oesch et al., 2005; Sivyer and Williams, 2013). In the outer retina, the horizontal cell (HC) dendrites, which are directly postsynaptic to the cone photoreceptors (cones) have recently been suggested to be plausible candidates for local signal processing (Grassmeyer and Thoreson, 2017; Jackman et al., 2011; Vroman et al., 2014) despite their involvement in global tasks such as contrast enhancement.

To test this hypothesis physiologically, I used two-photon imaging to record calcium (Ca^{2+}) signals in cones and HCs, as well as, cone glutamate release in mouse retinal slices. I used green (578 nm) and ultra violet (UV, 360 nm) light stimuli and recorded from different retinal regions to specifically activate different combinations of medium (M-) and short (S-) wavelength-sensitive opsin expressed in cones. This approach allowed to assess if signals from individual cones remain “isolated” within a local dendritic region of a HC, or if they spread across the entire dendritic tree or, in the electrically coupled HC network. In contrast to what one would expect in a purely globally acting HC (network), responses measured in neighbouring HC compartments varied markedly in their chromatic preference suggesting that HC dendrites are able to process cone input in a highly local manner. Moreover, I found local HC feedback to play a role in shaping the temporal properties of cone output.

Introduction

The central nervous system is composed of a great variety of neurons, each type being specialized to encode specific input. However, the power of neuronal processing can be greatly increased by subdividing neurons into subunits that can locally and independently process synaptic signals. In dendrites, this is commonly achieved by combining anatomical and physiological properties that locally restrict presynaptic signals in postsynaptic compartments (reviewed in Branco and Häusser, 2010). Dendritic processing is present at different levels of the central nervous system such as the cortex, hippocampus, cerebellum and retina (reviewed in Branco and Häusser, 2010; Kitamura and Kano, 2013; Schubert and Euler, 2010; Spruston, 2008).

The retina is an excellent model system to study dendritic processing: Dendrites can be recorded in *ex vivo* retinal preparation under natural stimulus (light flashes) and the detailed knowledge about neuronal types (Baden et al., 2016; Ghosh et al., 2004; Wässle et al., 2009) and the availability of anatomical reconstruction (Helmstaedter et al., 2013) make it a powerful model to study neuronal networks and circuitry (Wässle, 2004).

In this thesis, I used the first synapse of the visual system - between the cone axon terminal and the HC dendrites - as a model to study under physiological conditions, how presynaptic signals can be locally encoded in a globally acting network. In fact, HCs have been considered for many decades as an electrically coupled network responsible for sampling from a large number of cones. They provide global feedback to cones, and thus play an essential role in contrast enhancement, colour opponency and the generation of centre-surround receptive fields in cones and bipolar cells (BCs; reviewed by Thoreson and Mangel, 2012). Due to the presence of gap junctions and their global functions they were so far not considered to support local dendritic processing. However, recent studies suggest that HC feedback can also act at the level of a single HC dendritic tip and a cone axon terminal (Grassmeyer and Thoreson, 2017; Jackman et al., 2011; Vroman et al., 2014). This indicates that local dendritic signal processing might already exist at the first synapse of the visual system.

In this work, I therefore first introduce the basics of local dendritic processing. Then, I provide an overview of the first synapse of the visual system that I used as a model to study how local dendritic processing is generated in a neuronal class that was traditionally thought to play global functions.

Dendritic processing

The large variety in dendritic morphology, size and synapse location suggests that dendrites are involved in various tasks (reviewed in Lefebvre et al., 2015). Dendritic dysfunction and malformation in the brain has been associated with several pathologies such as autism spectrum disorders, schizophrenia, or Alzheimer's disease, (reviewed in Kulkarni and Firestein, 2012; Penzes et al., 2011) revealing their essential role in integrating and processing inputs. Moreover, the recent development of high spatial resolution microscopy has highlighted the role of sub-synaptic dendritic compartments (such as spines or varicosities) that were not accessible so far (reviewed in Adrian et al., 2014). Whereas spines are dendritic protrusions that can be connected to the dendritic branch by a high resistance structure called the spine neck, varicosities are enlargements in a thinner dendrite (reviewed in Harris and Spacek, 2016).They are both involved in biochemical and electrical compartmentalization (reviewed in Adrian et al., 2014). They can release neurotransmitters, (reviewed in Ludwig and Pittman, 2003) and switch between different processing modes depending on the strength of the stimulus (Grimes et al., 2010).

Moreover, spines are highly plastic (reviewed in Mel et al., 2017) and undergo drastic changes during development. Spine formation begins after birth in many species. Their number increases during the first months and decreases with age (reviewed in Yuste and Bonhoeffer, 2004). In addition, spines can have different morphologies and undergo morphological changes. Four major types of spine morphology have been described: Filopodium, thin, stubby and mushroom (**Figure 1**) (Risher et al., 2014). Filopodium and thin spines are more immature and dynamic and they have been associated with learning whereas large spine such as mushroom spines are more stable and contribute to memory function (reviewed in Kasai et al., 2003).

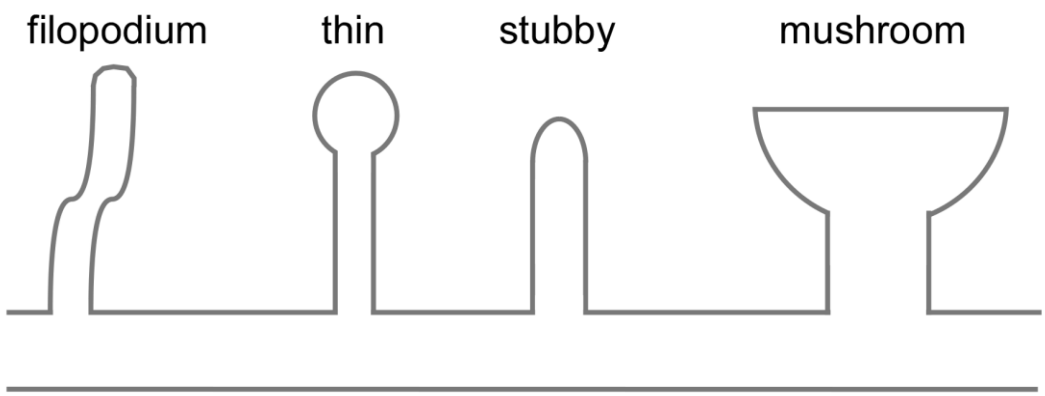

Figure 1. Diversity in spine morphology
Schematic representation of four main types of dendritic spine morphology: filopodium, thin, stubby and mushroom (*modified from Yuste and Bonhoeffer, 2004)*.

Here, I describe several well studied examples where Ca^{2+} signalling plays a key role in switching between different dendritic processing modes. These discoveries rely on the combination of experiments and biophysical modelling.

Purkinje cells

Cerebellar Purkinje cells are GABAergic (gamma-aminobutyric acid) neurons that play a role in motor coordination. They possess large dendritic trees covered with spines, each receiving excitatory inputs from a single climber fibre and from more than 100,000 parallel fibres. Depending on the source and the strength of the excitatory input, different pathways are activated. Weak stimulations via parallel fibres activate the metabotropic glutamate receptor mGluR1 leading to local Ca^{2+} increase that stays confined to a single spine (Finch and Augustine, 1998). However, strong stimulation by climber fibres (possibly together with parallel fibres) activates voltage gated Ca^{2+} channels (VGCCs), leading to the generation of dendritic spikes that propagate to the soma and synchronize the dendritic signal (Wang et al., 2000). Therefore, Purkinje cells can either process presynaptic inputs in a highly local manner (when receiving presynaptic input from parallel fibres) or on a global scale when electrical signal can spread

along the dendrites. Moreover, simultaneous activation of both fibres types can induce long-term depression (reviewed in Kitamura and Kano, 2013).

Pyramidal cells

Pyramidal neurons have been extensively studied in the cortex (layer V) and the hippocampus. They are composed of basal and apical dendritic trees which are covered with spines that receive mostly excitatory glutamatergic input. However, Villa and colleagues (2016) have recently shown that while excitatory input on dendritic spines is stable, some inhibitory input is present and highly plastic. Moreover, they show recurrent synapse formation at the same location. Pyramidal dendritic spines have also been found to be responsible for local signal processing. For example, in CA1 pyramidal cells, the spine neck has been found to create an electrical resistance that restrict signal spread along the dendritic branch. Even when strong depolarization of dendritic spines leads to VGCC activation, the high resistance in the spine neck create a voltage drop. This results in a compartmentalization of electrical signal to the spines as VGCCs localized on the dendritic branch or on neighbouring spines do not get activated (Bloodgood et al., 2009).

Retinal amacrine cells

Another example of local and global dendritic signalling is the retinal A17 amacrine cell (AC), which is involved in the rod photoreceptor (rod) pathway: Rods transfer the visual signal to rod BCs which in turn receive reciprocal inhibitory feedback from A17 ACs. A17 AC dendrites are covered with numerous spine-like structures, called varicosities, each of them being the basis for independent dendritic processing and therefore for highly local feedback to rod BCs. A17 ACs express Ca^{2+} permeable α-amino-3-hydroxy-5-methyl-4-isoxazolepropionic acid (AMPA) receptors. The increase of intracellular Ca^{2+} through these channels activates Ca^{2+} induced Ca^{2+} release (CICR) from internal stores which in turn amplifies the response (Grimes et al., 2010). To prevent spread of signals, the A17 ACs express large-conductance Ca^{2+}-activated potassium (K^{+})

channels (BK channels) that limit the depolarization and therefore prevent the activation of VGCCs (Grimes et al., 2009). Moreover, the uniform distribution of varicosities along the dendrites (every ~20 µm) prevents the activation of neighbouring varicosities at least for low-light conditions (sparse activation of few varicosities, Grimes et al., 2010). Similar to Purkinje cells, the A17 ACs may also be able to switch to a global processing mode. Strong stimulation likely overcomes the BK channel-mediated suppression of VGCC leading to a spread of electrical signals along the A17 dendrites (Grimes et al., 2010, 2009).

Dendritic spines vs. retinal horizontal cell dendritic tips

These examples presented above share common principles to increase dendritic integration and processing capacity of incoming signals. On a general level, these aptitudes are based on anatomical features (such as spines or varicosities) that can physically restrict the spread of signals along the dendrites and active functional properties that lead to nonlinear presynaptic input integration. The following steps summarize a general mechanism for local dendritic signalling at an excitatory synapse (**Figure 2**):

(1) Release of glutamate from the presynaptic terminal
(2) Binding of glutamate at postsynaptic glutamate receptors (Ca^{2+} permeable ionotropic or metabotropic glutamate receptors) on a dendritic spine (or other specialisation)
(3) Local increase in Ca^{2+} concentration
(4) Activation of CICR that further increases the Ca^{2+} concentration: Ca^{2+} can regulate gene transcription. It can also act on Ca^{2+} sensitive proteins such as calmodulin (CaM) that binds CaM dependent kinase type II (CaMKII). In turn, CaMKII phosphorylates AMPA receptors and strengthen the synaptic transmission (reviewed in Lisman et al., 2002). Moreover, Ca^{2+} can act on direct Ca^{2+}-activated enzymes such as calcineurin (phosphatase) or calpain (protease) but also on parvalbumin, calretinin and calbindin that buffer Ca^{2+} to modulate its time course (reviewed in Higley and Sabatini, 2012; Raghuram et al., 2012). Finally, the local depolarization following the Ca^{2+} inflow can

lead to release of neurotransmitter or to the generation of dendritic spike (reviewed by Branco and Häusser, 2010).

(5) Depending on the strength of the depolarization in the spine, VGCCs may be activated and may lead to spread of signals to the dendritic branch and possibly to neighbouring dendritic spines. For example, the interactions between spines and with the dendritic branch can lead to the discrimination of temporal input sequences along a dendritic branch (Branco et al., 2010). Moreover, spines have been suggested to play a role in the regulation of back-propagating action potentials along the dendrites (Trong et al., 2017; Tsay and Yuste, 2002). The depolarization along the dendritic branch can also lead to the generation of somatic action potential.

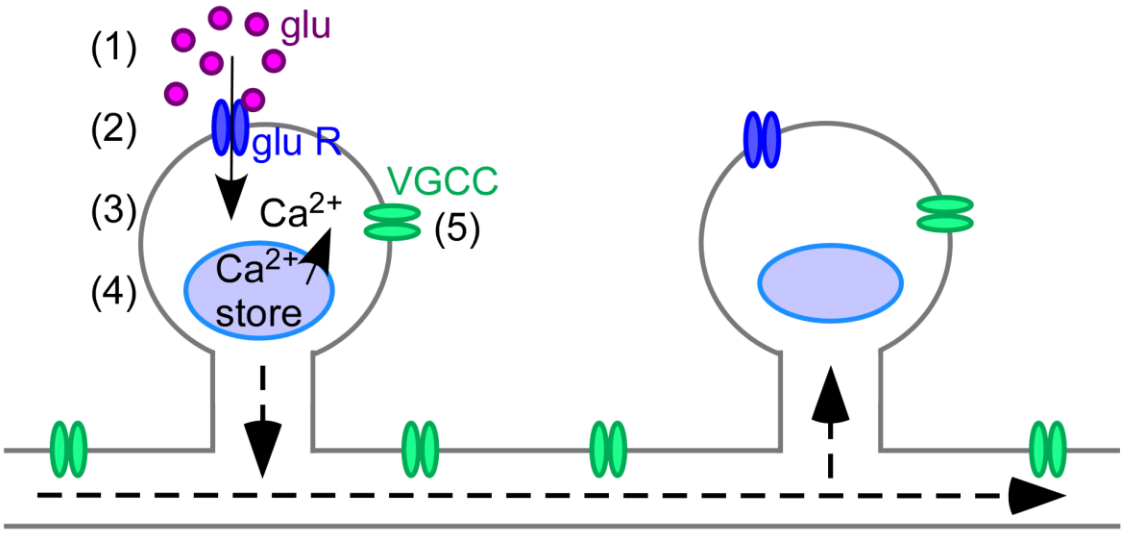

Figure 2. Ca^{2+} signalling in dendritic spines
Schematic representation of a dendritic branch with two neighbouring spines. The release of glutamate from the presynaptic terminal (1) leads to glutamate receptor activation (2) which triggers a local increase in Ca^{2+} concentration (3) and activates CICR (4). If the resulting depolarization in the dendritic spine exceeds the voltage gated Ca^{2+} channel activation threshold (5), the voltage signal may spread to the dendritic branch and to neighbouring spines (black dashed lines). CICR: Ca^{2+} induced Ca^{2+} release, glu: glutamate, glu R: glutamate receptor, VGCC: voltage gated Ca^{2+} channel (*modified from* Higley and Sabatini, 2012).

Local dendritic processing is a way to increase the computational power of the central nervous system, but it has never been directly demonstrated experimentally for the outer retina. Therefore, in this thesis, I evaluate the possibility for local dendritic processing at the level of the first synapse of the visual system, where the cones synapse onto HC dendritic tips – at the site of the feedback. Several factors need to be considered before evaluating local dendritic processing in HC dendrites. First, mammalian HCs do not possess clearly defined spine-like structure. Globular structures along the dendrites have been reported (personal communication, Christian Behrens) but if they play a role in Ca^{2+} signal compartmentalization is still unknown. Second, the HC dendritic tips and most of the dendritic spines can act as an input and output structure and can release neurotransmitter (Ludwig and Pittman, 2003). In the case of the HC dendritic tip, this input and output structure is also the site of the generation of a complex feedback to the cones (described in detail below). Taken together, the HC dendritic tip is a plausible candidate for local dendritic processing (Grassmeyer and Thoreson, 2017; Jackman et al., 2011; Vroman et al., 2014). I therefore use the HCs in the retina as a model to study the mechanisms and the functions of local dendritic processing in a neuron that does not possess spines and that is suggested to be responsible for global tasks.

Structure of the mammalian retina

In the retina, when a photon reaches a photoreceptor, the incoming signal is transduced into an electrical signal which is fed into parallel BC pathways. These, in turn, convey the visual information to ganglion cells (GCs), the output neurons of the retina (Baden et al., 2016; Euler et al., 2014). This excitatory feed forward pathway is modulated by two inhibitory interneuron classes. In the outer plexiform layer (OPL), HCs feedback to photoreceptors and modulate their responses, while, in the inner plexiform layer (IPL), ACs modulate BC and GC responses (**Figure 3**). In this thesis, I focused on the first synapse of the visual system. I therefore introduce the three partners of this synapse: the photoreceptors, HC and BC with an emphasis on HC.

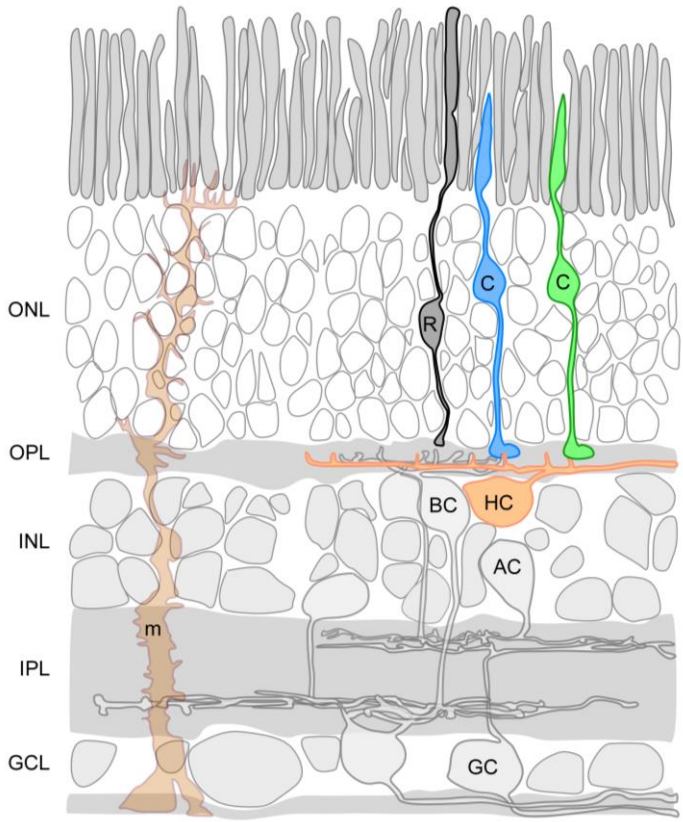

Figure 3. Schematic organization of a vertical section of the mouse retina
The retina is composed of two types of photoreceptors: rods (R) and cones (C) which transmit signals to ganglion cells (GCs) via bipolar cells (BCs). Two inhibitory interneurons modulate their signals, the horizontal cells (HCs) and amacrine cells (ACs). Müller cells (m) are glial cells that support retinal physiological functions. Retinal neurons are organized in different layers: outer nuclear layer (ONL), outer plexiform layer (OPL), inner nuclear layer (INL), inner plexiform layer (IPL) and ganglion cell layer (GCL) *(modified from Euler et al., 2009)*.

The photoreceptor synapse

Photoreceptors are responsible for capturing photons and are the site of phototransduction. Their terminals contain specialized synaptic site(s) called “ribbons” (reviewed in Schmitz, 2009). Ribbons are protein complexes located at the active zone and are surrounded by vesicles containing glutamate. They allow a graded neurotransmitter release. Mice cone axon terminals contain approximatively 10 ribbons whereas rod axon terminals possess only one ribbon (Tsukamoto et al., 2001). Each cone ribbon relays the light signal to one ON cone BC dendrite invaginated into the cone axon terminal and to several OFF cone BCs located at the base of the cone axon terminals (Haverkamp et al., 2000). However, this classical view has been recently challenged by Behrens and colleagues (2016) who showed exceptions to this rule: For example, the ON BC type X makes predominantly non-invaginating contacts with cones.

Each cone can be contacted by different types of BCs, indicating that the cone signal is distributed into multiple pathways: In total, the information of cones is divergently relayed into 14 types of BCs (reviewed in Euler et al., 2014). Moreover, two HC dendritic processes (belonging to possibly two different HCs) modulate the cone output via parallel feedback mechanisms (**Figure 4**). The first step of the visual information processing has a critical role as all the downstream neuronal processing relies on it. Moreover, HCs play a central role in this synapse as they are responsible for providing feedback to photoreceptors and feed-forward signals to BCs.

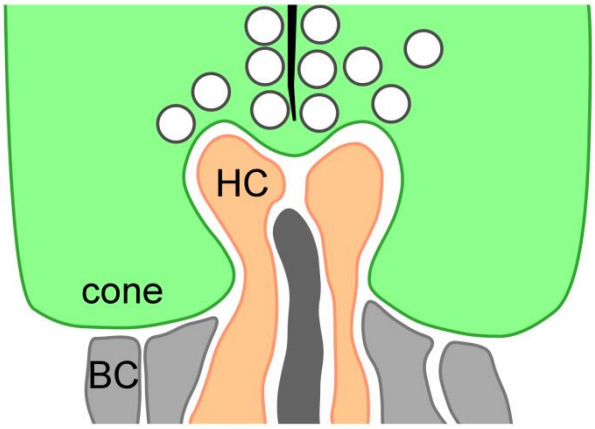

Figure 4. Schematic representation of the cone photoreceptor synapse
Cone axon terminal (green) possesses a specialized synaptic site called ribbon (black line) surrounded by vesicles containing glutamate (white circles). The cone axon terminal makes synaptic contacts with two invaginating HC dendritic tips (orange) and one ON cone BC dendrite (dark grey). Several OFF cone BCs (light grey) make synaptic contacts at the base of the cone axon terminal *(modified from Chapot et al., 2017)*.

Cone and rod photoreceptors

There are two types of photoreceptors, which are specialized to capture the light at different light intensities. Rods are highly sensitive to light and are therefore responsible for scotopic vision at low-light levels (“night” vision) whereas cones, are activated at higher light intensities and mediate photopic vision (“daylight” vision). Adaptation across a large range of light intensities is achieved mostly by modulation of the phototransduction cascade (Pugh et al., 1999). Moreover, HC feedback has often been suggested to contribute keeping the photoreceptors in their physiological range (see below).

Photoreceptors consist of four anatomical compartments having distinct functional specialization: The outer segment (OS) is responsible for the phototransduction, the inner

segment (IS) contains mitochondria and ribosomes to fulfil the high metabolic demands, the soma, responsible for gene expression and the axon terminal where synaptic transmission to postsynaptic neurons occurs. Cones are shorter than rods and have a conical shape whereas rod OS has an elongated shape formed by stacked discs containing pigments to increase the probability to catch a photon (**Figure 5**) (reviewed in Molday and Moritz, 2015).

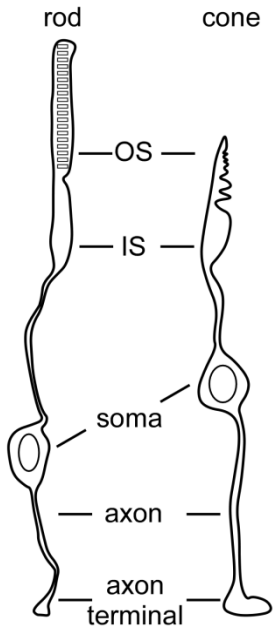

Figure 5. Schematic representation of rod and cone photoreceptors
Photoreceptors are composed of several anatomical and functional compartments: The outer segment (OS) contains the visual pigment and is responsible for the phototransduction, the inner segment (IS) contains ribosomes and mitochondria to supply energy, the soma is responsible for gene expression and the axon terminal is responsible for glutamate release.

In the OS of photoreceptors, the opsin protein is expressed and binds to the 11-cis retinal. The spectral sensitivity of the opsin depends on the amino acid sequence. Rods possess only one type of opsin (rhodopsin) and therefore do not mediate colour vision, which relies on the comparison of photoreceptor activity sensitive to different wavelengths. In contrast, cones mediate colour vision as they express different types of opsin, whose spectral sensitivities vary between species. In the mouse retina, the S-opsin (maximum absorbance wavelength, λ_{max}=360 nm) is maximally activated by UV light whereas the M-opsin (λ_{max}=508 nm) is maximally activated by green light (Nikonov et al., 2006). Most of M-cones co-express the M-opsin and the S-opsin. This co-expression is set up as a dorso-ventral gradient: The dorsal retina is dominated by mostly M-opsin expressing cones, whereas the ventral retina is dominated by almost exclusively S-opsin expressing cones (Baden et al., 2013; Röhlich et al., 1994; Szél et al., 1992). In addition, the retina is composed of 5% “true” S-cones with a constant density across the

retina that exclusively express the S-opsin. These “true” S-cones have been anatomically characterized by their connection to a cone BC type (Haverkamp et al., 2005).

Apart from mediating colour vision, cones can encode light contrast differentially: M-cones and few S-cones encode bright and dark contrast stimuli equally whereas most of S-cones show a clear preference for dark over bright stimuli (Baden et al., 2013). As S-cones are located in the ventral retina and therefore sample information from the sky, it has been speculated that their dark contrast preference is an evolutionary advantage to detect dark predators.

Horizontal cells

Horizontal cell connectivity

There are two types of HC, an axon-less type (A-type) and an axon-bearing type (B-type). The mouse retina is composed only of the B-type (Peichl and González-Soriano, 1994). Whereas rods contact HC axon terminals, cones contact HC dendrites. Specifically, HC dendrites sample information from all cones within their dendritic fields (Feigenspan and Babai, 2015; Schubert et al., 2010) and each cone is contacted by several HCs. However, despite the clear separation of cone and rod inputs into different anatomical HC compartments, their signals are not strictly sequestered to HC dendrites and axon terminals, respectively. Firstly, cones and rods are coupled to a great extent via gap junction-forming connexin36 (Cx36) (Asteriti et al., 2014; Deans et al., 2002); secondly, cone signals can travel from HC dendrites to the HC axon terminal system (Szikra et al., 2014; Trumpler et al., 2008), indicating that HC dendrites and axons receive a mixture of cone and rod signals. However, whether rod signals can also travel from the HC axon terminal system to the dendrites remains controversial (Szikra et al., 2014; Trumpler et al., 2008).

Horizontal cells express connexin57 (Cx57) and form a large electrically coupled network (Hombach et al., 2004; Janssen-Bienhold et al., 2009). As a consequence of this strong coupling, the receptive field of an HC is larger than its dendritic field (Shelley et al., 2006). Horizontal cell

coupling is modulated by dopamine, which is in turn regulated by both the circadian rhythm (reviewed in Besharse and McMahon, 2016) and the light adaptation state of the retina (Hampson et al., 1994; He et al., 2000; Tornqvist et al., 1988; Xin and Bloomfield, 1999). During the day, the dopamine is released by dopaminergic ACs in the inner retina, diffuses through the retina and reduces the HC electrical coupling (reviewed by Witkovsky, 2004). Bloomfield and Dacheux (2001) proposed that a reduction of the HC coupling during the day avoids lateral spread of signals and therefore preserves high spatial resolution. In contrast, in mesopic condition (e.g. dawn), when the coupling is high, HCs sample from a large number of cones and rods allowing a summation over a large area of the retina in order to capture as many photons as possible and therefore increasing the signal to noise ratio.

Horizontal cell feedback

HCs form a sign-conserving synapse with the cones: They both hyperpolarize in response to light stimulation. Glutamate released by cones binds to postsynaptic receptors expressed on HCs. HCs express AMPA- and kainate (KA) -type ionotropic glutamate receptors (Feigenspan and Babai, 2015; Kreitzer et al., 2009; Schubert et al., 2006; Schultz et al., 2001; Ströh et al., 2013). In turn, HCs modulate cone glutamate release using at least three different feedback mechanisms: ephaptic, proton (or pH) -mediated feedback and GABAergic mediated feedback (**Figure 6**).

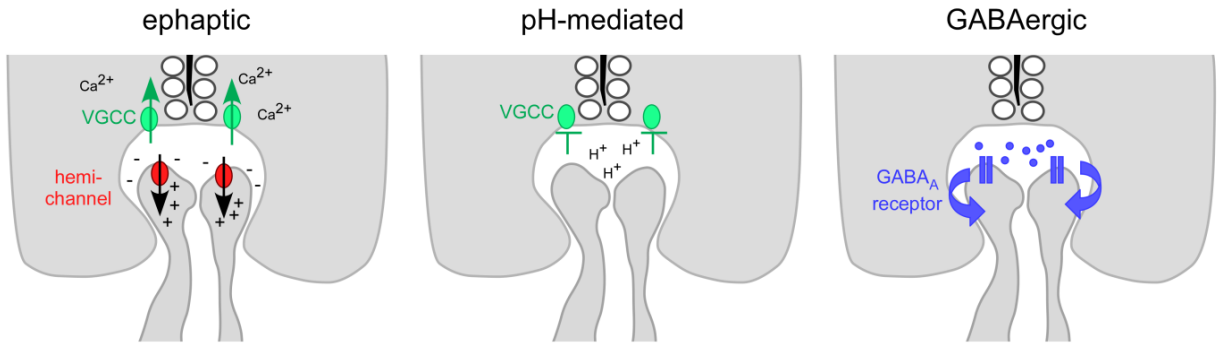

Figure 6. Three hypotheses for negative horizontal cell feedback
Schematic drawing that illustrates the mechanisms for ephaptic, pH-mediated and GABAergic feedback in the mouse. Ephaptic feedback is an instantaneous process due to flow of cations through hemichannels that leads to voltage gated Ca^{2+} channel (VGCC) activation. pH-mediated feedback is a slower process that occurs when the proton concentration exceeds the pH buffer capacity of the synaptic cleft leading to a reduction of VGCC conductance. GABAergic feedback is due to GABA release from HCs that binds to auto-receptors and modulates both ephaptic and pH-mediated feedback.

The *ephaptic mediated feedback* is an instantaneous process mediated by a flow of cations through hemichannels into the distal HC dendrites when HCs hyperpolarize to light (Vroman et al., 2014). This flow of cations produces a slight hyperpolarization within the synaptic cleft. Consequently, the voltage drop in the synaptic cleft is sensed as a depolarization by the VGCCs expressed in the cone axon terminals, promoting Ca^{2+} inflow and increasing the glutamate release (reviewed in Vroman et al., 2013). The basis of ephaptic mediated feedback relies on the high resistance within the extracellular synaptic cleft between a cone ribbon synapse and a HC dendritic tip, and the presence of hemichannels (e.g. connexin or pannexin). In zebrafish, Cx55.5 was shown to be involved in ephaptic feedback (Klaassen et al., 2011). Additionally, Pannexin1 has been found in the HC dendritic tips of mouse and zebrafish and may play a role in ephaptic feedback (Kranz et al., 2013; Prochnow et al., 2009).

The *proton mediated feedback* (also known as pH-mediated feedback; Vessey, 2005) is a slower process compared to the ephaptic mediated feedback (with a response time constants of both cones and HCs of ~200 ms for proton-mediated vs. ~35 ms for ephaptic feedback; Vroman et al., 2014). The release of protons in the synaptic cleft leads to an acidification of the cleft when its concentration exceeds the extracellular pH buffer capacity. Once the pH buffer capacity is exceeded, protons bind to negative residues present at the VGCC pore and reduce its conductance (Chen et al., 1996) and therefore decrease the rate of glutamate release (Wang et al., 2014). Several sources of protons in the synaptic cleft can contribute to the decrease of pH: the hydrolysis of adenosine triphosphate (ATP) extruded by HCs through hemichannels (Vroman et al., 2014), Na^{+}/H^{+} (sodium/hydrogen) exchangers (Molina et al., 2004), proton-bicarbonate permeable channels (Warren et al., 2016a), plasmalemma membrane Ca^{2+}/H^{+}

ATPases (Kreitzer et al., 2007) and proton pumps (Wang et al., 2014). Moreover, in low light condition, the cone axon terminal releases glutamate with free protons leading to an acidification of the synaptic cleft (DeVries, 2001) acting as a cone auto-feedback loop.

The *GABAergic mediated feedback* modulates both ephaptic and proton mediated feedback and acts in an indirect fashion (Kamermans and Werblin, 1992; Kemmler et al., 2014). Upon depolarization, HCs release GABA which binds to ionotropic $GABA_A$ auto-receptors (Liu et al., 2013). The intracellular increase in chloride (Cl^-) concentration through $GABA_A$ receptors may shunt the positive current flow through hemichannels, altering the ephaptic feedback (Endeman et al., 2012). Moreover, GABA receptors are also permeable for bicarbonate (Liu et al., 2013). A release of bicarbonate leads to an alkalinisation of the synaptic cleft resulting in an increase VGCC conductance. The role of GABA in HC feedback is still a matter of debate and there is currently no consensus on this topic as its function is highly dependent on species and experimental conditions (Tatsukawa et al., 2005; Verweij et al., 2003). For example, the light exposure used during (and before) the experiment may have an influence on the $GABA_A$ receptors expression and this directly affects the effect of GABA on HCs (unpublished data, FASEB poster 2016 “GABA mediated horizontal cell signalling switches back and forth between cones at night and ON cone bipolar cells in the days”, Mangel and colleagues). Moreover, whereas mouse cones do not express GABA receptors (Kemmler et al., 2014), fish cones express GABA receptors (and Ca^{2+} dependent Cl^- channels) allowing direct modulation of cone responses (Endeman et al., 2012). It is also conceivable that GABA acts on BC receptors (see BC section).

Horizontal cell functions

Horizontal cells play many roles in early visual processing that I review in the following section. Note that depending on the species, HCs may play different roles.

First, it has been proposed that HCs are responsible for *adjusting the operational range of cones* in the turtle (Burkhardt, 1995). By providing negative feedback to cones, HCs have been

thought to adjust the cone responses over a broad range of light intensities (reviewed by Thoreson and Mangel, 2012). However, the fact that the HC receptive field (from hundred of µm to mm in mice; Shelley et al., 2006) is larger than that of a cone indicates that the mean inputs received by cones and HCs are likely to be different and therefore that HC feedback may not play a critical role in adjusting the operational range of cones. Moreover, non-mammalian vertebrates possess different HC types that respond to different chromatic input with opposite polarities (Kamermans et al., 1991; Pottek et al., 1997), that may result in stronger difference between cone and HC inputs.

Second, HCs are involved in *contrast enhancement* (VanLeeuwen et al., 2009). This function relies on lateral inhibition: HCs provide an estimate of the background light level and subtract the mean ambient light level from local cone changes. It has also been suggested that contrast enhancement increases the BC's detection of small details from the visual field (reviewed in Thoreson and Mangel, 2012).

Third, HCs are involved in the *generation of centre-surround receptive fields* in cones, BCs and, indirectly, GCs. Already at the level of the cone, Warren and colleagues (2016b) found that blocking HC feedback with a pH buffer abolishes the surround responses in cone salamanders. In addition, depolarization of HCs leads to a depolarization in neighbouring ON BCs while producing a hyperpolarization in neighbouring OFF BCs in carps (Toyoda and Kujiraoka, 1982) indicating that HCs can also play a role in the generation of centre-surround receptive fields in BCs (see also BC section below). At the level of GCs, HCs have also been shown to contribute to the formation of surround antagonism in primate parasol (Davenport et al., 2008) and midget GCs (Crook et al., 2011).

Finally, HCs also play a role in colour processing. *Colour opponency* is a phenomenon that has been described in primate (Packer et al., 2010) but not yet in the mouse outer retina. This phenomenon is based on the centre-surround receptive field organization (described previously). In addition to S- and M-opsin, primates possess a long wavelength opsin (L-opsin, "red"), and therefore have trichromatic vision (reviewed in Neitz and Neitz, 2011). Moreover, primates possess two HC types. The HI type samples signals from L- and M-cones and avoids S-

cones (Dacey et al., 1996; Goodchild et al., 1996) whereas the HII type samples predominantly signals from S-cones and receives few inputs from L- and M-cones (Dacey et al., 1996). Under green and red light, HII sums up M- and L-cone signals and provides lateral inhibition to S-cones and therefore generates colour opponency with information from the cones (Packer et al., 2010) (**Figure 7**). Moreover, HCs have been suggested to be involved in *colour constancy* in primate and fish. Colour constancy is a mechanism allowing a constant colour perception of an object independently of the ambient light (Kamermans et al., 1998; Vanleeuwen et al., 2007).

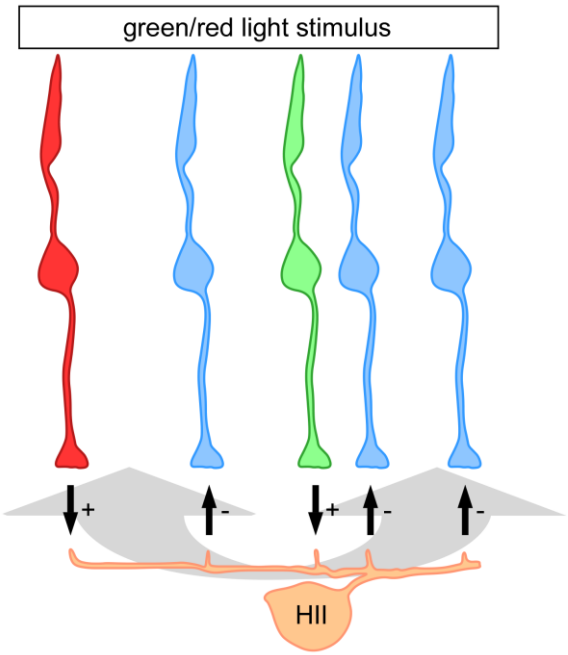

Figure 7. Generation of colour opponency in primate cones
Under green and red light stimulus, HII (orange) sums up signals from L- (red) and M-cones (green) that provide glutamatergic input. By sending global feedback (grey double arrow), HII provides inhibition to S-cones (blue). Black arrows and signs indicate the polarity of the signals *(modified from Chapot et al., 2017).*

Bipolar cells

Bipolar cells receive input from photoreceptors. In the mouse retina there are 14 types of BC responsible for relaying photoreceptor signals to GCs (Greene et al., 2016; Helmstaedter et al., 2013). Bipolar cells form parallel channels and are responsible for processing different features (reviewed in Euler et al., 2014). Each BC channel responds with different polarity, speed and chromatic preference (or different combination of these properties). Part of these functional differences originate from the fact that BC types express different types of glutamate receptors at their dendrites (reviewed in Brandstätter and Hack, 2001). For example, OFF cone BCs form a

sign-conserving synapse with cones as they express AMPA- or KA-type ionotropic glutamate receptors (DeVries, 2000). In contrast, ON cone BCs express the metabotropic glutamate receptor mGluR6 (Masu et al., 1995) and form a sign-inverting synapse with cones. The activation of mGluR6 leads to the closure of TRPM1 channels (transient receptor potential cation channel subfamily M member; Koike et al., 2010), resulting in a depolarization upon light. The distinct types of glutamate receptors expressed at BC dendrites modulate the kinetics of their responses (e.g. slow metabotropic glutamate receptors vs. relatively faster ionotropic glutamate receptors, DeVries, 2000). The shape of the BC response is also determined by the input from ACs at the BC axon terminals (reviewed in Eggers and Lukasiewicz, 2011). Even though most of the BCs contact all the cones within their dendritic field and are therefore achromatic, some BC types encode chromatic contrast by selectively contacting S- or M-cones (Haverkamp et al., 2005). Note that there is a single type of rod BC contacting predominantly rods. However, a recent study has revealed that rod BCs receive to a certain extent cone input (Pang et al., 2010).

As BCs express GABA receptors on their dendritic tips next to GABA release sites from HC dendrites (Haverkamp et al., 2000; Hoon et al., 2015), HCs may act either on BCs directly via GABA binding to GABA receptors expressed on BC dendrites (Hoon et al., 2015; Puller et al., 2014) or/and indirectly via the modulation of the cone neurotransmission. Previous studies provided evidence that GABA released by HCs can depolarize ON BCs and hyperpolarize OFF BCs (Toyoda and Kujiraoka, 1982). The action of Cl^- (depolarization vs. hyperpolarization) depends on intracellular Cl^- concentration that is regulated by Cl^- co-transporters. Therefore, differential expression of Cl^- co-transporter can result in two opposing signals (Vardi et al., 2000). The ON cone BCs have a high expression of NKCC (Na-K-Cl) co-transporter compared to OFF BCs which express predominantly KCC (K-Cl) co-transporter (Duebel et al., 2006). The NKCC co-transporter is responsible for an increase in the intracellular Cl^- concentration. Therefore, the release of GABA leads to an outflow of Cl^- depolarizing the cell. In contrast, the KCC co-transporter is responsible for the decrease of intracellular Cl^- concentration. In this case, the release of GABA leads to an inflow of Cl^- which hyperpolarizes the cell. However, depending on

the light condition used during experiments, the direct action of GABA released from HCs onto BCs is still controversial (Purgert and Lukasiewicz, 2015; Schubert et al., 2008).

Global vs. local signal processing in horizontal cell

As described earlier, due to their electrical coupling, HCs have been suggested to be involved in global signal processing such as contrast enhancement, colour opponency and generation of centre-surround receptive fields. However, recent studies suggest that HCs may provide local feedback (Grassmeyer and Thoreson, 2017; Jackman et al., 2011; Vroman et al., 2014). Indeed, Jackman and colleagues (2011) found that glutamate released from cones activate Ca^{2+} permeable AMPA receptors on HCs leading to a Ca^{2+} influx in HCs in zebrafish, tiger salamander, anole lizard and rabbit. The local Ca^{2+} increase in HC dendritic tips triggers in turn an unknown retrograde messenger that increases the conductance of glutamate channels. Note that this mechanism was abolished in slice preparation and has not been studied in mouse yet. Taken together, this indicates that HCs may play a role in both local and global visual signal processing. These two functional modes (local dendritic processing vs. global signal integration) would greatly increase the computational power of the retina (reviewed by Schubert and Euler, 2010): This would help to keep the accuracy of the signal encoded by the cones and give rise to a “personalized” feedback and, in parallel, would still serve global functions.

Aims

A growing interest in dendritic signal processing in the brain has revealed its essential role in increasing the computational power within a single neuron, a capacity extremely useful in the case of the retina which needs to be space-efficient regarding its thickness and transparency requirement. In this thesis, I focused on the first synapse of the visual system, between the cones and the HC dendrites and I assessed if and under which conditions signals from individual cones remain "isolated" within a local dendritic region of a HC or if (and how) they spread across the entire dendritic tree or in the electrically coupled HC network (Figure 8).

In the mouse retina, S- and M-cone inputs are processed by a single type of HC. Despite the fact that HCs form a large gap junctionally-coupled network involved in large scale lateral inhibition for spatial contrast enhancement, measurements at the cone-HC synapse in other species suggest that HC dendrites can feedback into cones in a highly local and independent manner supporting a role of HC dendrites in local signal processing (Grassmeyer and Thoreson, 2017; Jackman et al., 2011; Vroman et al., 2014).

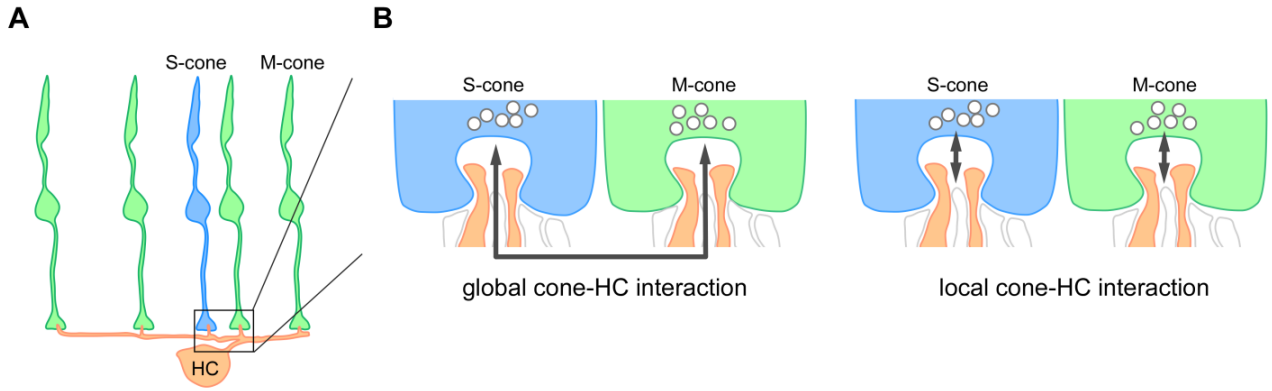

Figure 8. Two hypotheses of horizontal cell signal processing
A. Schematic representation of the connectivity between S- (blue) and M-cones (green) with a horizontal cell (HC, orange). The box corresponds to the enlarged schematic shown in B. **B.** Neighbouring S- and M-cones with postsynaptic HC dendrites. Bipolar cell dendrites are shown in white. The arrows indicate the hypothesized spread of signals in HCs. In case of global signal processing (*left*), cone signals can travel along HC dendrites and HCs send a global feedback to cones. In the second scenario (*right*), each postsynaptic HC dendrite sends local and "personalized" feedback to presynaptic cones (UV and green signals do not spread to neighbouring dendritic tips).

I tested this possibility physiologically using two-photon microscopy to record light-evoked Ca^{2+} signals in cone axon terminals and HC dendrites as well as glutamate release in the OPL in different areas of the retina (dorsal to ventral). Pharmacological approaches were used to dissect the mechanisms as well as the function of HC dendritic local processing. I performed all recordings in the mouse retinal slice preparation. Due to the angle between the laser beam and the photoreceptors, such a preparation allowed us to avoid bleaching of the OS of photoreceptors while recording light-evoked Ca^{2+} and glutamate responses in the first synapse of the visual system.

The aims of this thesis were the following:

(1) Retinal slice preparation to record light-evoked Ca^{2+} signals in HCs ($Cx57^{+/cre}$ x Ai38 mouse line), cones (HR2.1:TN-XL mouse line) and glutamate signals in the OPL (C57BL/6 mouse line expressing iGluSnFR after intra-vitral injection) using two-photon microscopy.
(2) Establishment of different light stimulus protocols to assess chromatic and contrast preferences as well as temporal receptive field of cones and HCs.
(3) Electrophysiological recording of HC somata ($Cx57^{+/cre}$ x Ai9 mouse line) to simultaneously record voltage and Ca^{2+} signals in HCs.
(4) Pharmacological dissection of the mechanisms involved in local dendritic signal processing in HCs using bath and puff drug application in combination with light stimulation.
(5) Evaluation of the function for local HC feedback by pharmacologically isolating HCs from their cone input.

I performed all tasks except the analysis of periodograms (Luke Edward Rogerson) and the intravitreal injection of iGluSnFR (Dr. Katrin Franke).

Methods

Animals

To perform Ca^{2+} imaging experiments in HCs, the transgenic mouse lines $Cx57^{cre/cre}$ (Ströh et al., 2013) and B6;129S-*Gt(ROSA)26Sor*$^{tm38(CAG\text{-}GCaMP3)Hze}$/J (Ai38, Zariwala et al., 2012) were crossed, yielding $Cx57^{+/cre}$ x Ai38 mice: The Ca^{2+} biosensor GCaMP3 (Tian et al., 2009) was selectively expressed under the control of the promoter for the gap junction-forming Cx57 present in HCs. GCaMP3 consist of a Ca^{2+} binding protein CaM and of a green fluorescent protein (GFP) (**Figure 9**).

For Ca^{2+} imaging in cone axon terminals, I used the HR2.1:TN-XL mouse line (Wei et al., 2012), which expresses the ratiometric Ca^{2+} biosensor TN-XL (Mank et al., 2006) exclusively in cones. TN-XL is composed of a Ca^{2+} sensor protein troponin C which is flanked by the fluorophores citrine and the enhanced cyan fluorescent protein (eCFP) (**Figure 9**).

For glutamate imaging, iGluSnFR (Marvin et al., 2013) was virally expressed after intra-vitreal virus injection in C57BL/6 mice (see Virus injection). iGluSnFR is composed of a circularly permutated green fluorescent protein (cpGFP) and a glutamate transporter (**Figure 9**).

For electrophysiology recording of HCs, the transgenic mouse lines $Cx57^{cre/cre}$ (Ströh et al., 2013) and B6;129S6-*Gt(ROSA)26Sor*$^{tm9(CAG\text{-}tdTomato)Hze}$/J (Ai9, the Jackson laboratory, ME, USA) were crossed, yielding $Cx57^{+/cre}$ x Ai9 mice that express tdTomato under the control of the promoter for Cx57.

Both male and female adult mice (4-18 weeks of age) were used. All procedures were performed in accordance with the law on animal protection (Tierschutzgesetz) issued by the German Federal Government and approved by the institutional committee on animal experimentation of the University of Tübingen.

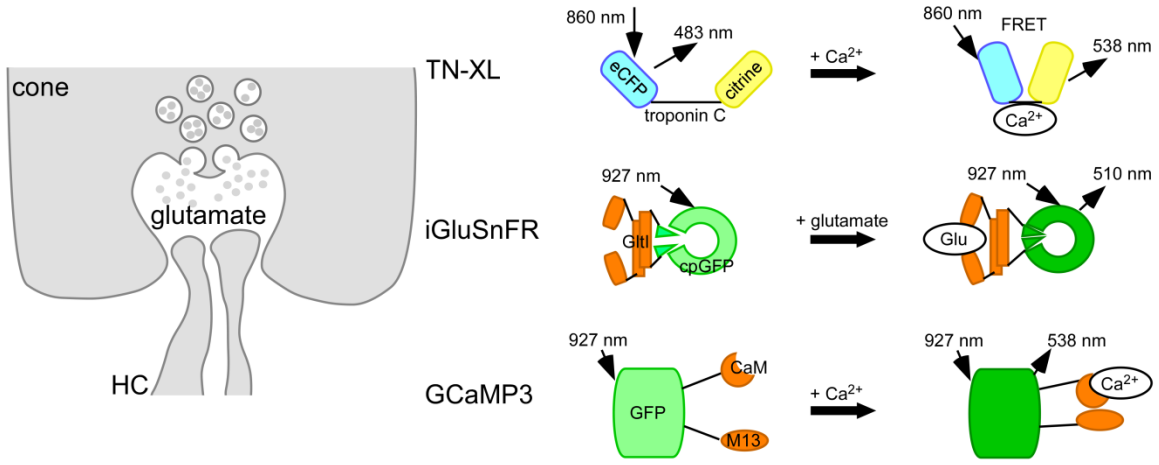

Figure 9. Ca^{2+} and glutamate imaging in the outer plexiform layer
Schematic representation of biosensors used to record light-evoked Ca^{2+} signals in cones (TN-XL), glutamate released in the synaptic cleft (iGluSnFR) and Ca^{2+} signals in HCs (GCaMP3). TN-XL is a Förster resonance energy transfer (FRET) -based Ca^{2+} biosensor between eCFP (enhanced cyan fluorescent protein, donor) and citrine (acceptor) which are linked by the Ca^{2+} sensor Troponin C. iGluSnFR consists of cpGFP (circularly permutated green fluorescent protein) linked to a glutamate transporter from E. coli (gltI). GCaMP3 is a genetically encoded Ca^{2+} indicator formed by a Ca^{2+} sensor calmodulin (CaM), a peptide (M13 myosin light chain kinase) and a green fluorescent protein (GFP). Glu: glutamate *(modified from www.amsbio.com, Marvin et al., 2013; Tainaka et al., 2010).*

Retinal tissue preparation

For all imaging experiments, mice were dark adapted for two hours. They were deeply anesthetized with isoflurane (CP-Pharma, Germany) and killed by cervical dislocation. All preparations were performed under dim red light in carboxygenated (95% O_2 / 5% CO_2) extracellular solution with (in mM): 125 NaCl, 2.5 KCl, 1 MgCl2, 1.25 NaHCO3, 20 glucose, 2 CaCl2, 0.5 L-glutamine and supplemented with 150 µM pyridoxal 5-phosphate (Deniz et al., 2011), a cofactor of the glutamic acid decarboxylase (Sigma-Aldrich or Merck, Germany). To maintain retinal orientation, both eyes were marked at the ventral side. Eyes were quickly enucleated and hemisected. Cornea, lens and vitreous body were carefully removed (**Figure 10A**). The retina was separated from the eye-cup, cut in half, flattened and mounted photoreceptor side-up on a nitrocellulose membrane (0.8 µm pore size, Millipore, Ireland). 300 µm thick acute vertical slices were cut along the nasal-temporal axis using a custom-made slicer

(Werblin, 1978) (**Figure 10B**). Slices attached to the membrane were fixed with high vacuum grease on individual glass coverslips (**Figure 10C**). They were kept in the dark in a storing chamber at room temperature for later use. Each retinal slice was transferred to the recording chamber which was maintained at ~36°C and perfused continuously with carboxygenated extracellular solution containing 0.5 µM sulforhodamine 101 (SR101; Sigma-Aldrich, Germany) to visualize cone axon terminals.

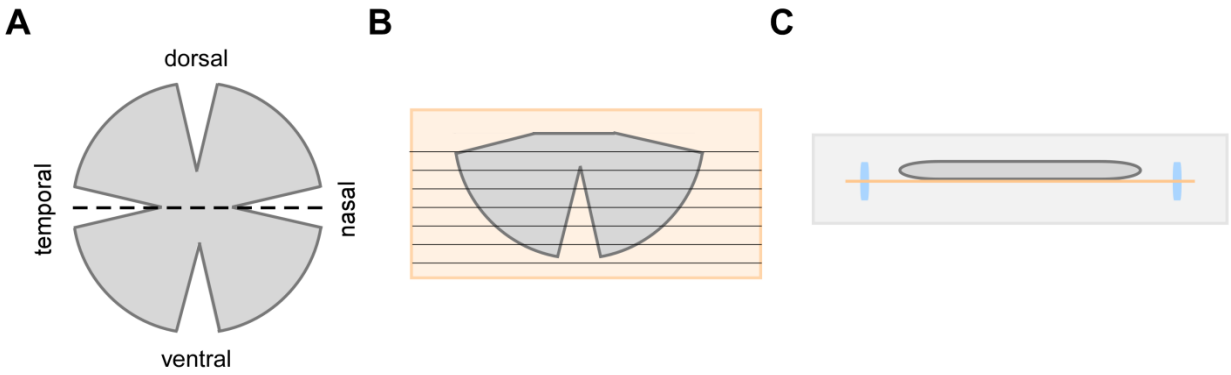

Figure 10. Retinal slice preparation
A. To prepare retinal slices, the retina (grey) was carefully dissected and vitreous body was removed. **B.** The retina was cut in half and fixed photoreceptor side-up on a nitrocellulose membrane (yellow). 300 um thick slices were cut (black lines). **C.** For recording purpose, individual slices were turned at an angle of 90° and fixed on coverslip (light blue) using high vacuum grease (dark blue).

Virus injection

Mice (5-7 weeks) were anaesthetized with 10% ketamine (Bela-Pharm GmbH, Germany) and 2% xylazine (Rompun, Bayer Vital GmbH) in 0.9% NaCl (Fresenius, Germany). A Hamilton syringe (syringe: 7634-01, needle: 207434, point style 3, length 51 mm, Hamilton Messtechnik GmbH) was filled with the virus AAV9.hSyn.iGluSnFR.WPRE.SV40 (Penn Vector core, PA, USA) and fixed on a micromanipulator (World Precision Instruments, Germany) at an angle of 15°. 1 µl of the virus was injected into the naso-ventral part of the vitreous body (Franke et al., 2017). Recordings were performed three weeks after the injection.

Two-photon imaging

A customized MOM-type two-photon microscope (Sutter Instruments, Novato, CA; designed by W. Denk, MPI for Neurobiology, Martinsried, Germany) (Denk et al., 1990; Euler et al., 2009) was used to record both Ca^{2+} and glutamate signals. Microscope was equipped with a mode-locked Ti:Sapphire laser (MaiTai-HP DeepSee; Newport Spectra-Physics, Germany) tuned to different wavelengths depending on fluorescence excitation (**Table 1**). Two photomultiplier tubes (PMTs) with different combinations of band-pass filters (BP) were used to detect the fluorescence emission (**Table 1** and **Figure 11**). Image series were acquired using a 20x water-immersion objective (either XLUMPlanFL, 0.95 NA, Olympus, Germany, or W Plan-Apochromat 20x/1.0 DIC M27, Zeiss, Germany) with the custom software ScanM (by M. Müller, MPI for Neurobiology, and T. Euler) running under IgorPro 6.37 (Wavemetrics, Lake Oswego, OR, USA). Different image configurations were used: 128 x 64 pixels (51.8 x 28.2 µm or 38.7 x 20.8 µm, at 7.8125 Hz) for all visual stimuli except the "coloured noise" and binary noise stimulus, where I used images of 128 x 16 (51.8 x 7.1 µm or 38.7 x 5.2 µm, at 31.25 Hz). To prevent bleaching of the cone outer segments by the scanning laser, recording fields were always located at the OPL (Baden et al., 2013; Wei et al., 2012).

Fluorescence		**Band-pass filters**		**Excitation wavelength (nm)**
Channel #1	**Channel #2**	**Channel #1**	**Channel #2**	
TN-XL/citrine	TN-XL/eCFP	538 BP 50	483 BP 32	860
iGluSnFR	SR101	510 BP 84	630 BP 60	927
GCaMP3	SR101	538 BP 50	630 BP 60	927
OGB1	tdTomato	538 BP 50	630 BP 60	927

Table 1. Fluorescent biosensors or dyes with respective band-pass filters and fluorescence excitation wavelength.
BP, band-pass filters; eCFP, enhanced cyan fluorescent protein; OGB1, Oregon Green 488 BAPTA-1; SR101, sulforhodamine 101.

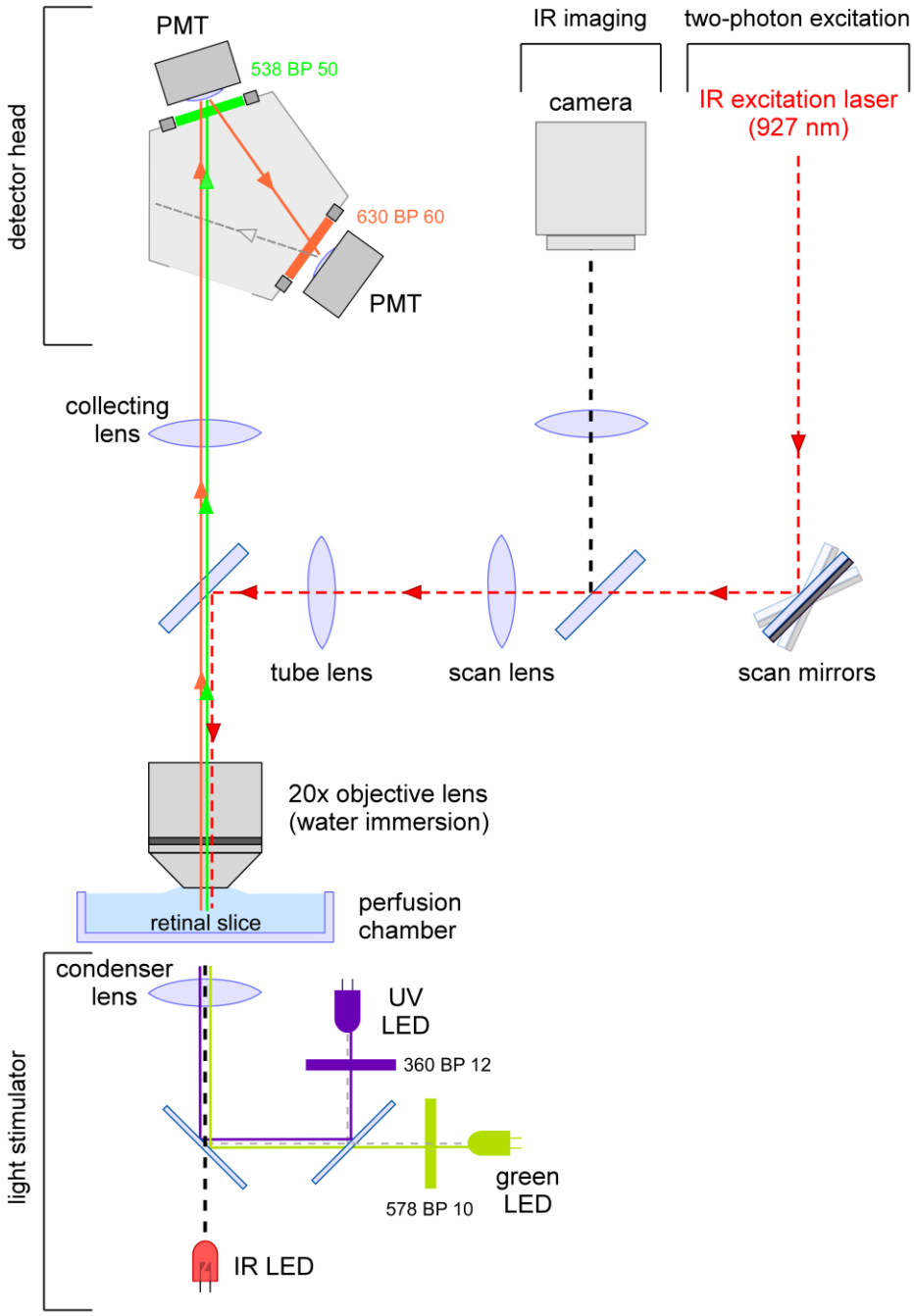

Figure 11. Two-photon Ca^{2+} imaging in horizontal cells in retinal slices
A retinal slice was placed in the perfusion chamber. The objective was centre to the OPL layer using infrared (IR) light-emitting diode (LED) and IR camera. For two-photon imaging, IR excitation laser was tuned to 927 nm and Ca^{2+} signals in HCs were detected using a 538 BP 50 filter and a photomultiplier (PMT). An additional 630 BP 60 filter was used to detect sulforhodamine (SR101) emission. Light stimulator consists of UV and green LEDs focused on the retinal slice through the bottom of the perfusion chamber *(modified from Euler et al., 2009)*.

Electrophysiology

For current clamp recording of HCs, patch electrodes (~8 to 12 MΩ) were filled with (in mM): 125 K-gluconate, 10 NaCl, 1 $MgCl_2$, 1 EGTA, 5 HEPES, 5 ATP-Na and 0.1 guanosine triphosphate (GTP)-Na. In addition, 100 µM of Oregon green 488 BAPTA-1 (OGB1, Life Technologies OR, USA) was added in the electrode to simultaneously record membrane potential and Ca^{2+} changes. The pH was then adjusted to 7.2 with KOH (solution modified from Akrouh and Kerschensteiner, 2013). The liquid junction potential was corrected (14.5 mV, calculated using Clampex's Junction Potential Calculator, Axon instruments, CA, USA). Signals were amplified using the Axopatch 200B amplifier (molecular devices, Biberach and der Riss, Germany) and digitized at 10 kHz.

Light stimulation

To stimulate photoreceptors with full-field stimuli, an open-source microprocessor board (http://www.arduino.cc/) was used to drive two band-pass-filtered LEDs (UV, 360 BP 12; green, 578 BP 10; AHF). LEDs were synchronized with the scanner retrace to avoid light stimulus artefacts during image acquisition. The light was combined by a beam-splitter (400 CDLP, AHF) and focused on the retinal slice through the bottom of the recording chamber via a condenser lens (H DIC, 0.8 NA, Zeiss) (**Figure 11**).The intensity of each LED was adjusted such that the photoisomerisation (P*) rate in S-cones elicited by the UV LED was equal to the P* rate elicited by the green LED in M-cones (Breuninger et al., 2011; Chang et al., 2013). A background illumination (I_{BKG}) of approximatively 10^4 P^*s^{-1}/cone was always present due to the scanning two-photon excitation laser (Baden et al., 2013; Wei et al., 2012). Five stimuli protocols were used (**Table 2**). In all cases, except the binary noise stimulus, the minimal light intensity (I_{MIN}) was set to $0.5 \cdot 10^3$ P^*s^{-1}/cone whereas the maximal light intensity was set to $6.5 \cdot 10^3$ (I_{MAX}) P^*s^{-1}/cone. For the binary noise stimulus, a different light stimulator was used (for details, see Franke et al., 2017) and the following light intensities were applied: $I_{MIN}=0.6 \cdot 10^3$ P^*s^{-1}/cone and $I_{MAX}=19 \cdot 10^3$ P^*s^{-1}/cone. In case of the contrast and colour flash protocol, the intensity between

flashes was set to $3 \cdot 10^3$ P*s^{-1}/cone. All stimuli protocols were preceded by a 15-s period of photoreceptor adaptation to the background (I_{MIN} + I_{BKG}). Note that throughout the manuscript, "white" is used to refer to the simultaneous stimulation with both LEDs at the same P* rate.

Protocol	Description	Function
white flash	1-s bright white flashes at 0.2 Hz 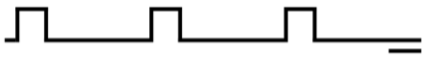	assess drug effects on light-evoked Ca^{2+} responses
colour flash ("GUW")	bright green, UV and white 1-s flashes ("GUW") at 0.2 Hz (x10) 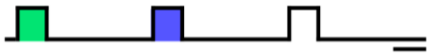	determine Spectral Contrast (*SC*)
contrast and colour flash	1-s bright and dark flashes, with the respective LED combinations (green, UV, and white) at 0.2 Hz (x8) 	determine *SC* and Dark-Light index (*DLi*)
"coloured noise" stimulus	25-Hz pseudo-random sequence of green, UV, white, and dark flashes 	probe correlation between neighbouring cones and HC processes and calculate time kernels
binary noise stimulus	60-Hz pseudo-random sequence of dark and bright flashes 	calculate time kernels

Table 2. Light stimulus protocols
Protocols with schematic representations and functions. GUW, green, UV and white flashes. Scale bars, 1s.

Immunohistochemistry

After two-photon Ca^{2+} imaging of retinal slices from $Cx57^{+/cre}$ x Ai38 mice, a subset of slices was used for immunostaining purposes. First, slices were fixed with 4% paraformaldehyde (PFA) in 0.1 M phosphate-buffered saline (PBS) at 4°C for 15 min. Slices were then washed in 0.1 M PBS, and kept in blocking solution (0.1 M PBS, 0.3% Triton X-100, 10% donkey serum) over night at 4°C. Afterwards, slices were incubated for 4 days at 4°C with primary antibodies (rabbit anti-M-opsin (1:1,000) from EMD Millipore, Billerica MA, USA; goat anti-S-opsin (1:500) from Santa Cruz Biotechnology, Germany) in 0.1 M PBS, 0.3 Triton X-100, and 5% donkey serum. The following day, slices were washed in 0.1 M PBS and incubated with the secondary antibodies (donkey anti-rabbit conjugated to Alexa-Fluor 568 (1:1000) and donkey anti-goat conjugated to Alexa-Fluor 660 (1:1000), both Invitrogen, Carlsbad, CA, USA). A confocal laser-scanning microscope (Leica TCS SP8, Germany) equipped with green (552 nm) and far-red (638 nm) lasers and a x10 0.3 NA objective lens (Leica) was used to acquire image stacks (15 frames of 1024 x 1024 pixels, 15 µm Z-steps). Maximum-intensity projections of the image stacks were performed using Fiji (http://fiji.sc/Fiji).

Pharmacology and drug application

All drugs were prepared as stock solutions in distilled water or, in the case of thapsigargin, in dimethyl sulfoxide (DMSO, 0.1% in the extracellular medium), and were stored at -20°C. Before each experiment, drugs were freshly diluted from stock solution in carboxygenated extracellular solution. For bath application, the tissue was perfused with the drug added to the bathing solution (perfusion rate of ~1.5 ml/min) for 5 min (except for thapsigargin with 20 min). For puff application, a glass electrode (tip diameter: 1-2 µm) was placed ~100 µm above the recorded region of the slice and drug solution was puffed for 10 s using a pressure application system (~0.2-1 bar, Sigmann Elektronik GmbH, Germany). The lateral spread of the puff was about 200 µm in diameter, as measured by puffing SR101 (**Table 3**).

Drug	[µM]	Application	Effect
6,7-dinitroquinoxaline-2,3-dione (NBQX)	200	puff	AMPA/KA-type glutamate receptor antagonist
	100	bath	
cyclothiazide (CTZ)	200	puff	positive allosteric modulator of ionotropic glutamate receptors
AMPA	50	puff	AMPA and KA receptor agonist
KA	25	puff	AMPA and KA receptor agonist
muscimol (musc)	100	puff	$GABA_A$ receptor agonist
SR-95531 hydrobromide (gabazine, gbz)	100	puff	$GABA_A$ receptor antagonist
verapamil (vera)	100	bath	L-type VGCC blocker
thapsigargin (thap)	5	bath	sarco-endoplasmic reticulum Ca^{2+}-ATPase (SERCA) blocker

Table 3. Drugs, applications and targets
Drugs with their respective concentrations (µM), applications and targets. All drugs were purchased from Tocris Bioscience (Bristol, England) except for KA and CTZ, which were purchased from Sigma-Aldrich.

Data analysis

For all light-evoked imaging experiments and electrophysiological recordings, I analysed the data with custom-written scripts in IgorPro (Wavemetrics) and semi-automated routines for functional image analysis (SARFIA, Dorostkar et al., 2010), a freely available package for IgorPro. For Ca^{2+} imaging (GCaMP3 and TN-XL fluorescence), regions-of-interest (ROIs) were semi-automatically detected using SARFIA: Image series were filtered and averaged. Then Laplace operator (threshold of 0.4) was used to assign ROIs. The resulting ROI mask was manually corrected in case two nearby structures shared one ROI. ROIs with an area < 10 pixels were discarded. Note that for TN-XL, the ratio between acceptor (citrine) and donor fluorescence (eCFP) was calculated on the image series, prior to signal extraction.

For glutamate imaging (iGluSnFR fluorescence), the correlation over time between neighbouring pixels was measured and ROIs were determined based on a correlation threshold

defined for each recording in function of the signal to noise ratio. ROI diameters were limited to range between 5 to 8 µm (expected diameter of a cone axon terminal).

For all recording, Ca^{2+} or glutamate traces were extracted for each ROI, de-trended by high-pass filtering at ~0.1 Hz (except for the analysis of drug effects on the baseline) and z-normalized (ratio between de-trended trace subtracted from its average and standard deviation (s.d.) noise). For all flash stimuli, I determined response amplitude (ΔF) and area-under-the-curve (F_{Area}). Ca^{2+} baseline level (F_0) was determined for NBQX, CTZ, muscimol and gabazine puff experiment as well as for the contrast and colour flash protocols. These parameters were calculated on the trace smoothed using IgorPro's boxcar algorithm with 2 passes for all stimuli (except drug experiments with 5 passes due to fewer stimulus repeats). Moreover, for all HC recordings (GCaMP3 fluorescence), I also determine the distance of each ROI to the cone axon terminal base. To this end, I used SR101 fluorescence to localize cone axon terminals in each field, I then manually drew a straight line at their bases and measure the distance of each HC ROI to the cone axon terminal base (d_{base}).

For light-evoked Ca^{2+} imaging, two quality criteria were defined to identify responsive ROIs and only ROIs passing both criteria were used for further analysis:

(1) The quality index (Qi) is defined as the ratio between ΔF in response to a white flash and the s.d. of the noise of the trace (measured on the raw trace subtracted from the smoothed trace using boxcar algorithm with 2 passes). Note that for the contrast and colour flash protocol, Qi was calculated for both dark and bright flashes independently. Depending on stimulus and experiment type, I used different Qi thresholds ($Qi \geq 1$ for all flash protocols except contrast and colour flashes protocol, where I used $Qi \geq 1.5$; drug experiments: $Qi \geq 1.3$ for CTZ puffs, $Qi \geq 3$ for AMPA/KA puffs).

(2) The consistency index (Ci) is defined as the ratio between the variance of the mean and the mean of the variance across n=8 to 10 stimulus trials depending on stimulus. ROIs with $Ci \geq 0.2$ were considered to show consistent light responses over time.

Depending on the stimulus protocol, I determined additional parameters for each ROI: I calculated the spectral contrast preference, $SC = \left(F_{Area(G)} - F_{Area(UV)}\right)/\left(F_{Area(G)} + F_{Area(UV)}\right)$, using the F_{Area} for the responses to green (G) and UV flashes (for colour flash and colour and contrast flash protocols). The dark-light index, $DLi = \left(F_{Area(B)} - F_{Area(D)}\right)/\left(F_{Area(B)} + F_{Area(D)}\right)$ (Baden et al., 2013), was determined using the F_{Area} for the responses to bright (B) and dark (D) white flashes (colour and contrast flash protocol).

To analyse the two noise protocols, I determined the time kernel for each ROI by calculating the negative-transient-triggered average which was weighted by the transients' amplitudes. ROIs were considered responsive if the maximum amplitude of the kernel (A_{LRF}) for green and/or UV was $A_{LRF} > 2$ s.d. of the noise for the coloured noise stimulus and if $A_{LRF} > 3$ s.d. noise for the binary noise. All kernels were then normalized to 1.

I determined additional parameters in function of noise stimuli:

(1) For the coloured noise stimulus, I calculated the correlation between ROIs present in the same field either for the full Ca^{2+} traces or for negative events (with amplitudes < -2 s.d. of the noise) in a time window of -750 to 250 ms around the event (with negative event at 0 ms). The mean of the correlation for each field was then used for further analysis.
(2) For the binary noise stimulus, periodograms of time kernels were generated using a discrete Fourier transform without zero padding. The power spectral densities at each frequency component followed approximately a log-normal distribution, and so to improve Gaussianity (assumed in the subsequent t-tests), a log transform was applied to each periodogram, and the transformed data was used for statistical comparisons.

Statistics

All statistical tests (except for the ones for the periodograms) were performed using the Wilcoxon signed-rank test or the Wilcoxon rank-sum test. Alpha was set to 0.05 and p-values (*p*)

< 0.05 were considered as significant (*), $p < 0.01$ (**), $p < 0.001$ (***). For multiple comparisons, Bonferroni correction was used and $p < 0.025$ was considered as significant (+), $p < 0.005$ (++), $p < 0.0005$ (+++). Spearman rank correlation test was used to estimate the correlation between negative events and distance along the slice (*cf.* **Figure 21**) as well as the relationships between *DLi*, *SC*, slice position and F_0 (*cf.* **Figure 22**). Differences between dorsal and ventral *DLi* were assessed with t-test and Bartlett test (*cf.* **Figure 22**). For periodograms, a dependent sample t-test was computed for each positive frequency component and Bonferroni correction was used (15 comparisons, *cf.* **Figure 23**). Errors are given as standard error of the mean (SEM), median absolute deviation (MAD) or standard deviation (s.d.).

Results

Identification of cone axon terminals and horizontal cell processes in the mouse retinal slice

To study signal processing in HCs, I used the $Cx57^{+/cre}$ x Ai38 mouse line in which the genetically encoded Ca^{2+} indicator GCAMP3 is selectively expressed in HCs under the control of the promoter Cx57. This mouse line results in the deletion of one Cx57 allele which plays an important role in gap junction-coupling between HCs (Hombach et al., 2004). Despite reduced receptive field size, HC coupling and feedback were still functional and the connection between photoreceptors and HCs was not affected (Shelley et al., 2006). Therefore, I do not expect this genetic modification to affect the conclusions (see also discussion).

I recorded GCaMP3 fluorescent signals from HCs in the OPL in retinal slices (**Figure 12A**). Simultaneously to GCaMP3 recording, I used SR101 fluorescence to identify the cone axon terminals (Euler et al., 2009). SR101 is a dye which labels active photoreceptor axon terminals due to its uptake during vesicle endocytosis (Miller et al., 2001). To confirm that SR101 labels cone axon terminals, I performed a control experiment using the HR2.1:TN-XL mouse line (Wei et al., 2012), in which cones exclusively express the Ca^{2+} biosensor TN-XL and I compared SR101 and TN-XL fluorescence (**Figure 12B**). I found that SR101 can reliably locate cone axon terminals. Therefore, I routinely bath-applied SR101 and for each recording I manually drew a line at the cone axon terminal base to estimate the distance of each ROI to this line (d_{base}) for each HC ROI.

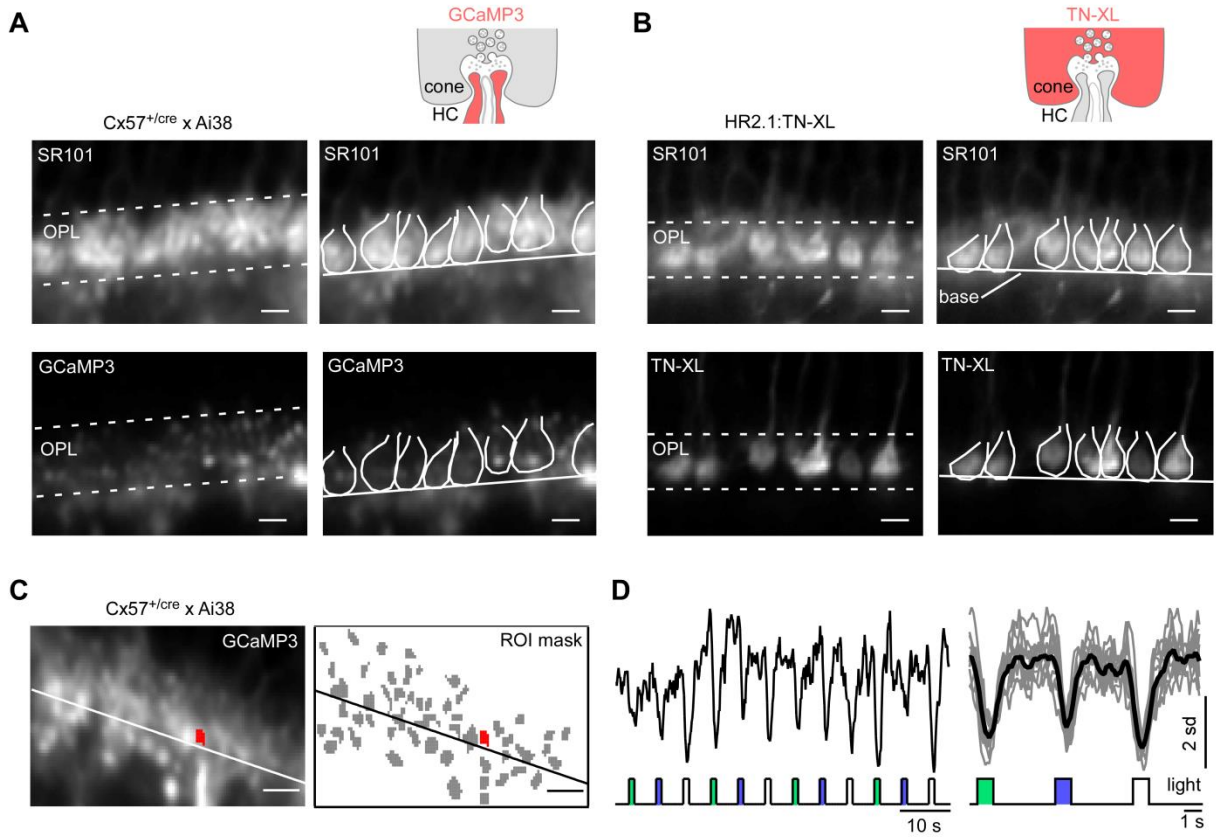

Figure 12. Identification of cone axon terminals and horizontal cell processes in mouse retinal slices

A,B. Bath application of sulforhodamine 101 (SR101) (top images in A,B) to identify cone axon terminals in retinal slices of the $Cx57^{+/cre}$ x Ai38 (A) and HR2.1:TN-XL mouse lines (B). Outlines of cone axon terminals were manually drawn for illustration purposes; solid lines indicate cone axon terminal base; dotted lines indicate outer plexiform layer (OPL) borders. Upper right diagram depicts imaged synaptic compartment and biosensor used (red). **C.** *left*: GCaMP3-labeled HC processes, with line marking cone axon terminal base (analogous to A and B). *Right*: Regions-of-interest (ROIs, grey; exemplary ROI marked red) on HC processes were automatically determined (Methods). **D.** Ca^{2+} responses to green, UV and "white" (GUW) 1-s light flashes of exemplary ROI (in C); continuous Ca^{2+} trace (left) and average of n=10 trials for each stimulus condition (right) are shown (Ca^{2+} signals de-trended by high-pass filtering at ~0.1 Hz and z-normalized, Methods). Scale bars, 5 µm.

Light-evoked Ca^{2+} signals in horizontal cell processes

I applied green, UV or "white" flashes ("GUW" protocol, **Table 2**) to record light-evoked Ca^{2+} signals in HC dendrites. Regions-of-interest (ROIs) were anatomically defined (based on GCaMP3 fluorescence) and Ca^{2+} signals were extracted (**Figure 12C,D**). To select ROIs responding to the light protocol, I determined two quality criteria based on "white" Ca^{2+} response: a quality index (*Qi*; **Figure 13A**) and a consistency index (*Ci*; **Figure 13B**) (Methods). From a total of 9,912 ROIs, 423 (4.3%) were selected for further analysis with reliable light-evoked Ca^{2+} response (**Figure 13C**). HC dendritic tips are invaginated in cone axon terminals and HC axon terminals contact rods well above cone terminals whereas ROIs below their bases correspond to HC primary dendrites (Haverkamp et al., 2000). Therefore, I used HC d_{base} to get an estimation of each ROI identity (**Figure 13D-F**). I found that ROIs located close to the cone axon terminal base show larger *Qi* and larger F_{Area}: 61.5% of responsive ROIs were localized within $0 < d_{base} < 5$ µm of the OPL band occupied by cone axon terminals. However, the analysis of ROI area in function of d_{base} did not reveal any significant difference ($d_{base} > 0$; 2.45 ± 0.07 μm^2, n=292 and below $d_{base} < 0$; 2.87 ± 0.30 μm^2, n=131; p=0.248). Together, my data show that I can record light-evoked Ca^{2+} signals in HC dendritic tips in the cone synapse.

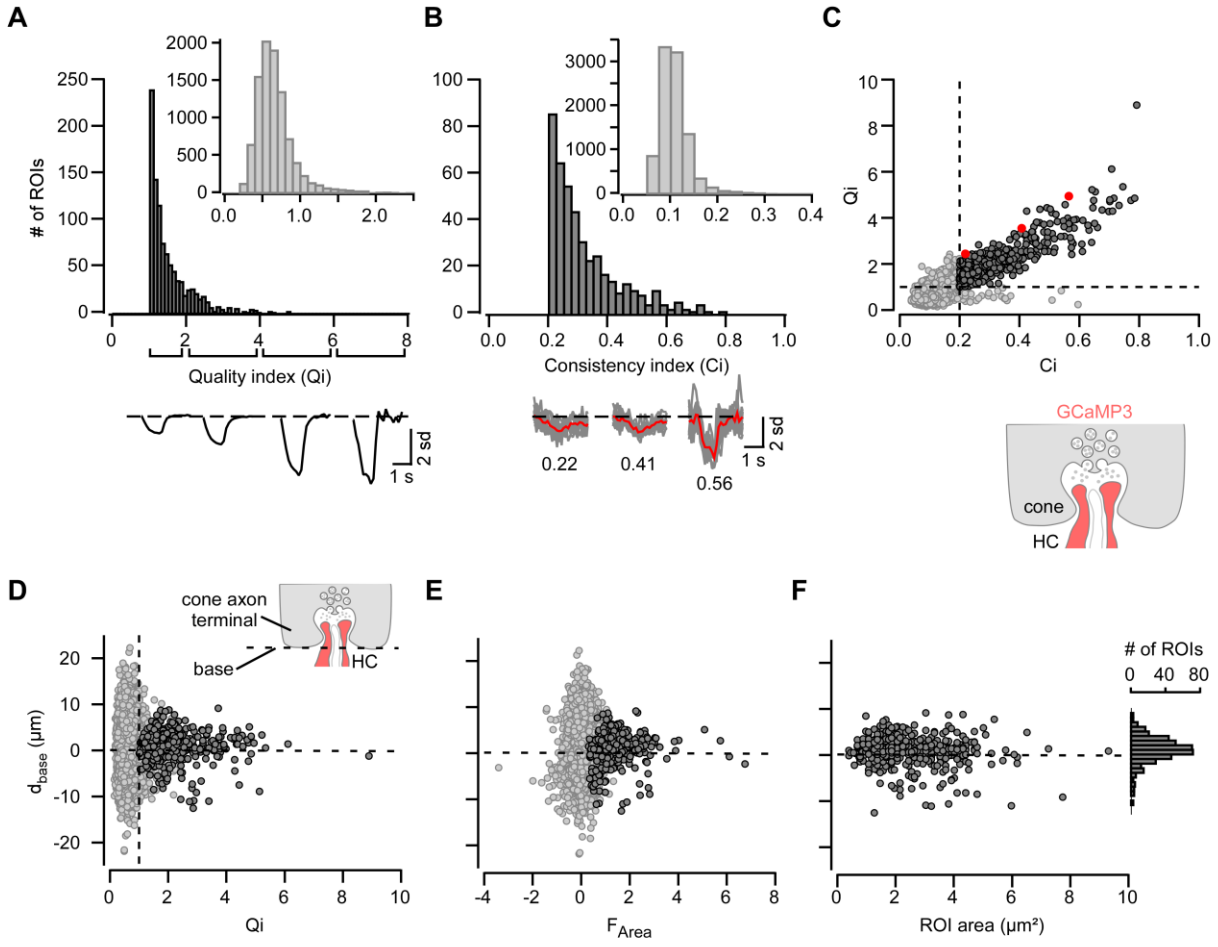

Figure 13. Selection of ROIs on horizontal cell processes based on their light-evoked Ca^{2+} signals

A. Distribution of quality index (*Qi*), defined as ratio between Ca^{2+} response amplitude to white flash and s.d. of noise (Methods). Only ROIs with $Qi \geq 1$ (dark grey) were considered for further analysis (inset shows distribution of discarded ROIs). *Below*: Average Ca^{2+} responses across ROIs for different *Qi* intervals. **B.** Distribution of consistency index (*Ci*), defined as ratio between variance of the mean and mean of variance (Methods). Only ROIs with $Ci \geq 0.2$ (dark grey) were considered for further analysis (inset shows distribution of discarded ROIs). *Below*: Exemplary Ca^{2+} traces for different *Ci* values (mean in red, n=10 trials in grey). **C.** *Qi* as a function of *Ci*, with ROIs passing both criteria shown as dark-grey dots (n=423 of 9,912 ROIs passed both criteria). Red dots indicate ROIs of example traces in B. **D,F.** Distance of ROI (centre of mass) to cone axon terminal base (d_{base}) as a function of *Qi* (D, the dashed line indicates the cone base), area-under-the-curve (F_{Area}, E) and ROI area (F). Histogram shows distribution of ROIs along the cone terminal base. Diagram on the right depicts imaged synaptic compartment and used biosensor (red).

Light-evoked Ca^{2+} responses in horizontal cells are mediated by AMPA/kainate-type glutamate receptors

Cones release glutamate that binds to postsynaptic AMPA and KA-type glutamate HC receptors leading to an increase in the intracellular Ca^{2+} concentration (Schubert et al., 2006). To confirm that light-evoked Ca^{2+} responses I measured in HC dendrites were mediated by cone glutamate release, I combined light flashes together with a pharmacology approach: I puff-applied the AMPA/KA-type glutamate receptor antagonist NBQX (200 µM) while presenting "white" flashes (**Figure 14A,B** and **Table 2**). NBQX significantly decreased the Ca^{2+} baseline level (F_0) in HC processes (by -1.47 ± 0.07 s.d., mean ± SEM, $p=2.384 \cdot 10^{-7}$; n=23 ROIs from 4 slices, 2 mice) and greatly reduced response amplitude (ΔF; control, 1.24 ± 0.16; NBQX, 0.16 ± 0.03; $p=2.384 \cdot 10^{-7}$) and F_{Area} (F_{Area}; control, 1.02 ± 0.17; NBQX, -0.01 ± 0.04; $p=4.768 \cdot 10^{-7}$, **Figure 14C-E** and **Table 4**). Washing out the drug partially restored these light responses (**Table 4**).

I also puff-applied cyclothiazide (CTZ, 200 µM) (Cadetti et al., 2005; Huang et al., 2004), a positive allosteric modulator of ionotropic glutamate receptors while presenting "white" flashes (**Figure 14F,G** and **Table 4**). I found a small but non-significant increase in response amplitude (ΔF; control, 0.92 ± 0.18; CTZ, 1.21 ± 0.23; p=0.031) and F_{Area} (F_{Area}; control, 0.82 ± 0.14; CTZ, 1.11 ± 0.22; p=0.047) but no effect on Ca^{2+} baseline (**Figure 14H-J** and **Table 4**). Taken together, my data indicate that light-evoked Ca^{2+} signals recorded in HC processes result from the activation of AMPA/KA receptors (Feigenspan and Babai, 2015; Schubert et al., 2006; Ströh et al., 2013).

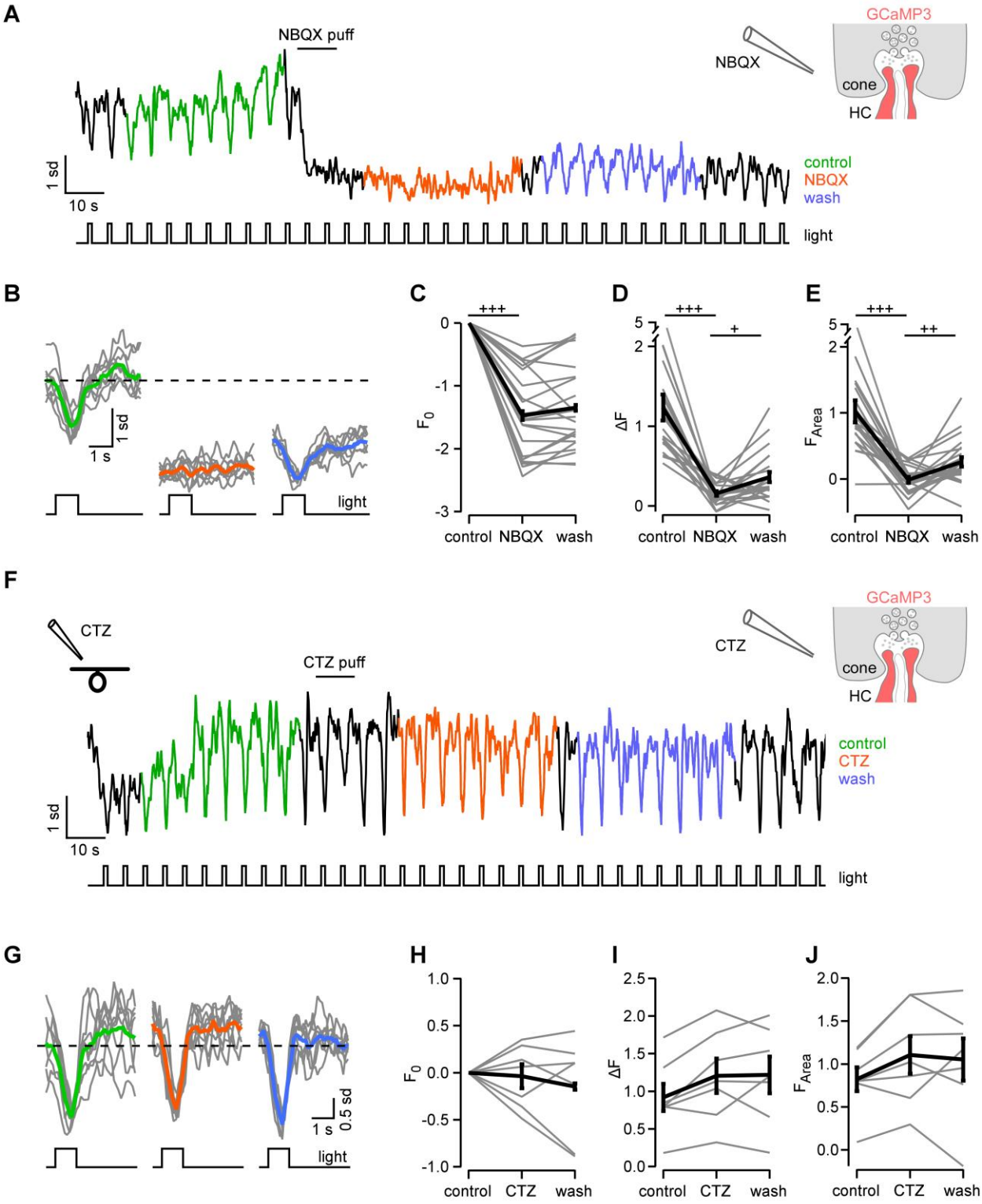
A
NBQX puff
NBQX
GCaMP3
cone
HC
1 sd
10 s
control
NBQX
wash
light
B
1 sd
1 s
light
C
+++
F0
control NBQX wash
D
+++
+
ΔF
control NBQX wash
E
+++
++
FArea
control NBQX wash
F
CTZ
CTZ puff
CTZ
GCaMP3
cone
HC
control
CTZ
wash
1 sd
10 s
light
G
1 s
0.5 sd
light
H
F0
control CTZ wash
I
ΔF
control CTZ wash
J
FArea
control CTZ wash

Figure 14. Light-evoked Ca^{2+} responses in horizontal cell processes are mediated by activation of AMPA/kainate-type glutamate receptors

A. Exemplary Ca^{2+} response of a HC process to white flashes before (control), after a puff of NBQX and during wash-out. **B.** Averaged responses for control (green), NBQX (orange) and wash (blue) (individual trials in grey). **C-E.** Quantification of NBQX effects on response baseline, (F_0, C), amplitude (ΔF, D), and area-under-the-curve (F_{Area}, E) (average of n=23 ROIs from 4 slices, 2 mice). **F.** Experiment as in (A) but for the cyclothiazide (CTZ). **G.** Averaged responses for control, CTZ and wash-out. **H-J.** Quantification of CTZ effects as in (C-E) (average of n=7 ROIs, 3 slices, 2 mice). Error bars indicate SEM. +, p≤0.025; ++, p≤0.005; +++, p≤0.0005 (Bonferroni corrected significance threshold).

	Number of mice/slices/ROIs	Control	Drug	Wash
NBQX puff application				
F_0 [s.d.]	2/4/23	0	-1.470 ± 0.069 ($p=2.384\cdot10^{-7}$ +++)	-1.348 ± 0.046 (p=0.033)
ΔF [s.d.]		1.235 ± 0.163	0.156 ± 0.029 ($p=2.384\cdot10^{-7}$ +++)	0.362 ± 0.064 (p=0.007 +)
F_{Area} [a.u.]		1.024 ± 0.167	-0.012 ± 0.044 ($p=4.768\cdot10^{-7}$ +++)	0.257 ± 0.071 (p=0.003 ++)
CTZ puff application				
F_0	2/3/7	0	-0.037 ± 0.128 (p=0.813)	-0.148 ± 0.034 (p=0.469)
ΔF		0.917 ± 0.182	1.206 ± 0.229 (p=0.031)	1.219 ± 0.243 (p=0.938)
F_{Area}		0.822 ± 0.139	1.105 ± 0.219 (p=0.047)	1.053 ± 0.247 (p=0.938)

Table 4. Pharmacology for AMPA/kainate-type glutamate receptors

NBQX, AMPA/KA-type glutamate receptor blocker; CTZ, positive allosteric modulator of ionotropic glutamate receptors; Ca^{2+} baseline (F_0), amplitude (ΔF) and area-under-the-curve (F_{Area}) of light-evoked Ca^{2+} responses, a.u., arbitrary unit.

$GABA_A$ receptor activation modulates the intracellular Ca^{2+} level in horizontal cell processes

Horizontal cell are GABAergic interneurons. In mouse, they also express $GABA_A$ receptors (see Introduction for details) but cones do not express GABA receptors. Therefore GABA release from HCs can binds to auto-receptors and modulate cone responses indirectly (Kemmler et al., 2014; Liu et al., 2013; Vroman et al., 2014).

I tested how light-evoked Ca^{2+} signals in HCs were modulated by GABA by puff-applying the $GABA_A$ receptor agonist muscimol (musc, 100 µM) while presenting "white" flashes (**Figure 15A,B** and **Table 2**). I found a small and significant increase in F_0 (by 0.32 ± 0.13 s.d., p=0.011 for muscimol vs. control; n=20 ROIs from 4 slices, 2 mice; **Figure 15C** and **Table 5**) which was reversed during wash-out (0.03 ± 0.15 s.d., p=0.007 for muscimol vs. wash-out). However the size of the light responses was not affected (**Figure 15D,E** and **Table 5**). I also puff-applied the $GABA_A$ receptor antagonist SR95531 (gabazine or gbz, 100 µM) but I did not find any significant effects (n=33 ROIs from 4 slices, 2 mice; **Figure 14F-J** and **Table 5**).

Horizontal cells express NKCC co-transporters on their dendritic tips (Li et al., 2008; Vardi et al., 2000) which is consistent with the increase in Ca^{2+} baseline I observed: Due to the high intracellular Cl^- levels in HC dendritic tips, $GABA_A$ receptor activation caused a Cl^- efflux leading to VGGC activation and Ca^{2+} inflow. The fact that $GABA_A$ receptor antagonist had no effect on HC responses was also consistent with a previous study performed under similar conditions (Kemmler et al., 2014). One plausible explanation is that due to the perfusion of carboxygenated extracellular solution and the slice preparation, endogenous GABA might be wash out in my experimental condition (see discussion in Kemmler et al., 2014).

Taken together, my data show that GABA auto-reception plays a role in modulating the activity in distal HC processes and may indirectly shape cone output (see introduction and Endeman et al., 2012; Hirano et al., 2016; Liu et al., 2013).

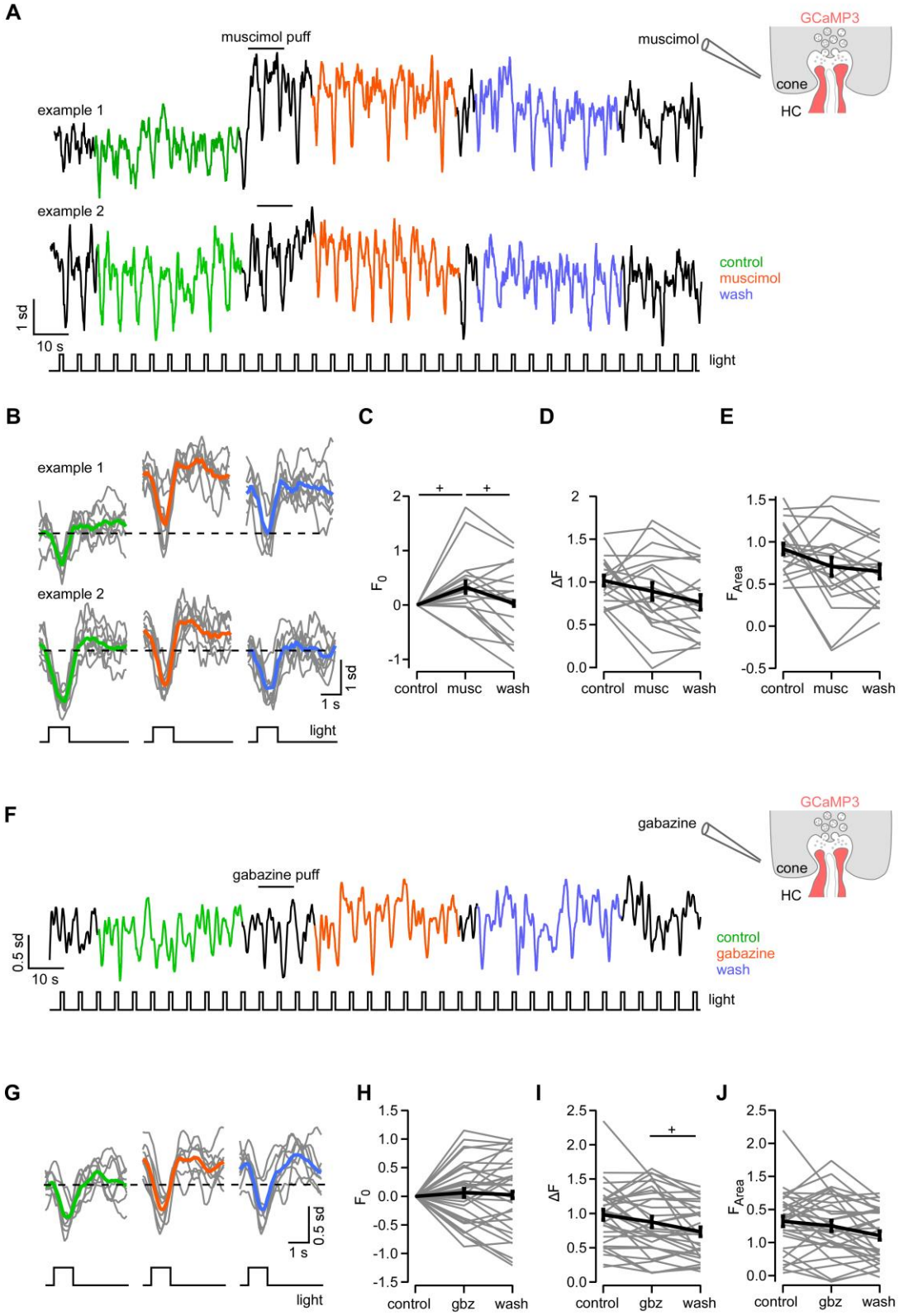
A
muscimol puff
muscimol
GCaMP3
cone
HC
example 1
example 2
control
muscimol
wash
1 sd
10 s
light
B
example 1
example 2
1 sd
1 s
light
C
D
E
control
musc
wash
F
gabazine
GCaMP3
cone
HC
gabazine puff
0.5 sd
10 s
control
gabazine
wash
light
G
0.5 sd
1 s
light
H
I
J
control
gbz
wash

Figure 15. GABA modulates light-evoked Ca^{2+} signals in horizontal cell dendrites
A. Two exemplary Ca^{2+} responses of HC processes to white flashes before (control), after a puff of the $GABA_A$ receptor agonist muscimol (musc) and during wash-out to illustrate the variability of the response to the musc puff. **B.** Averaged responses for control (green), musc (orange) and wash-out (blue) for the two exemplary traces in A. **C-E.** Quantification of musc effects on response baseline (F_0, C), amplitude (ΔF, D) and area-under-the-curve (F_{Area}, E) (average of n=20 ROIs from 4 slices, 2 mice). **F.** Experiment as in (A) but for the $GABA_A$ receptor antagonist gabazine (gbz). **G.** Averaged responses for control, gbz and wash-out. **H-J.** Quantification of gbz effects as in (C-E) (average of n=33 ROIs, 4 slices, 2 mice). Error bars indicate SEM. +, p≤0.025 (Bonferroni corrected significance threshold).

	Number of mice/slices/ROIs	Control	Drug	Wash
Muscimol puff application				
F_0 [s.d.]	2/4/20	0	0.323 ± 0.126 (p=0.011 +)	0.029 ± 0.149 (p=0.007 +)
ΔF [s.d.]		1.0166 ± 0.061	0.891 ± 0.102 (p=0.330)	0.762 ± 0.087 (p=0.040)
F_{Area} [a.u.]		0.915 ± 0.067	0.707 ± 0.110 (p=0.154)	0.649 ± 0.086 (p=0.452)
Gabazine puff application				
F_0	2/4/33	0	0.062 ± 0.076 (p=0.525)	0.024 ± 0.060 (0.437)
ΔF		0.981 ± 0.0762	0.874 ± 0.082 (0.126)	0.733 ± 0.067 (p=0.009 +)
F_{Area}		0.822 ± 0.079	0.751 ± 0.081 (p=0.296)	0.606 ± 0.068 (p=0.027)

Table 5. Pharmacology for $GABA_A$ auto-receptors on horizontal cell dendrites.
Muscimol, $GABA_A$ receptor agonist; gabazine, $GABA_A$ receptor antagonist; Ca^{2+} baseline (F_0), amplitude (ΔF) and area-under-the-curve (F_{Area}) of light-evoked Ca^{2+} responses, a.u., arbitrary unit.

Ca^{2+} signals in horizontal cell processes are mediated by voltage gated Ca^{2+} channels and intracellular Ca^{2+} stores

To dissect the cellular basis of Ca^{2+} signalling in HC dendrites, I performed pharmacology experiments and assess if Ca^{2+} permeable AMPA and KA receptors, VGCCs and Ca^{2+} release from intracellular stores play a role (Schubert et al., 2006). First, I puff-applied a mixture of

AMPA (50 µM) and KA (25 µM) on HC dendrites. As I found a decrease over time of the Ca^{2+} responses to AMPA/KA puffs (possibly due to downregulation of VGCCs or strong depletion of the Ca^{2+} stores), I estimated this run-down by calculating the ratio of the response amplitudes ($\Delta F_2/\Delta F_1$) for two consecutive puffs at two intervals (5 and 20 mins, **Figure 16A,D** and **Table 6**. Secondly I used the same approach in the presence of the bath-applied VGCC blocker, verapamil (vera, 5 mins, 100 µM). I found a significantly smaller response ratio compared to control (**Figure 16B,C** and **Table 6**, control, 5 mins: $\Delta F_2/\Delta F_1$=0.44 ± 0.14; verapamil, 5 mins: $\Delta F_2/\Delta F_1$=0.13 ± 0.15; n=18 ROIs from 3 slices, 2 mice, $p=9.088\cdot10^{-5}$), confirming that VGCCs contributed to the signals. Thirdly I bath-applied the SERCA inhibitor thapsigargin (thap, 20 mins, 5 µM), which blocks Ca^{2+} store refill and leads to depletion of intracellular Ca^{2+} stores (Lv et al., 2014). I found a decrease of the amplitude ratio (**Figure 16D-F** and **Table 6** (control, 20 min: $\Delta F_2/\Delta F_1$=0.86 ± 0.28, n=28 ROIs from 3 slices, 2 mice; thapsigargin, 20 min: $\Delta F_2/\Delta F_1$=0.50 ± 0.14, n=14 ROIs from 4 slices, 2 mice, $p=9.163\cdot10^{-4}$). Taken together, my data support that Ca^{2+} signals in HC processes results from the combination of permeable AMPA and KA receptors, VGCCs and Ca^{2+} release for intracellular stores. My data were consistent with earlier experiments on isolated mouse HCs (Schubert et al., 2006).

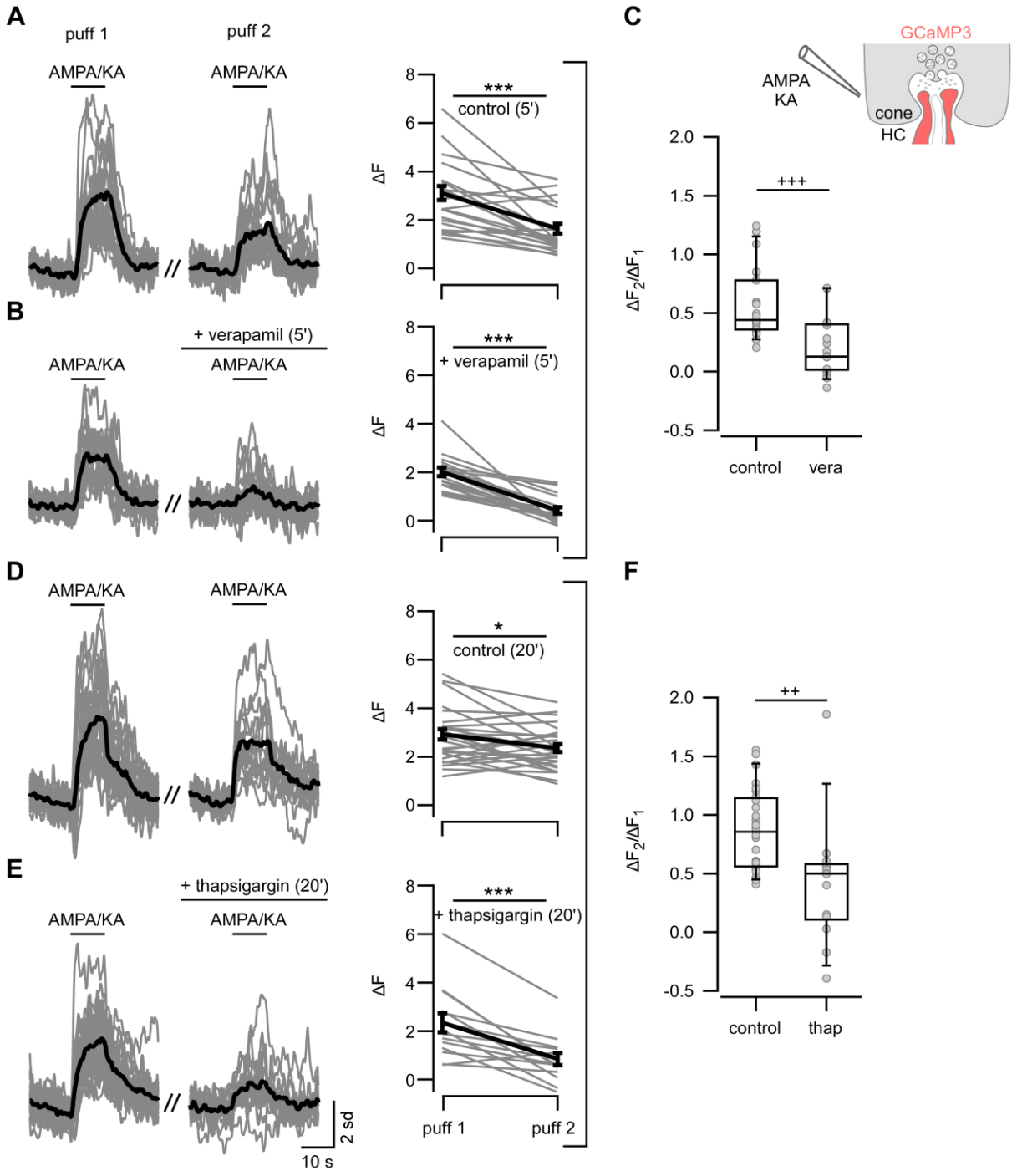

Figure 16. Ca^{2+} signals in horizontal cell processes are mediated by Ca^{2+} permeable AMPA and kainate receptors, voltage gated Ca^{2+} channels and intracellular Ca^{2+} stores

A-C. Ca^{2+} signals in HC processes evoked by two consecutive AMPA/KA puffs with 5 min interval (short bars indicate puff timing). **D-F.** 20 min interval between the two consecutive AMPA/KA puffs. *Left row*: in standard bathing medium; *middle row*: normal medium for 5 min (A, n=23 ROIs from 2 slices, 2 mice), during bath application of verapamil for 5 min (B, n=18, 3 slices, 2

mice), normal medium for 20 min (C, n=28, 3 slices, 2 mice) and during bath application of thapsigargin for 20 min. *Right row*: Quantification of drug effects on response amplitude ΔF (error bars indicate SEM; *, $p \leq 0.05$; ***, $p \leq 0.001$). **C,F.** Ratios between ΔF_2 (2nd puff) and ΔF_1 (1st puff) for control, verapamil (vera) and thapsigargin (thap) (++, $p \leq 0.005$; +++, $p \leq 0.0005$) (Bonferroni corrected significance threshold).

	Number of mice/slices /ROIs	**AMPA/KA puff 1 ΔF_1 [s.d.]**	**AMPA/KA puff 2 ΔF_2 [s.d.] (ΔF_2 vs. ΔF_1)**	**$\Delta F_2/\Delta F_1$ median [MAD] (vs. control)**
Control (5')	2/2/23	3.106 ± 0.286	1.648 ± 0.198 ($p=1.025\cdot10^{-5}$ ***)	0.439 ± 0.137
Verapamil (5')	2/3/18	2.011 ± 0.177	0.426 ± 0.130 ($p=7.629\cdot10^{-6}$ ***)	0.127 ± 0.145 ($p=9.088\cdot10^{-5}$ +++)
Control (20')	2/3/28	2.842 ± 0.209	2.293 ± 0.167 (p=0.014 *)	0.855 ± 0.284
Thapsigargin (20')	2/4/14	2.297 ± 0.387	0.814 ± 0.256 ($p=3.662\cdot10^{-4}$ ***)	0.499 ± 0.140 ($p=9.163\cdot10^{-4}$ ++)

Table 6. Pharmacology to block voltage gated Ca^{2+} channels and Ca^{2+} release from intracellular stores

Verapamil, L-type VGCC blocker; thapsigargin, inhibitor of sarco-endoplasmic reticulum Ca^{2+}-ATPases; amplitude puff 1 (ΔF_1); amplitude puff 2 (ΔF_2); ratio puff 2/puff 1 ($\Delta F_2/\Delta F_1$); MAD, median absolute deviation.

Light-evoked Ca^{2+} signals in horizontal cells reflect the dorso-ventral opsin expression gradient

Next, to confirm that I recorded from HC dendrites that directly receive cone inputs (and not rods) I applied the GUW stimulus protocol (**Table 2**) in different retinal regions along the dorso-ventral axis to activate different combination of S- and M- cones. The dorsal mouse retina contains mostly functional M-cones and only 5% "true" S-cones (Baden et al., 2013; Haverkamp et al., 2005), whereas the ventral retina is dominated by "functional S-cones" (ontogenetic M-cones that are mainly UV-sensitive due to massive expression of S-opsin, Röhlich et al., 1994; Szél et al., 1992). Therefore, if the spectral preference of the HCs reflects the dorso-ventral

opsin expression gradient, this indicates that cones and not rods dominantly drive the Ca^{2+} responses and therefore that I record from HC dendrites.

For each HC response, I calculated the spectral contrast (*SC*, Methods). I sorted the data for dorsal and ventral retina and found that the dorsal retina was mainly composed of HC dendrites responding to green flashes (**Figure 17A**) whereas UV responses were predominant in the ventral retina (**Figure 17B**), consistent with the cone opsin gradient (Baden et al., 2013).

Moreover, the analysis of d_{base} as a function of $|SC|$ revealed that ROIs localize close to the cone axon terminal base ($-4 \leq d_{base} \leq 4$ µm) have on average higher absolute *SC* ($|SC_{-4...+4}|$=0.72 ± 0.02, n=342) in comparison to ROIs below the base ($d_{base} < -4$ µm, $|SC_{<-4}|$=0.42 ± 0.05, n=28, $p=1.611 \cdot 10^{-5}$; **Figure 17C**). This suggests that HC dendritic tips invaginated in cone axon terminals can locally encode presynaptic input whereas primary dendrites (and soma) receive a mixture of S- and M-cone inputs.

I also analysed *SC* as a function of its slice location (**Figure 17D**) and found that the most dorsal slices (slice 6 and 5) were composed of only green sensitive responses whereas only UV sensitive responses were present in the most ventral slices (slices -5 and -6). Interestingly, in the central slices, where the opsin transitional zone is located, both UV- and green-dominated dendrites co-existed. I used immunohistochemical approach on recorded slices to confirm that the *SC* distribution followed the cone opsin expression along a slice: In the nasal part of the slice, where ROIs were UV-sensitive, S-opsin predominated, whereas in the temporal part of the slice, where green-sensitive ROIs were present, M-opsin predominated (**Figure 17E**). The fact that the *SC* preference in HC dendrites follows the cone opsin distribution along the dorso-ventral axis indicates that light-evoked Ca^{2+} signals in HCs reflect cone input and that I can exclude (direct) rod contributions.

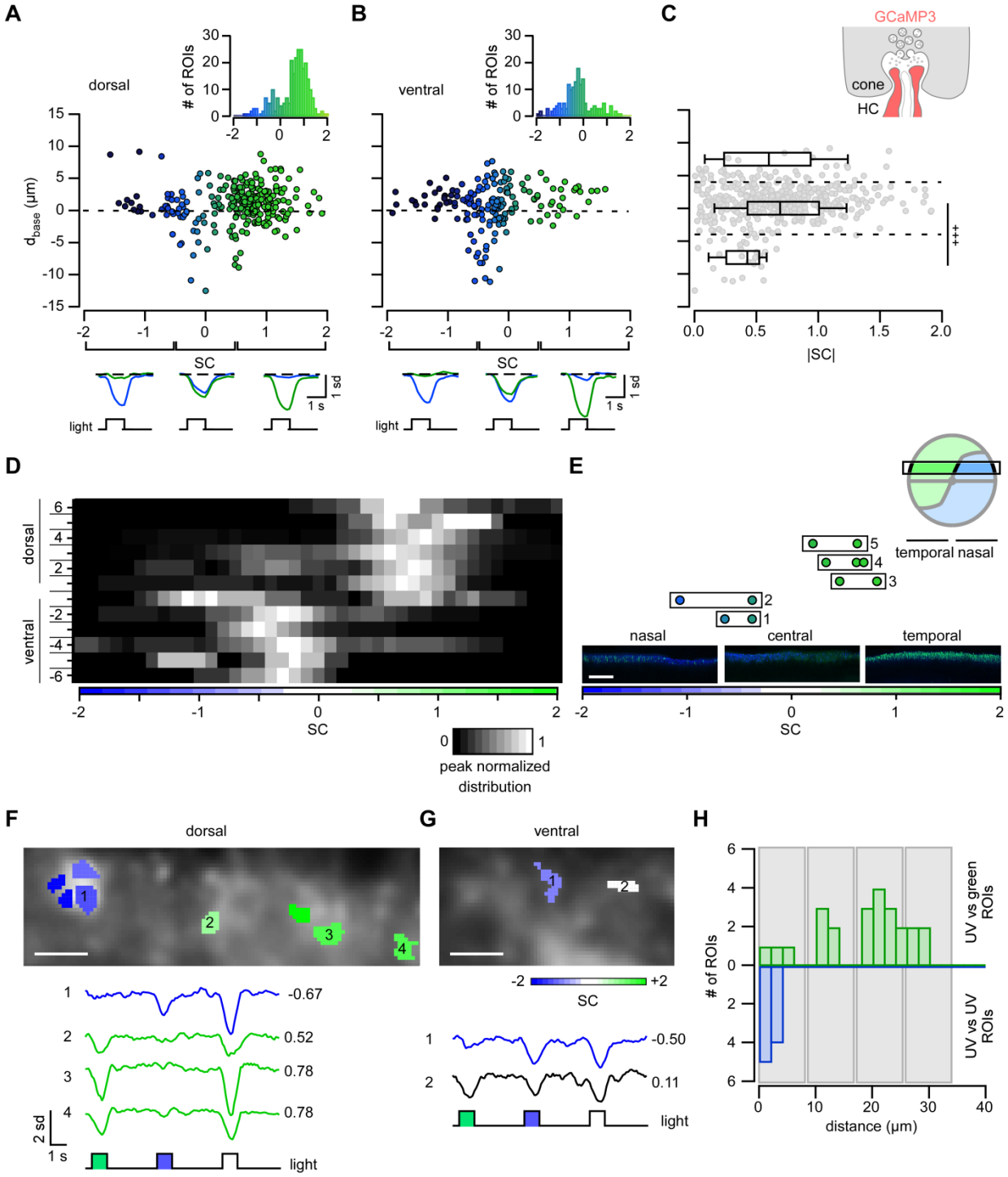

Figure 17. Light-evoked Ca^{2+} signals in horizontal cell dendrites reflect the dorso-ventral cone opsin expression gradient

A,B. Plots showing distance between ROI and cone axon terminal base (d_{base}) as a function of spectral contrast (*SC*, see Methods) for dorsal (n=262 ROIs) (A) and ventral retina (n=161) (B). Insets show respective histograms of *SC* distributions. Below: Averaged Ca^{2+} signals in response

to green and UV light flashes for different *SC* intervals (averages of n=10 trials). **C.** ROI distance to d_{base} as a function of |*SC*| (ROIs from both dorsal and ventral retina). ROIs were separated into three groups (indicated by dashed lines) depending on d_{base}: above ($d_{base} > 4$ µm), below ($d_{base} < -4$ µm), and near the cone axon terminal base ($-4 \leq d_{base} \leq 4$ µm). **D.** *SC* distribution sorted by retinal slice position (from dorsal to ventral; distributions peak normalized for every slice position). **E.** *SC* of ROIs from 5 different locations on the same slice (boxes 1-5) cut along the naso-temporal axis (position +3, see D) and corresponding S- (blue) and M-opsin (green) immunolabeling in the temporal, central and nasal region. **F,G.** Examples of recording fields that contain ROIs with different *SC* for dorsal (F) and ventral (G) retina, with respective Ca^{2+} signals shown below (averages of n=10 trials). Colours reflect *SC* preference of each ROI (see colour bar in G). **H.** Spatial distribution of UV- (top histogram) and green- (bottom histogram) preferring ROIs relative to each UV ROI (at 0 µm) (for ROIs with |*SC*| > 0.3; n=22 ROIs from 7 fields, 4 dorsal and 3 ventral fields). Grey boxes illustrate expected location of neighbouring cone axon terminals. +++, $p \leq 0.0005$ (Bonferroni corrected significance threshold). Scale bars, 200 µm in E; 5 µm in F, G.

Light-evoked Ca^{2+} signals in horizontal cell dendritic tips reflect local activity

Next I assessed if signals from individual cones remain "isolated" within HC distal dendrites or if they spread across the cells' dendritic arbours (or the electrically coupled HC network). I focused my analysis on fields that were composed of ROIs with different *SC* preferences (fields composed of ROIs with *SC* > 0 <u>and</u> ROIs with *SC* < 0) and I analysed the spatial distribution of UV and green preferring ROIs. In case signals from individual cones would spread within one HC or even in the whole network, I would expect neighbouring HC dendritic tips to respond with similar *SC* preference. The alternative would be to observe neighbouring "purely" UV and green sensitive HC dendritic tips: This would suggest that HC dendritic tips reflect the contacted cone's chromatic preference and therefore, local signals. In both dorsal (5 fields) and ventral retina (10 ventral), I found neighbouring HC dendrites that drastically vary in their *SC* preference (**Figure 17F,G**) suggesting that HC dendritic tips encode cone inputs in an independent manner.

By measuring the distance between UV ROIs and the distance between UV vs. green ROIs per field (|*SC*|=0.3; 7 fields, **Figure 17H**), I found that UV sensitive HC dendrites clustered together (< 10 µm) suggesting that they receive input from the same cone whereas most of green HC

dendrites are localized further away (> 10 µm) and may receive input from neighbouring green cones. In addition, the distribution of green HC dendrites seems to be periodic with a length corresponding approximatively to the width of a cone axon terminal (~8 µm). My data are therefore in favour of the local signal processing hypothesis.

Note that GCaMP3 was expressed ubiquitously in HCs and that I could not differentiate individual HCs and their processes. Therefore I could not assign ROIs to individual HCs. However, because only one HC type contact indiscriminately both S- and M-cones (Feigenspan and Babai, 2015; Schubert et al., 2010) and because HCs are electrically coupled, it is unlikely that my data are solely explained by recording of neighbouring HCs, one receiving exclusively S-input and the other exclusively M-cone input.

Somatic signal integration in horizontal cells

The "funnel" shape of the *SC* distribution (*cf.* **Figure 17C**) suggests that local and global signal processing co-exist in HCs: The dendritic tips can locally encode the cone input whereas soma are likely to receive a mixture of S- and M-cones input. To test this hypothesis and assess how signals are integrated at the level of the soma, I performed electrophysiology experiments: I used the $Cx57^{+/cre}$ x Ai9 (tdTomato) mouse line where HCs were selectively labelled (**Figure 18A**) to target individual HC soma using an electrode filled with intracellular solution and OGB1 (100 µM) (**Figure 18B**). I recorded simultaneously the membrane potential and light-evoked Ca^{2+} signals in response to the GUW protocol (**Figure 18C,D** and see Methods). Due to the difficulties of the experimental procedure, only few cells could be recorded and only one cell passed my quality criteria for both voltage and Ca^{2+} signals. Here, I present the result from this exemplary HC soma. The soma had a resting membrane potential of –38.8 mV (baseline before light stimulus, **Figure 18C**). The average somatic voltage and Ca^{2+} responses to green, UV and white flashes show that this exemplary HC located in the central part of the retina (slice +3; *cf.* **Figure 17D**) responded similarly to the different flashes (voltage amplitude, green: 2.0 mV, UV: 2.6 mV, white: 3.5 mV; Ca^{2+} amplitude, green: 1.4 s.d., UV: 2.5 s.d., white: 3.2 s.d.; *SC*=-0.3) (**Figure**

18D,E) which is in agreement with my hypothesis and suggests that HC soma receive a mixture of S- and M-cones.

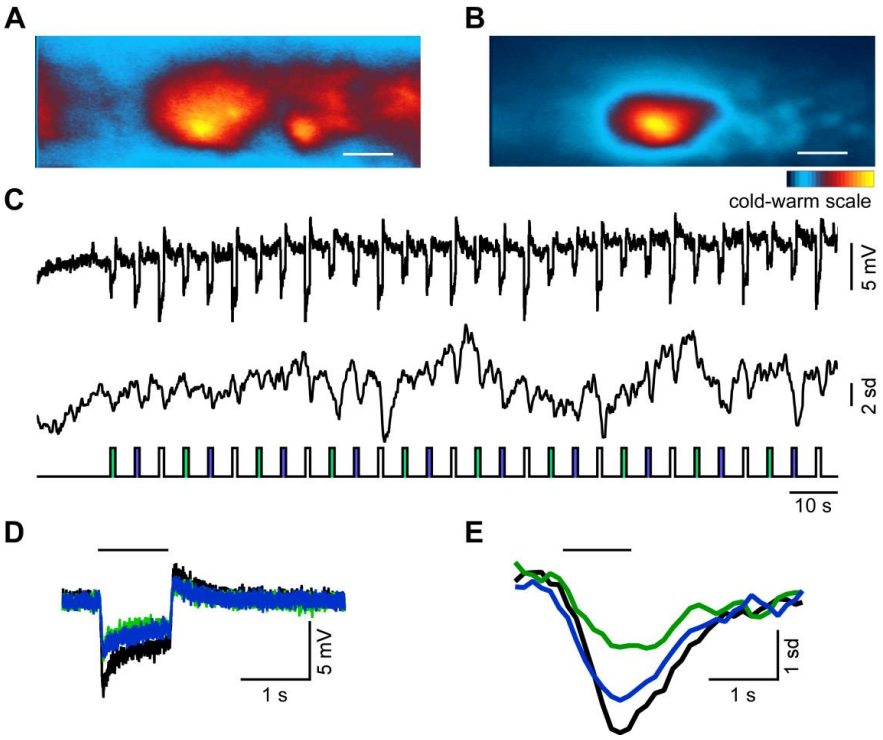

Figure 18. Voltage and Ca^{2+} signals in horizontal cell soma
A,B. To target a HC soma, I used the $Cx57^{+/cre}$ x Ai9 (tdTomato) mouse line (A). I current-clamped the HC using an electrode filled with the Ca^{2+} indicator OGB1 in intracellular solution (see Methods) (B). **C-E.** Membrane potential (C, *top* and D) and light-evoked Ca^{2+} signals (C, *bottom* and E) in response to the GUW protocol and corresponding averaged responses. The black bars indicate the light stimulus (D,E). Scale bars, 20 µm.

Horizontal cell dendritic processes "inherit" properties of the presynaptic cone

As I found HC dendrites to locally encode cone inputs, I studied to which extent cone signals are preserved in HC dendrites. To this end, I presented a 25 Hz full-field coloured noise stimulus (see Methods and **Table 2**) on retinal slices and recorded from cone axon terminals (HR2.1:TN-XL mouse, **Figure 19A-D**), glutamate release sites (from neighbouring cone terminals; intra-vitral injection of iGluSnFR, see Methods, **Figure 19E-H**) and HC dendritic tips ($Cx57^{+/cre}$ x Ai38 mouse, **Figure 19I-L**) (*cf*. **Figure 9**).

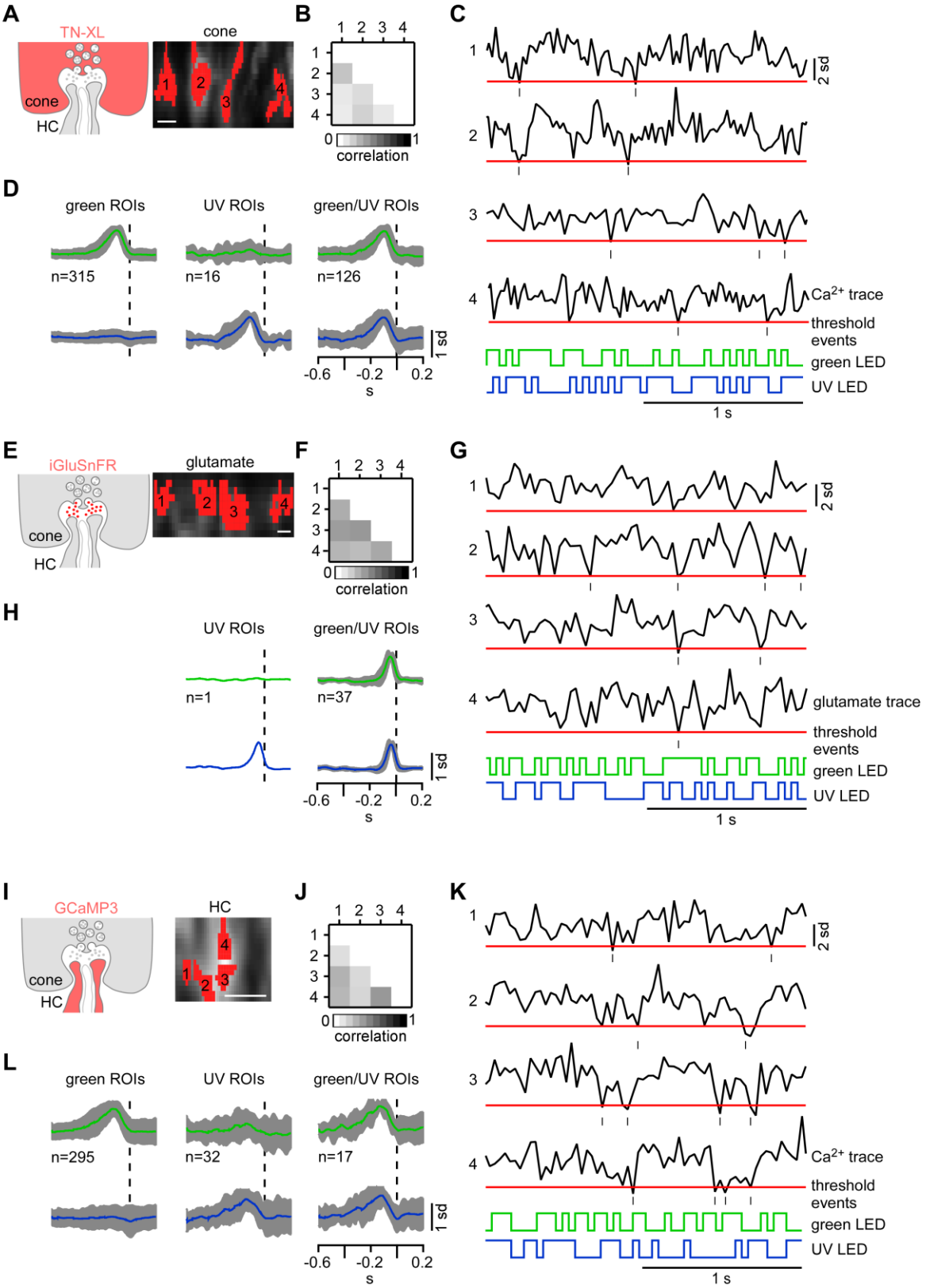
A
TN-XL
cone
HC
cone
1
2
3
4
B
1 2 3 4
0
1
correlation
C
2 sd
Ca2+ trace
threshold events
green LED
UV LED
1 s
D
green ROIs
UV ROIs
green/UV ROIs
n=315
n=16
n=126
1 sd
-0.6
-0.2
0.2
s
E
iGluSnFR
glutamate
cone
HC
F
correlation
G
glutamate trace
H
n=1
n=37
I
GCaMP3
HC
J
correlation
K
L
n=295
n=32
n=17

Figure 19. Light-evoked Ca^{2+} signals in neighbouring cone axon terminals and neighbouring horizontal cell dendrites and light-evoked glutamate signals in neighbouring glutamate release sites

A-L. Exemplary neighbouring cone axon terminals in the HR2.1:TN-XL retina (A), neighbouring site of glutamate release in the OPL from retina expressing iGluSnFR (E) and HC dendritic processes in the $Cx57^{+/cre}$ x Ai38 retina (I) with respective correlation matrix (B,F,J) of negative events in response to full-field 25-Hz coloured noise (Methods) (C,G,K). **D,H,L.** Normalized time kernels of green ROIs (amplitude green kernel > 2 s.d. noise, left), UV ROIs (amplitude UV kernel > 2 s.d. noise; middle) and mixed ROIs (amplitude green and UV kernel > 2 s.d. noise; right) for cones (D), glutamate release (H) and HCs (L). Scale bars, 5 µm.

To select ROIs responding to the coloured noise stimulus, I extracted their temporal receptive field kernels (time kernels) by computing the Ca^{2+}- or glutamate-transient-triggered average for negative events only (see Methods and Baden et al., 2016) and ROIs were considered responsive if the amplitude of their time kernels were >2 s.d. noise (**Figure 19 D,H,L**). I sorted the ROIs responding exclusively to green or UV and ROIs responding to both green and UV light (see Methods). Interestingly, I found that responses recorded from dorsal retina (Ca^{2+} signals in cone terminals and HC dendritic tips) were consistent with the percentage of "true" UV cones present in the dorsal retina (~4% for cones and 9% for HCs; Haverkamp et al., 2005). Moreover, glutamate signals that were recorded from the ventral retina (see Methods) were also consistent with the opsin distribution as I found mostly mixed responses and a single purely UV responses.

I found that the negative events for Ca^{2+} (in cones and HC dendrites) and glutamate (released from cones) signals were driven by robust positive deflections of the light stimulus: Pre- and postsynaptic signal decreases were triggered by an increase in light intensity ("OFF responses"). The differences between the time kernels I observed might be related to the origin of signals (slow Ca^{2+} signal vs. transient glutamate release from ribbons), biosensor kinetics or affinity (**Table 7**).

Biosensors	τ_{decay} (ms)	K_D in vitro (µM)	References
TN-XL	200	2.20	Hendel et al., 2008
iGluSnFR	92	4.9	Marvin et al., 2013
GCaMP3	230	0.66	Tian et al., 2009; Zariwala et al., 2012

Table 7. Biosensors kinetics and affinity
Decay time constant (τ_{decay}) and dissociation constant (K_D) for TN-XL, iGluSnFR and GCaMP3 biosensors.

Next, I calculated the correlations between neighbouring signals from cone axon terminals (HR2.1:TN-XL mouse), glutamate release sites in the OPL (intra-vitral injection of iGluSnFR, see Methods) and between HC dendritic tips ($Cx57^{+/cre}$ x Ai38 mouse). I used the degree of correlation to assess to what extent pre- and postsynaptic signals share response properties (**Figure 20**).

I calculated the linear correlation coefficient (ρ) between traces from cone ROIs and from glutamate ROIs present in the same recording field in response to the coloured noise and GUW stimuli (or GU (green and UV flashes only) in the case of glutamate recording). I found a significant decrease in correlation of negative events (<-2 s.d. noise) when presenting the coloured noise in comparison to the GUW stimulus (or GU stimulus for iGluSnFR recordings) for neighbouring ROIs for both cones (GUW: ρ=0.39 ± 0.04, n=26 ROIs (6 fields), 3 slices, 1 mouse; noise: ρ=0.08 ± 0.03, n=457 ROIs (65 fields), 7 slices, 3 mice; $p=3.888\cdot10^{-5}$) and glutamate signals (GU: ρ=0.76 ± 0.10, n=23 ROIs (6 fields), 2 slices, 1 mouse; noise: ρ=0.34 ± 0.014, n=38 ROIs (9 fields), 2 slices, 1 mouse; p=0.001) (**Figure 20A** and **Table 8**). A significant difference was also found when comparing whole traces for cones (GUW: ρ=0.45 ± 0.04; noise: ρ=0.24 ± 0.04; p=0.007) and glutamate signals (GU: ρ=0.77 ± 0.07; noise: ρ=0.47 ± 0.08; p=0.004) (**Figure 20B** and **Table 8**).

To estimate if cone properties are encoded locally in HC dendritic tips, I used a similar approach and calculated the correlation of neighbouring HC traces in response to the GUW and coloured noise stimulus protocols. My hypothesis was that if HC dendritic tips locally encode cone input,

I should observe a similar decrease in correlation when applying the coloured noise stimulus. However, in case of global signal averaging in HCs, the degree of correlation should remain high. As observed at the level of the cones and glutamate release, I found a decrease in correlation for both negative events (GUW: ρ=0.19 ± 0.08, n=262 ROIs (60 fields), 21 slices, 9 mice; noise: ρ=0.03 ± 0.02, n=344 ROIs (57 fields), 21 slices, 7 mice; $p=1.27 \cdot 10^{-17}$; **Figure 20A** and **Table 8**) and whole trace (GUW: ρ=0.31 ± 0.08; noise: ρ=0.21 ± 0.06; p=0.0009; **Figure 20B** and **Table 8**) when applying the coloured noise stimulus on HC dendritic tips in comparison to flashes. Note that the measurement of the correlation is not a direct read-out of pre-and post-synaptic signals and may therefore be influenced by the use of different biosensors (**Table 7**) or different scan rates for the GUW (7.8125 Hz) and the coloured noise stimuli (31.25 Hz).

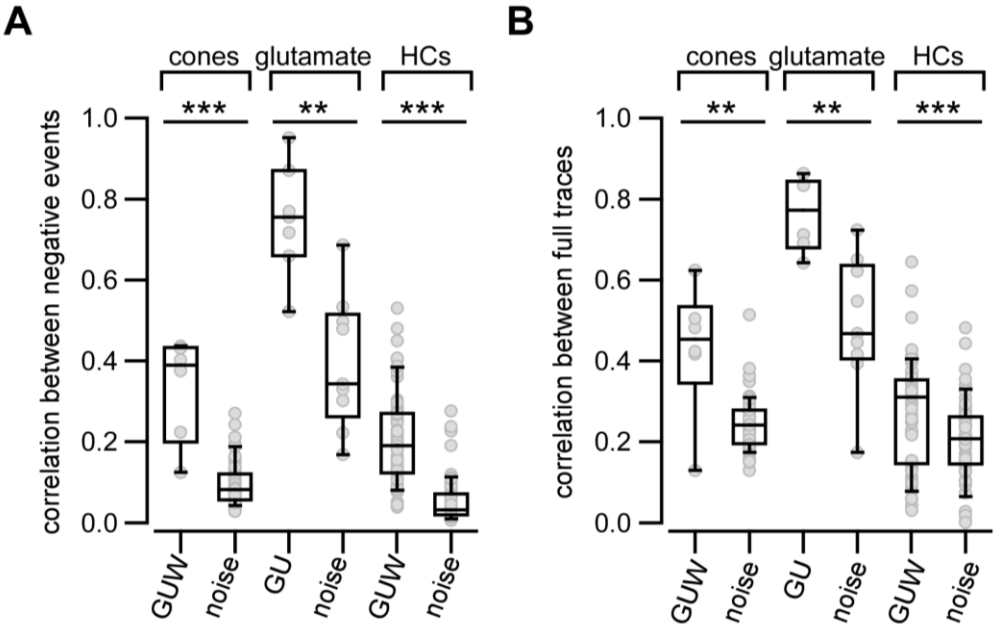

Figure 20. Correlation between neighbouring horizontal cell ROIs in response to GUW and noise stimuli

A,B. Average correlation per field for negative events only (A) and full traces (B) for cones, glutamate release sites and HCs in response to green, UV and white flashes (GUW or GU for glutamate recording) (cones: n=6 fields; glutamate: n=6 fields; HCs: n=60 fields) and to coloured noise (cones: n=65 fields; glutamate: n=9 fields; HCs: n=57 fields). **, p ≤ 0.01; ***, p ≤ 0.001.

		GU(W) (ρ) median [MAD]	noise (ρ) median [MAD]	Δmedian
Cone axon terminals	Negative events	0.390 ± 0.044	0.082 ± 0.030 ($p=3.888\cdot10^{-5}$ ***)	0.308
	Full traces	0.453 ± 0.044	0.242 ± 0.040 (p=0.007 **)	0.211
Glutamate release sites	Negative events	0.756 ± 0.096	0.344 ± 0.135 (p=0.001 **)	0.412
	Full traces	0.773 ± 0.072	0.468 ± 0.080 (p=0.004 **)	0.305
HC distal dendrites	Negative events	0.190 ± 0.078	0.032 ± 0.020 ($p=1.27\cdot10^{-17}$ ***)	0.158
	Full traces	0.310 ± 0.084	0.207 ± 0.059 (p=0.0009 ***)	0.103

Table 8. Linear correlation coefficient between traces from cones, glutamate release sites and horizontal cells

Linear correlation coefficient (ρ) between negative events and full traces, for cone axon terminals, glutamate release sites and HC distal dendrites. GUW, green, UV and white flashes (or GU for glutamate recordings); MAD, median absolute deviation.

Taken together, the finding that noise stimulation results in similarly low levels of correlation of the pre- (cone) and the postsynaptic (HC) signal as well as glutamate signals in OPL is consistent with the hypothesis of highly local and independent signal processing in HC distal dendrites. Moreover, when looking at the spatial distribution of the correlation between neighbouring HC dendrites, I found that HC dendrites that receive input from the same cones (distance < 8 µm) show higher degree of correlation for both the GUW and the colour noise stimuli (**Figure 21**, correlation between negative events vs. distance for GUW stimulus: r=-0.056,p=0.150, n=663 combinations; for noise stimulus: r=-0.271, $p=2.28\cdot10^{-20}$, n=1125 combinations).

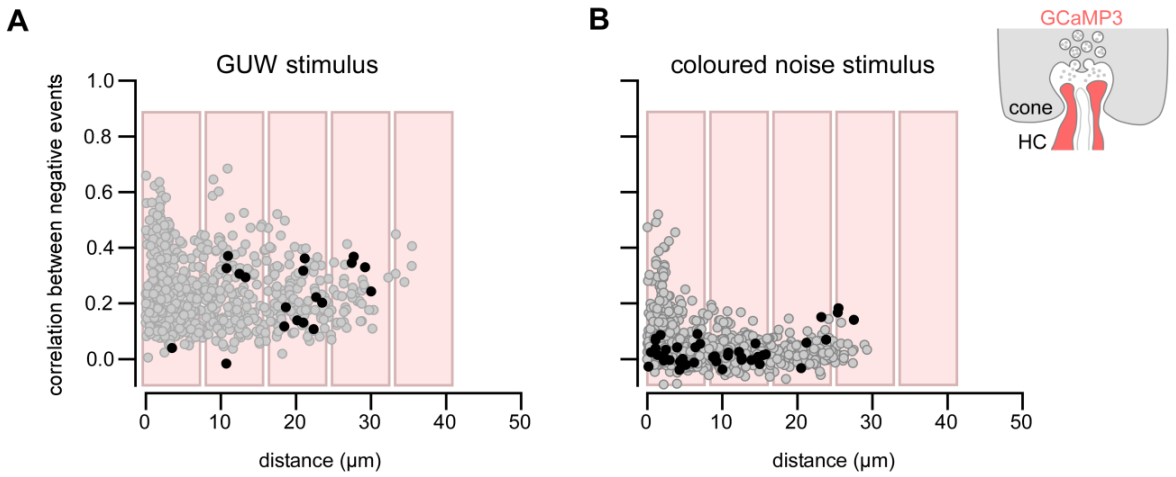

Figure 21. Correlation between negative events in horizontal cell dendrites
A-B. Correlation between negative events for all combinations of ROIs present in the same field as a function of their distance for HC dendrites ($Cx57^{+/cre}$ x Ai38 mice) for the GUW (A) and for the coloured noise stimulus (B). The dark circles indicate the combinations between "purely" green and "purely UV" ROIs (GUW, $|SC| > 0.4$; coloured noise, amplitude UV or green kernel > 2 s.d. noise). The boxes illustrate expected location of neighbouring cone axon terminals.

Are cone contrast preferences encoded in horizontal cell dendrites?

Mouse cones have been shown to encode contrast signal differently: M-cones respond equally to dark and bright flashes whereas most of S-cones encode preferentially dark contrast over bright one (see Introduction and Baden et al., 2013). Therefore, here I tested if cone contrast preferences are also encoded in HC dendritic tips (**Figure 22**). I applied a contrast and colour protocol (see **Table 2**) and I analysed for each ROI the *SC* as well as a dark-light index (*DLi*, see Methods).

HC dendrites generally responded preferentially to dark over bright stimuli (green: ΔF_{dark}=1.44 ± 0.60 vs. ΔF_{bright}=0.62 ± 0.46, p=8.389·10^{-9}, n=57; UV: ΔF_{dark} 1.63 ± 0.56 vs. ΔF_{bright}=0.55 ± 0.35, p=2.288·10^{-25}, n=99; **Figure 22A-D**) which is consistent with the "dark suppression effect", reported by Yang and colleagues (1994) who showed that dark-adapted HCs have smaller responses to bright flashes in comparison to dark flashes. Nevertheless, my data revealed that HCs located in the ventral retina encode darker contrast in comparison to

dorsal HCs (DLi means: ventral=-0.70 vs. dorsal=-0.51, p=0.0093; DLi variance: ventral=0.06 vs. dorsal=0.22, $p=4 \cdot 10^{-6}$, **Figure 22E**). This finding was consistent with what was earlier shown for cones (Baden et al., 2013). However, the *DLi* was independent on *SC* (**Figure 22F**) or baseline (F_0) (**Figure 22G**).

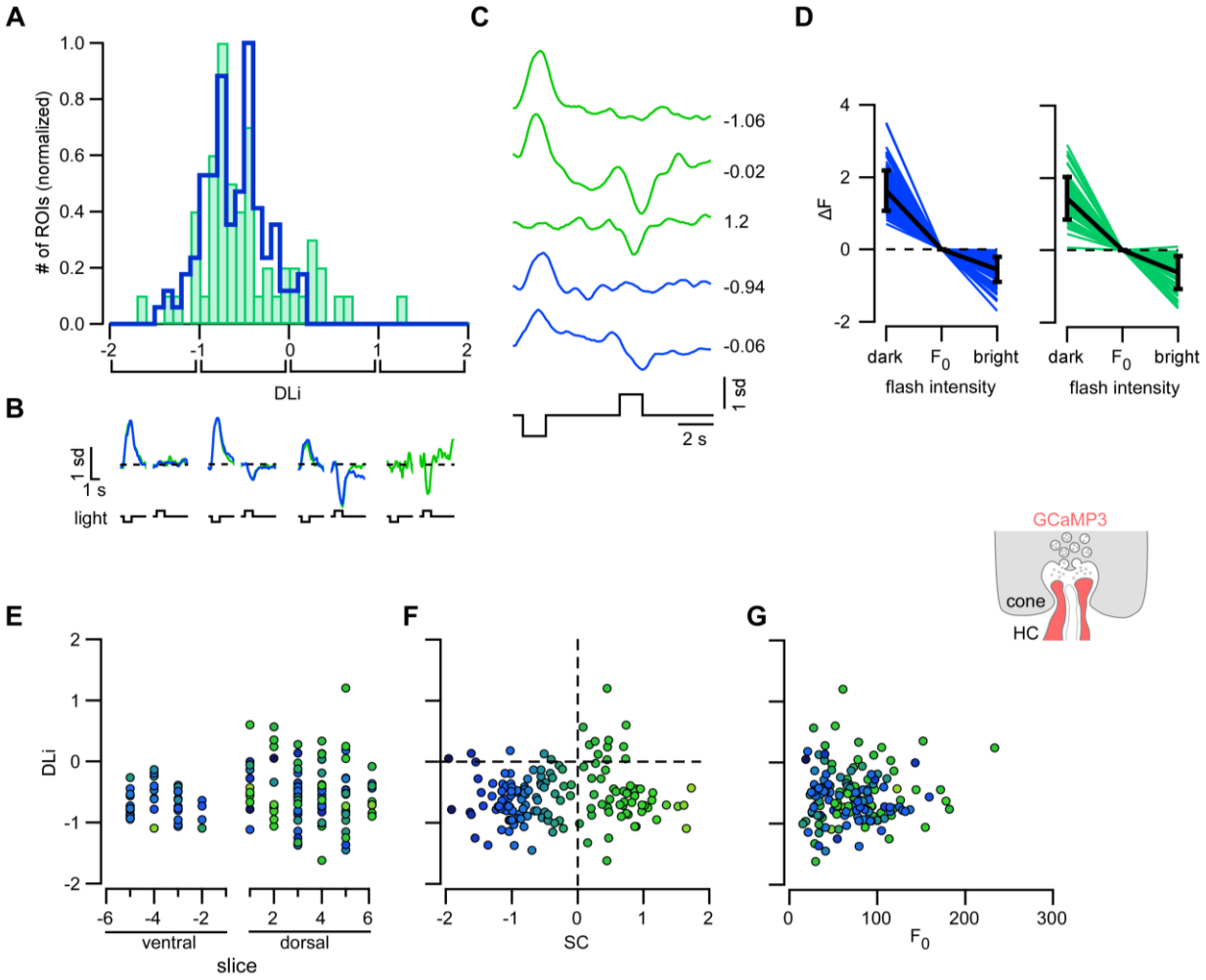

Figure 22. Contrast preference of Ca^{2+} responses in horizontal cell processes

A. Histogram of dark-light index distribution (*DLi*; see Methods) for green (*SC*>0; n=57 ROIs) and UV (SC<0; n=99 ROIs). **B.** Averaged Ca^{2+} signal in response to green and UV, dark and bright flashes for different *DLi* intervals (averages of n=8 trials). **C.** Exemplary green and UV ROIs responding to dark and bright flashes (averages of n=8 trials). Values indicate *DLi*. **D.** Response amplitudes (ΔF) for UV (left) and green ROIs (right) to dark and bright flashes (F_0, baseline). **E-G.** *DLi* plotted as a function of slice position (E), *SC* (F) and baseline (F_0, G). Colours reflect *SC* preference of each ROI. E. Error bars indicate s.d.

Local horizontal cell feedback may shape temporal properties of cone responses

To test the effect of local HC feedback on the cone response, I applied a 60 Hz full-field binary noise to slices prepared from HR2.1:TN-XL mice and mice expressing iGluSnFR (**Figure 23**). I used a similar approach as explained previously to analyse the data (*cf.* **Figure 19**): I calculated the time kernels for cone Ca^{2+} signals (**Figure 23A**) and glutamate signals (from cone release; **Figure 23B**). I either performed two consecutive recordings (with an interval of 5 min) in a control condition (cone Ca^{2+}, n=61 ROIs, 11 slices, 3 mice; glutamate, n=76 ROIs, 15 slices, 3 mice) or after bath-applying NBQX (100 µM) to deprive HCs of their input (cone Ca^{2+}, n=48 ROIs, 15 slices, 3 mice; glutamate, n=47 ROIs, 18 slices, 3 mice). No differences were found for the time-to-peak and the F_{Area} for both control and NBQX experiments (**Figure 23E**, Sinha et al., 2017). However, when the time kernel periodograms were analysed using discrete Fourier transforms (see Methods and Vroman et al., 2014), significant differences in the power spectral density at low frequencies were found in the NBQX condition for both cone Ca^{2+} and glutamate release (**Figure 23F**, dependent samples t-test; cone Ca^{2+}, at 1 Hz, $p=3\cdot10^{-4}$; cone glutamate release, at 0 Hz, $p=3.2\cdot10^{-7}$, at 1 Hz, $p=4.7\cdot10^{-5}$) suggesting that local HC feedback plays a role in increasing the sensitivity of the cone signal to low frequencies.

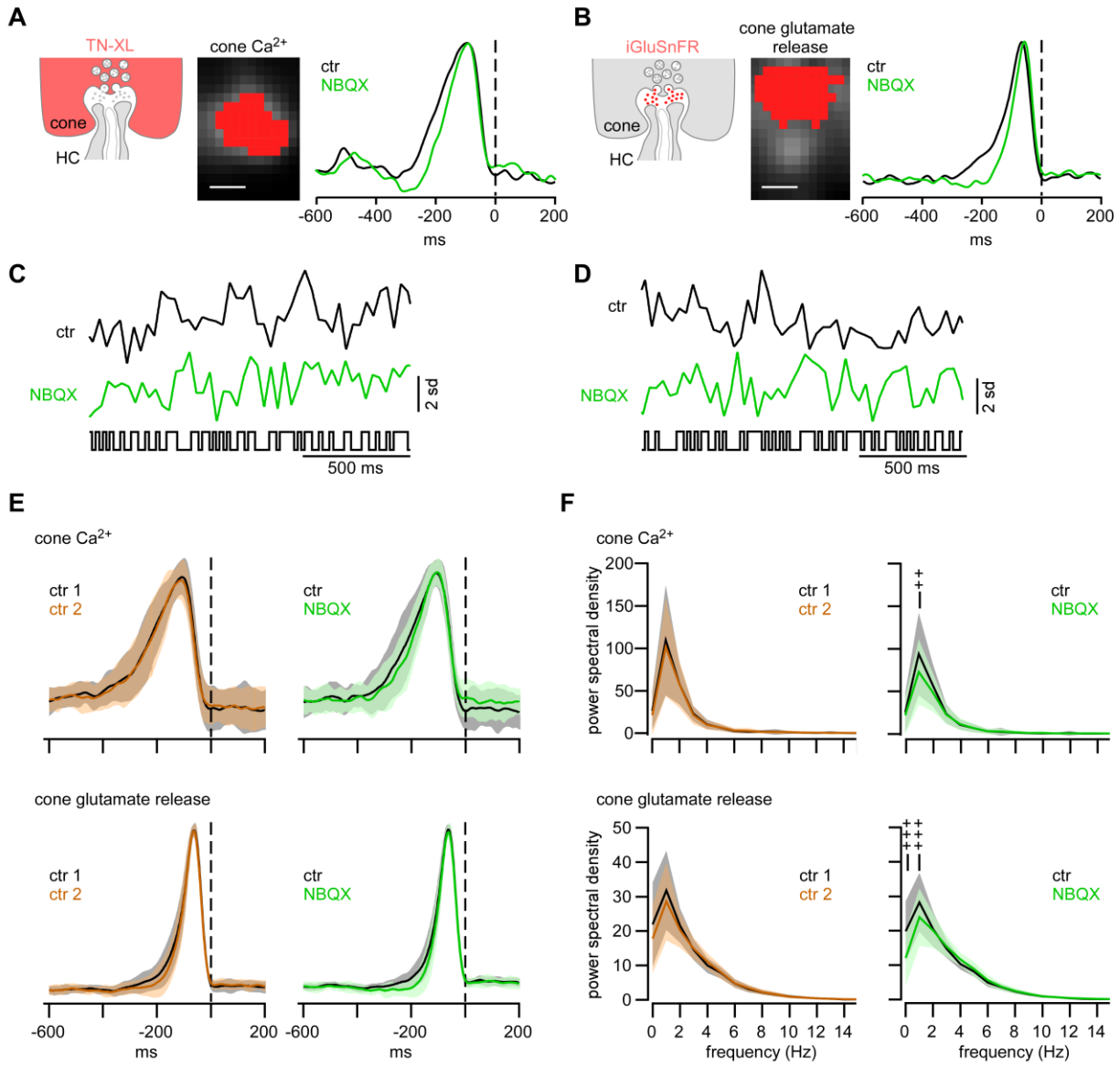

Figure 23. Local horizontal cell feedback modulates temporal properties of cone response
A-D. Exemplary ROIs of cone axon terminals, defined by TN-XL expression (A) or by iGluSnFR activity (B, Methods), with respective temporal receptive field kernels calculated from response to a full-field 60-Hz binary noise stimulus (raw traces in C, D; Methods) for control condition (black traces in A-D) and during bath application of NBQX (green traces in A-D). **E.** Normalized time kernels for cone Ca^{2+} (upper panel) and glutamate release (lower panel) for control condition (ctr1, ctr2; left) and with NBQX (right) (cone Ca^{2+}: ctr, n=61 ROIs; NBQX, n=48 ROIs; cone glutamate release: ctr, n=76 ROIs; NBQX, n=47 ROIs; shaded areas indicate 1 s.d.). **F.** Periodograms (Methods) generated from cone kernels (E) using a discrete Fourier transform: cone Ca^{2+} (upper panel) and glutamate release (lower panel) for control condition (left) and with NBQX (right) (shaded areas indicate 1 s.d.). ++, $p \leq 6.66 \cdot 10^{-4}$; +++, $p \leq 6.66 \cdot 10^{-5}$ (Bonferroni corrected significance threshold). Scale bars, 2.5 µm.

Discussion

In this thesis, I studied how cone signals are integrated in HCs in the mouse retina. To test the spatial resolution of HC feedback, I used two-photon Ca^{2+} and glutamate imaging at three different "levels" of the cone synapse: (i) cone Ca^{2+} signals, (ii) glutamate release from cones and (iii) HC Ca^{2+} signals (**Figure 9**). By applying light-evoked stimulus, I found that HC dendritic tips can locally process cone signal. First, using green and UV light-evoked Ca^{2+} signals in HCs from different retinal area, I found that the *SC* preference of neighbouring HCs differ markedly (neighbouring "purely" UV and green HC dendrites) indicating that HC dendritic tips can locally encode cone signals (**Figure 17**). Second, using a coloured noise stimulus applied on (1) cones, (2) glutamate release sites from cones and (3) HCs, I found that the degree of correlation in neighbouring HC signals was similarly reduced as for cone Ca^{2+} signals and for glutamate signals (in comparison to light flashes, **Figure 19** and **20**). This indicates that HC dendritic tips do not average signals from cones, in which case, a decrease in correlation between neighbouring HC dendrites would have not been observed.

These finding were in line with three other recent studies (Grassmeyer and Thoreson, 2017; Jackman et al., 2011; Vroman et al., 2014) that have shown that a (positive) local feedback occurs within the synaptic cleft of an individual cone-HC synapse. They were also consistent with a biophysical realistic model built based on my data by Christian Behrens (see below). This finding were surprising considering the fact that HCs form a large gap junction-coupled network that have been thought to be involved in global signal processing, such as contrast enhancement. Moreover, using a pharmacology approach, I found local HC feedback to play a role in shaping the temporal properties of the cones.

Do rods contribute to the Ca^{2+} signals in horizontal cell dendrites?

For the interpretation of the data, it is important to assess whether the light-evoked response were based on cone only or on cone/rod activation. As already described above, the

$Cx57^{+/cre}$ x Ai38 mouse line expressed GCaMP3 in all HC compartments and because dendritic and axonal HC processes are intermingled in the OPL, they could not be distinguished based on their morphology. In the present study, I think that I predominantly recorded from HC dendrites for the following reasons. First, I found light-evoked Ca^{2+} signals to be larger close to the cone axon terminal base (**Figure 13**), where HC dendritic tips make synaptic invaginated contacts with cones (**Figure 4**). Second, rods can respond to both green and UV light (due to higher light sensitivity than cones, reviewed in Ingram et al., 2016). However, I found that the *SC* preference was dependent on the slice position along the dorso-ventral axis and reflected the S- and M-opsin expression gradient. In case of direct rod activation, I would have observed an additional UV response in dorsal slices or/and green response in ventral slices (**Figure 17D**, see slices 6, 5, -5 and -6). Third, photoreceptor excitation by the laser already generates a background illumination equivalent to ~10^4 $P^*\cdot s^{-1}$/cone (Baden et al., 2013) which is probably similar in rods (Euler et al., 2009). Electrical recordings from mouse rods in slices indicate that rod photoresponses disappears around 10^4 $P^*\cdot s^{-1}$/rod (Szikra et al., 2014), suggesting that under my experimental conditions rods were not operational.

Why any rod responses could be detected is unclear as Franke and colleagues (Franke et al., 2017) recently showed that rod BCs respond to light flashes under similar experimental conditions. One possible explanation is that rods were indeed saturated and that rod BCs were driven by cones, because in mice, ~70% of the rod BCs contact at least one cone (Behrens et al., 2016) and therefore may receive substantial cone input.

However, it is also conceivable that rods contribute indirectly to the measurements either via spread of signals via gap junction between cones and rods (Asteriti et al., 2014) or via spread of signals from HC dendrites to the HC axon terminal system (Szikra et al., 2014).

Lateral interaction in horizontal cells in retinal slices?

The presented data are in favour of local signal processing in HCs. In contrast to the high *SC* variability found in the HC dendritic tips, more proximal dendrites showed less *SC* variability

(with *SC* closer to 0, **Figure 17**), which indicates that HC soma received and integrated signals from both S- and M-cones, arguing for global signal processing at the level of HC somata.

Whether lateral interaction between HCs is functional in these experimental conditions is unclear. Several pieces of evidence indicate that lateral interactions are preserved to some extent in slices. First, Kemmler and colleagues (2014) found that surround inhibition was already present in cones when applying a light stimulus more than 200 µm away from the measured cone in 300 µm thick slices. Second, AII ACs show intact gap junction-coupling in slice preparation (Habermann et al., 2003; Veruki et al., 2008). Third, Jackman and colleagues (2011) found that local feedback was affected in slice preparation but not the global feedback.

Nevertheless, the retinal slice preparation may alter to some extent the HC network. For example, it has been suggested that glutamate spillover to neighbouring cones (and therefore to neighbouring postsynaptic HC dendrites) might be affected in slices due to fast diffusion of neurotransmitters in the perfused solution (see discussion in Vroman and Kamermans, 2015). Another potentially limiting factor of lateral interaction in the experiments presented here is that in the $Cx57^{+/cre}$ x Ai38 mouse line, one *Cx57* allele is deleted and replaced by a *cre* gene. This results in a decreased size of the HC receptive field by a third (Shelley et al., 2006) and the number of HC coupled cells was reduced by half. Nonetheless, on average ~100 HCs were still electrically coupled. Moreover, no change in dendritic arbour size was reported even when fully deleting Cx57 (Shelley et al., 2006).

Taken together, while retinal slices turned out to be very useful to study local HC signal processing, they have some caveats when addressing questions at a larger scale (i.e. across the HC network). Therefore, it would be interesting to develop a method to study outer retina signalling in the whole mount preparation where the large HC network is intact. This would allow studying, for example, with spatially structured visual stimuli whether local and global signal processing happen in concert. If this is the case, HCs could serve, in parallel, global averaging of cone input (contrast enhancement) but also keep “intact” the visual information received by cones. However, in the whole mount retina, the laser focal plane would be very

close to the photoreceptors leading to strong laser effects and it is therefore unclear if this could work.

Mechanisms of local Ca^{2+} signalling in horizontal cell dendrites

In this thesis, I showed that Ca^{2+} signals in HC dendrites are mediated by AMPA/KA-type glutamate receptors, VGCCs and possibly Ca^{2+} released from intracellular stores (Feigenspan and Babai, 2015; Schubert et al., 2006; Ströh et al., 2013). It is therefore conceivable that HCs employ similar mechanisms as the A17 ACs (see Introduction) to be able to process presynaptic signals locally and globally depending on the strength of the input. In the following section, I summarize the similarities and differences in the dendritic signal processing between HCs and A17 ACs.

First, in this thesis, I found that VGCCs were activated by AMPA/KA puff. However, I used a relatively high concentration to reliably evoke detectable Ca^{2+} responses, and it is possible that (dim) light-evoked Ca^{2+} responses in HC dendrites do not lead to a similar level of activation of VGCCs. Therefore, while weak depolarization could result in local signalling in HC dendritic tip, strong depolarization could result in VGCC activation and spread of signal along the dendrite. This is consistent with a study from Jackman and colleagues (2011) who found that, local HC feedback in zebrafish, tiger salamander, anole lizard and rabbit HCs can be triggered directly by AMPA receptor activation (without VGCC activation). A similar mechanism is present in A17 ACs. Grimes and colleagues (2009) used an electrophysiological approach to record the inhibitory postsynaptic current elicited in rod BCs by the GABA released from A17 ACs in response to glutamate puffs at different concentration (50 and 500 µM) in a control condition and in the presence of cadmium, a VGCC pore blocker. Whereas they found that cadmium had a rather miner effect on the response to the glutamate puff at low concentration, cadmium strongly reduced the inhibitory postsynaptic current (by ~50%) in response to the glutamate puff at high concentration. Therefore, in both HC dendritic tips and A17 AC varicosities, the activation of VGCCs may depend on the strength of the excitatory input.

Second, a recent study showed that BK channels are expressed in HCs (Sun et al., 2017). BK channels are voltage- and Ca^{2+}-dependent and are responsible for limiting the membrane depolarization. Therefore, BK channels may help to restrict the signal locally by preventing the activation of VGCCs, in a similar fashion as in A17 AC varicosities (Grimes et al., 2009).

Third, Ca^{2+} signals in HC dendrites rely on intracellular Ca^{2+} stores (Schubert et al., 2006) and can increase the intracellular Ca^{2+} concentration following the activation of Ca^{2+} permeable glutamate receptors. In the A17 ACs, Chavez and colleagues (2006) found that the intracellular Ca^{2+} concentration increase following the Ca^{2+} permeable AMPA receptors activation, activates CICR and amplify the Ca^{2+} signal. Moreover, they found that this Ca^{2+} pathway is sufficient to trigger GABA release and do not require membrane depolarization or VGCC activation.

Finally, the HC morphology may support electrical isolation between dendritic tips. Using a simple biophysical, morphologically realistic model of a HC dendritic branch including cone contacts based on electron microscopy reconstruction (Behrens et al., 2016; Helmstaedter et al., 2013; Rogerson et al., 2017), preliminary data indicate that the HC dendritic morphology supports electrical isolation of distal tips and, thereby, local signal processing (Christian Behrens, personal communication). Similarly, Grimes and colleagues (2010) used a model to show that the A17 AC morphology supports local processing : A17 AC dendrites are covered by varicosities that restrict signal spread to neighbouring varicosities, at least for weak stimulation (see Introduction for details).

Taken together, the results presented in this thesis indicate that both A17 ACs and HCs share common principles to regulate the spatial processing of their inputs. However, an important difference to the A17 ACs is that mouse HCs can affect their own activities not only by modulating the output of their presynaptic partners (the cones), but also by sensing their GABA release via $GABA_A$ auto-receptors (Hirano et al., 2016; Kemmler et al., 2014). In comparison, A17 cells also express $GABA_A$ receptors but GABA auto-reception has not yet been found (Menger and Wässle, 2000). This suggests that HC dendrites can regulate their own level of depolarization and points to yet another level of complexity in dendritic HC processing.

Functions of HC dendritic tips in the retina and functions of dendritic spines in the central nervous system

Using a pharmacological approach to deprive the cones from HC feedback, I found that HC feedback may shape the transmission of low-frequency signals in the cone output. Therefore, local HC feedback appears to play a role in the time domain. The data show that an increase in (local) HC feedback leads to a slower presynaptic cone. In contrast, when the (local) HC feedback decreases, the presynaptic cone responses become more transient. However, a different mechanism seems to regulate the cone kinetics in primate: A recent study (Sinha et al., 2017) in primate retina showed that foveal cones have slower time-to-peak and are less transient than peripheral cones. They show that primate HCs do not play a role in setting the cone properties but the difference in cone response kinetics originates from differences in the phototransduction cascade in the cone OS.

It is interesting to note that another distinction between primate and mouse is the presence of colour opponency in the primate cones that has never been found in mouse cones. As colour opponency requires a global average of several cone responses, the absence of colour opponency in mouse outer retina would be in line with the predominant function of mice HCs being the local modulation of the cone response.

My finding that local Ca^{2+} signalling in mouse HC dendritic tips may be to modulate the temporal responses of cones is reminiscent of the idea that dendritic spines can modulate the temporal filtering properties of the neuron (Rose and Call, 1992). However, one major difference between dendritic tip and spine is that whereas mouse HC dendritic tips are unlikely to be plastic (at least under physiological condition; see below for details), dendritic spines are highly plastic: They can undergo change of morphology, formation or degradation of new spines and can be influenced by sensory perception. This plastic property has also been found to be the basis for learning and memory.

First, sensory perception can influence the formation of dendritic spines. For example, mice kept in an enriched environment from birth show higher number of dendritic spines and higher rate of dendritic spine turnover in pyramidal cells from layer II/III and V of the somatosensory cortex (Jung and Herms, 2014). In contrast, a study on dark-rearing mice (from birth) shows that dendritic spines from layer V of visual cortex stay in an immature stage (Tropea et al., 2010). Similar results have been found after unilateral whisker trimming, with reduced spine motility in the contralateral barrel cortex (Lendvai et al., 2000). Taken together, these different examples show how sensory perception can affect the spine physiology and provide evidence that dendritic spines are the substrate for encoding sensory signals (reviewed in Fu and Zuo, 2011).

Second, learning tasks such as rotarod training (Yang et al., 2009), pellet reaching task (Xu et al., 2009) in mice or learning song in zebra finches (Roberts et al., 2010), have all been associated with increasing spine turnover and/or new spine formation in the brain area that supports the learnt task.

Finally, the persistence of new spines formed during the learning process has been associated with the retention of the task (Yang et al., 2009). Moreover, long-term study of mice has shown that while dendritic spines of young mice are highly plastic, those of adult mice are stable over years and provide the subtract for long term memory (Grutzendler et al., 2002).

In this thesis, I studied HCs in adult mice but it is possible that mouse HC dendrites may be more plastic during development as it has been shown for zebrafish. Zebrafish HC dendrites possess structures called “spinules” that have been found to play a role in feedback to cone mechanisms and are involved in the opposite responses to different wavelengths in the HII type (reviewed in Kröger and Wagner, 1996). Spinules are reminiscent of dendritic spines and are highly plastic during development: They can be modulated by the sensory perception (Biehlmaier et al., 2003) and their presence is regulated by both the light adaptation (they are formed at down and undergo degradation at dusk) (Biehlmaier et al., 2003) and by circadian rhythm (their formation is regulated by dopamine).

Therefore, in the context of this thesis, such plastic functions are unlikely to be involved under physiological condition in adult mouse HC dendritic tips. However, under non-physiological condition in adult mice, HC remodelling has been reported. For example, retinitis pigmentosa is a retinal disorder that is characterized by photoreceptor degeneration and subsequently leads to remodelling of the OPL. In particular, HCs undergo loss of dendrites before a second phase of neurite extension (reviewed in Kalloniatis et al., 2016) indicating that mouse HC dendrites can be plastic to some extent after loss of photoreceptor input.

Outlook

Dendrites are a specialized part of the neurons responsible for receiving signals. However, they can also directly release neurotransmitter without further somatic and axonal integration (reviewed in Ludwig and Pittman, 2003). Keeping this system flexible by allowing both local and global signal integration is of great interest in many neuronal types. It allows various and sophisticated tasks to happen in a compact system avoiding metabolic overhead. The spatial extent of the postsynaptic response depends entirely on the morphological and electrophysiological state of the dendrites. In general, spine-like structures play a key role in neuronal compartmentalisation: They limit both biochemical diffusion and electrical signal spread. Therefore, if spines possess excitable channels and high resistance in the spine neck, they can even locally generate spikes (reviewed in Sjöström et al., 2008). Moreover, spines have been shown to be highly plastic at least *in vitro* (Matsuzaki et al., 2004). Taken together, the presence of multiple subunits along individual dendrites considerably increases the amount of presynaptic signals that can be encoded at a time.

In this thesis, I have shown that already at the first synapse of a sensory system, local dendritic processing is present in a neuronal class that was unlikely to be responsible for local synaptic integration – the mouse HC. In fact, HCs are known to play roles that require global processing such as contrast enhancement and the presence of gap junctions near the dendritic tips argues against local processing. However, my functional data suggest that HC dendrites support local signal integration. But how exactly are signals from neighbouring cones segregated in HC dendritic tips? And how do HCs switch between a local and a global processing mode? These questions remain to be investigated (reviewed in Chapot et al., 2017). The recent development of high spatial resolution microscopy, the development of new biosensors for imaging inhibition and voltage (e.g. Arosio et al., 2010; St-Pierre et al., 2014), together with biophysically realistic model are promising approach to address these questions.

A better knowledge of the first synapse of the visual system is also crucial to understand how the information from the outside world is processed before being separated into parallel pathways downstream. Moreover, since HC remodelling has been associated with

photoreceptor loss (Kalloniatis et al., 2016), a better understanding of HC functions under physiological condition and in the context of retinal disorders may help to improve current therapeutic strategies by taking into account the distinct aspects of HC functions.

Publications

- Camille A. Chapot, Thomas Euler and Timm Schubert, 2017. How do horizontal cells "talk" to cone photoreceptors? Different levels of complexity at the cone-horizontal cell synapse. The Journal of Physiology 595, 5495-5506. DOI: 10.1113/JP274177.
- Camille A. Chapot, Christian Behrens, Luke E. Rogerson, Tom Baden, Sinziana Pop, Philipp Berens, Thomas Euler and Timm Schubert. Local signals in mouse horizontal cell dendrites. *Currently under review*.

Acknowledgment

Many people have contributed to this work and I therefore would like to express my thanks to:

- **Dr. Timm Schubert** and **Prof. Dr. Thomas Euler** for letting me the opportunity to work on such an exciting project and to present this work on several conferences and also for guidance, valuable suggestions, constructive criticisms and support throughout these years.
- **Prof. Dr. Frank Schaeffel** and **Prof. Dr. Cornelius Schwarz** for being part of my advisory board and for constructive feedback.
- **Sinziana Pop**, **Christian Behrens**, **Luke E. Rogerson**, **Dr. Philipp Berens** and **Dr. Tom Baden** for their help, suggestions and their contribution to this project.
- **Gordon Eske** for excellent technical support and for taking care of the mice.
- **Valeska Botzenhardt** for her help and patience.
- **Dr. Katrin Franke** for her advice and friendship.
- **Prerna Srivastava**, **Michael Power**, **Dr. Zhijian Zhao**, **André Maia Chagas**, **Yanli Ran**, **Miroslav Román Rosón** and **Dr. Manoj Kulkarni**, for helpful discussions and for creating such a nice atmosphere in the lab. I especially would like to thank Michael Power for his time to revise this thesis as a native English speaker.

Finally, I would like to extend my thanks to:

- **Devesh** for sharing joy and frustration and for our week-ends that always came as breaths of fresh air.
- **My parents** for supporting me and for always encouraging me to learn English and to travel abroad, merci.

References

Adrian, M., Kusters, R., Wierenga, C.J., Storm, C., Hoogenraad, C.C., Kapitein, L.C., 2014. Barriers in the brain: resolving dendritic spine morphology and compartmentalization. Front. Neuroanat. 8, 1–12. doi:10.3389/fnana.2014.00142

Akrouh, A., Kerschensteiner, D., 2013. Intersecting circuits generate precisely patterned retinal waves. Neuron 79, 322–334. doi:10.1016/j.neuron.2013.05.012

Arosio, D., Ricci, F., Marchetti, L., Gualdani, R., Albertazzi, L., Beltram, F., 2010. Simultaneous intracellular chloride and pH measurements using a GFP-based sensor. Nat. Methods 7, 516–518. doi:10.1038/nmeth.1471

Asteriti, S., Gargini, C., Cangiano, L., 2014. Mouse rods signal through gap junctions with cones. Elife 3, e01386. doi:10.7554/eLife.01386

Baden, T., Berens, P., Franke, K., Román Rosón, M., Bethge, M., Euler, T., 2016. The functional diversity of retinal ganglion cells in the mouse. Nature 529, 345–50. doi:10.1038/nature16468

Baden, T., Schubert, T., Chang, L., Wei, T., Zaichuk, M., Wissinger, B., Euler, T., 2013. A tale of two retinal domains: Near-optimal sampling of achromatic contrasts in natural scenes through asymmetric photoreceptor distribution. Neuron 80, 1206–1217. doi:10.1016/j.neuron.2013.09.030

Behrens, C., Schubert, T., Haverkamp, S., Euler, T., Berens, P., 2016. Connectivity map of bipolar cells and photoreceptors in the mouse retina. Elife 5, e20041. doi:10.7554/eLife.20041.

Besharse, J.C., McMahon, D.G., 2016. The retina and other light-sensitive ocular clocks. J. Biol. Rhythms 31, 223–43. doi:10.1177/0748730416642657

Biehlmaier, O., Neuhauss, S.C.F., Kohler, K., 2003. Synaptic plasticity and functionality at the cone terminal of the developing zebrafish retina. J. Neurobiol. 56, 222–236. doi:10.1002/neu.10243

Bloodgood, B.L., Giessel, A.J., Sabatini, B.L., 2009. Biphasic synaptic Ca influx arising from compartmentalized electrical signals in dendritic spines. PLoS Biol. 7. doi:10.1371/journal.pbio.1000190

Bloomfield, S.A., Dacheux, R.F., 2001. Rod vision: Pathways and processing in the mammalian retina. Prog. Retin. Eye Res. 20, 351–384. doi:10.1016/S1350-9462(00)00031-8

Branco, T., Clark Beverley A., Häusser, M., 2010. Dendritic discrimination of temporal input sequences in cortical neurons. Science. 329, 1671–1675.

Branco, T., Häusser, M., 2010. The single dendritic branch as a fundamental functional unit in the nervous system. Curr. Opin. Neurobiol. 20, 494–502. doi:10.1016/j.conb.2010.07.009

Brandstätter, J.H., Hack, I., 2001. Localization of glutamate receptors at a complex synapse: The mammalian photoreceptor synapse. Cell Tissue Res. 303, 1–14. doi:10.1007/s004410000304

Breuninger, T., Puller, C., Haverkamp, S., Euler, T., 2011. Chromatic bipolar cell pathways in the mouse retina. J. Neurosci. 31, 6504–6517. doi:10.1523/JNEUROSCI.0616-11.2011

Burkhardt, D.A., 1995. The influence of center-surround antagonism on light adaptation in cones in the retina of the turtle. Vis. Neurosci. 12, 877–885.

Cadetti, L., Tranchina, D., Thoreson, W.B., 2005. A comparison of release kinetics and glutamate receptor properties in shaping rod-cone differences in EPSC kinetics in the salamander retina. J. Physiol. 569, 773–88. doi:10.1113/jphysiol.2005.096545

Chang, L., Breuninger, T., Euler, T., 2013. Chromatic coding from cone-type unselective circuits in the mouse retina. Neuron 77, 559–571. doi:10.1016/j.neuron.2012.12.012

Chapot, C.A., Euler, T., Schubert, T., 2017. How do horizontal cells “talk” to cone photoreceptors? Different levels of complexity at the cone-horizontal cell synapse. J. Physiol. 595, 5495–5506. doi:10.1113/JP274177

Chávez, A.E., Singer, J.H., Diamond, J.S., 2006. Fast neurotransmitter release triggered by Ca influx through AMPA-type glutamate receptors. Nature 443, 705–8. doi:10.1038/nature05123

Chen, X.H., Bezprozvanny, I., Tsien, R.W., 1996. Molecular basis of proton block of L-type Ca2+ channels. J. Gen. Physiol. 108, 363–74. doi:10.1085/jgp.108.5.363

Crook, J.D., Manookin, M.B., Packer, O.S., Dacey, D.M., 2011. Horizontal cell feedback without cone type-selective inhibition mediates “red–green” color opponency in midget ganglion cells of the primate retina. J. Neurosci. 31, 1762–1772. doi:10.1523/JNEUROSCI.4385-10.2011

Dacey, D.M., Lee, B.B., Stafford, D.K., Pokorny, J., Smith, V.C., 1996. Horizontal cells of the primate retina: cone specificity without spectral opponency. Science. 271, 656–659. doi:10.1126/science.271.5249.656

Davenport, C.M., Detwiler, P.B., Dacey, D.M., 2008. Effects of pH buffering on horizontal and ganglion cell light responses in primate retina: evidence for the proton hypothesis of surround formation. J Neurosci 28, 456–464. doi:10.1523/JNEUROSCI.2735-07.2008

Deans, M.R., Volgyi, B., Goodenough, D.A., Bloomfield, S.A., Paul, D.L., 2002. Connexin36 is essential for transmission of rod-mediated visual signals in the mammalian retina. Neuron

36, 703–712.

Deniz, S., Wersinger, E., Schwab, Y., Mura, C., Erdelyi, F., Szabó, G., Rendon, A., Sahel, J.A., Picaud, S., Roux, M.J., 2011. Mammalian retinal horizontal cells are unconventional GABAergic neurons. J. Neurochem. 116, 350–362. doi:10.1111/j.1471-4159.2010.07114.x

Denk, W., Strickler, J.H., Webb, W.W., Series, N., Apr, N., 1990. Two-photon laser scanning fluorescence microscopy. Science. 248, 73–76. doi:10.1126/science.2321027

DeVries, S.H., 2001. Exocytosed protons feedback to suppress the Ca2+ current in mammalian cone photoreceptors. Neuron 32, 1107–1117. doi:10.1016/S0896-6273(01)00535-9

DeVries, S.H., 2000. Bipolar cells use kainate and AMPA receptors to filter visual information into separate channels. Neuron 28, 847–856. doi:10.1016/S0896-6273(00)00158-6

Dorostkar, M.M., Dreosti, E., Odermatt, B., Lagnado, L., 2010. Computational processing of optical measurements of neuronal and synaptic activity in networks. J. Neurosci. Methods 188, 141–150. doi:10.1016/j.jneumeth.2010.01.033

Duebel, J., Haverkamp, S., Schleich, W., Feng, G., Augustine, G.J., Kuner, T., Euler, T., 2006. Two-photon imaging reveals somatodendritic chloride gradient in retinal ON-type bipolar cells expressing the biosensor clomeleon. Neuron 49, 81–94. doi:10.1016/j.neuron.2005.10.035

Eggers, E.D., Lukasiewicz, P.D., 2011. Multiple pathways of inhibition shape bipolar cell responses in the retina. Vis Neurosci 28, 95–108. doi:10.1017/s0952523810000209

Endeman, D., Fahrenfort, I., Sjoerdsma, T., Steijaert, M., Eikelder, H., Kamermans, M., 2012. Chloride currents in cones modify feedback from horizontal cells to cones in goldfish retina. J. Physiol. 590, 5581–5595. doi:10.1113/jphysiol.2012.240325

Euler, T., Detwiler, P.B., Denk, W., 2002. Directionally selective calcium signals in dendrites of starburst amacrine cells. Nature 418, 845–852. doi:10.1038/nature00931

Euler, T., Hausselt, S.E., Margolis, D.J., Breuninger, T., Castell, X., Detwiler, P.B., Denk, W., 2009. Eyecup scope—optical recordings of light stimulus-evoked fluorescence signals in the retina. Eur. J. Physiol. 457, 1393–1414. doi:10.1007/s00424-008-0603-5

Euler, T., Haverkamp, S., Schubert, T., Baden, T., 2014. Retinal bipolar cells: elementary building blocks of vision. Nat. Rev. Neurosci. 15, 507–519. doi:10.1038/nrn3783

Feigenspan, A., Babai, N., 2015. Functional properties of spontaneous excitatory currents and encoding of light/dark transitions in horizontal cells of the mouse retina. Eur. J. Neurosci. 42, 2615–2632. doi:10.1111/ejn.13016

Finch, E.A., Augustine, G.J., 1998. Local calcium signalling by inositol-1,4,5-trisphosphate in Purkinje cell dendrites. Nature 396, 753–756.

Franke, K., Berens, P., Schubert, T., Bethge, M., Euler, T., Baden, T., 2017. Balanced excitation and inhibition decorrelates visual feature representation in the mammalian inner retina. Nature 542, 439–444. doi:10.1101/040642

Fu, M., Zuo, Y., 2011. Experience-dependent structural plasticity in the cortex. Trends Neurosci. 34, 177–187. doi:10.1016/j.tins.2011.02.001

Ghosh, K.K., Bujan, S., Haverkamp, S., Feigenspan, A., Wässle, H., 2004. Types of bipolar cells in the mouse retina. J. Comp. Neurol. 469, 70–82. doi:10.1002/cne.10985

Goodchild, A.K., Chan, T.L., Grünert, U., 1996. Horizontal cell connections with short-wavelength-sensitive cones in macaque monkey retina. Vis. Neurosci. 13, 833–45.

Grassmeyer, J.J., Thoreson, W.B., 2017. Synaptic ribbon active zones in cone photoreceptors operate independently from one another. Front. Cell. Neurosci. 11. doi:10.3389/fncel.2017.00198

Greene, M.J., Kim, J.S., Seung, H.S., 2016. Analogous convergence of sustained and transient inputs in parallel On and Off pathways for retinal motion computation. Cell Rep. 14, 1892–1900. doi:10.1016/j.celrep.2016.02.001

Grimes, W.N., Li, W., Chávez, A.E., Diamond, J.S., 2009. BK channels modulate pre- and postsynaptic signaling at reciprocal synapses in retina. Nat. Neurosci. 12, 585–592. doi:10.1038/nn.2302

Grimes, W.N., Zhang, J., Graydon, C.W., Kachar, B., Diamond, J.S., 2010. Retinal parallel processors: more than 100 independent microcircuits operate within a single interneuron. Neuron 65, 873–885. doi:10.1016/j.neuron.2010.02.028

Grutzendler, J., Kasthuri, N., Gan, W., 2002. Long-term dendritic spine stability in the adult cortex 420. doi:10.1038/nature01151.1.

Habermann, C.J., O'Brien, B.J., Wässle, H., Protti, D.A., 2003. AII amacrine cells express L-type calcium channels at their output synapses. J Neurosci 23, 6904–6913.

Hampson, E., Weiler, R., Vaney, D., 1994. pH-gated dopaminergic modulation of horizontal cell gap junctions in mammalian retina. Proceedings. Biol. Sci. 255, 67–72.

Harris, K.M., Spacek, J., 2016. Dendrite structure. In: Stuart et al. (Eds) Dendrites. 3rd Edition, Oxford University Press.

Haverkamp, S., Grünert, U., Wässle, H., 2000. The cone pedicle, a complex synapse in the retina. Neuron 27, 85–95. doi:10.1016/S0896-6273(00)00011-8

Haverkamp, S., Wässle, H., Duebel, J., Kunner, T., Augustine, G.J., Feng, G., Euler, T., 2005. The primordial, blue-cone color system of the mouse retina. J. Neurosci. 25, 5438–5445.

doi:10.1523/JNEUROSCI.1117-05.2005

He, S., Weiler, R., Vaney, D.I., 2000. Endogenous dopaminergic regulation of horizontal cell coupling in the mammalian retina. J. Comp. Neurol. 418, 33–40. doi:10.1002/(SICI)1096-9861(20000228)418:1<33::AID-CNE3>3.0.CO;2-J

Helmstaedter, M., Briggman, K.L., Turaga, S.C., Jain, V., Seung, H.S., Denk, W., 2013. Connectomic reconstruction of the inner plexiform layer in the mouse retina. Nature 500, 168–174. doi:10.1038/nature12346

Hendel, T., Mank, M., Schnell, B., Griesbeck, O., Borst, A., Reiff, D.F., 2008. Fluorescence changes of genetic calcium indicators and OGB-1 correlated with neural activity and calcium in vivo and in vitro. J. Neurosci. 28, 7399–7411. doi:10.1523/JNEUROSCI.1038-08.2008

Higley, M.J., Sabatini, B.L., 2012. Calcium signaling in dendritic spines. Cold Spring Harb Perspect Biol 4, a005686. doi:10.1101/cshperspect.a005686

Hirano, A.A., Liu, X., Boulter, J., Grove, J., de Sevilla Müller, L.P., Barnes, S., Brecha, N.C., 2016. Targeted deletion of vesicular GABA transporter from retinal horizontal cells eliminates feedback modulation of photoreceptor calcium channels. eNeuro 3, ENEURO.0148-15.2016. doi:10.1523/ENEURO.0148-15.2016

Hombach, S., Janssen-Bienhold, U., Söhl, G., Schubert, T., Büssow, H., Ott, T., Weiler, R., Willecke, K., 2004. Functional expression of connexin57 in horizontal cells of the mouse retina. Eur. J. Neurosci. 19, 2633–2640. doi:10.1111/j.1460-9568.2004.03360.x

Hoon, M., Sinha, R., Okawa, H., Suzuki, S.C., Hirano, A.A., Brecha, N., Rieke, F., Wong, R.O.L., 2015. Neurotransmission plays contrasting roles in the maturation of inhibitory synapses on axons and dendrites of retinal bipolar cells. Proc. Natl. Acad. Sci. U. S. A. 112, 12840–5. doi:10.1073/pnas.1510483112

Huang, S.Y., Liu, Y., Liang, P.J., 2004. Role of Ca2+ store in AMPA-triggered Ca2+ dynamics in retinal horizontal cells. Neuroreport 15, 2311–2315. doi:10.1097/00001756-200410250-00002

Ingram, N.T., Sampath, A.P., Fain, G.L., 2016. Why are rods more sensitive than cones? J. Physiol. doi:10.1113/JP272556

Jackman, S.L., Babai, N., Chambers, J.J., Thoreson, W.B., Kramer, R.H., 2011. A positive feedback synapse from retinal horizontal cells to cone photoreceptors. PLoS Biol. 9, 1001058. doi:10.1371/journal.pbio.1001057

Janssen-Bienhold, U., Trümpler, J., Hilgen, G., Schultz, K., de Sevilla Müller, L.P., Sonntag, S., Dedek, K., Dirks, P., Willecke, K., Weiler, R., 2009. Connexin57 is expressed in dendro-dendritic and axo-axonal gap junctions of mouse horizontal cells and its distribution is

modulated by light. J. Comp. Neurol. 513, 363–374. doi:10.1002/cne.21965

Jung, C.K.., Herms, J., 2014. Structural dynamics of dendritic spines are influenced by an environmental enrichment : An in vivo imaging study. Cereb. Cortex 24, 377–384. doi:10.1093/cercor/bhs317

Kalloniatis, M., Nivison-Smith, L., Chua, J., Acosta, M.L., Fletcher, E.L., 2016. Using the rd1 mouse to understand functional and anatomical retinal remodelling and treatment implications in retinitis pigmentosa: A review. Exp. Eye Res. 150, 106–121. doi:10.1016/j.exer.2015.10.019

Kamermans, M., Kraaij, D.A., Spekreijse, H., 1998. The cone/horizontal cell network: a possible site for color constancy. Vis. Neurosci. 15, 787–97. doi:10.1017/S0952523898154172

Kamermans, M., van Dijk, B.W., Spekreijse, H., 1991. Color opponency in cone-driven horizontal cells in carp retina. Aspecific pathways between cones and horizontal cells. J. Gen. Physiol. 97, 819–43.

Kamermans, M., Werblin, F., 1992. GABA-mediated positive autofeedback loop controls horizontal cell kinetics in tiger salamander retina. J. Neurosci. 12, 2451–2463.

Kasai, H., Matsuzaki, M., Noguchi, J., Yasumatsu, N., Nakahara, H., 2003. Structure-stability-function relationships of dendritic spines. Trends Neurosci. 26, 360–368. doi:10.1016/S0166-2236(03)00162-0

Kemmler, R., Schultz, K., Dedek, K., Euler, T., Schubert, T., 2014. Differential regulation of cone calcium signals by different horizontal cell feedback mechanisms in the mouse retina. J. Neurosci. 34, 11826–43. doi:10.1523/JNEUROSCI.0272-14.2014

Kitamura, K., Kano, M., 2013. Dendritic calcium signaling in cerebellar Purkinje cell. Neural Networks 47, 11–17. doi:10.1016/j.neunet.2012.08.001

Klaassen, L.J., Sun, Z., Steijaert, M.N., Bolte, P., Fahrenfort, I., Sjoerdsma, T., Klooster, J., Claassen, Y., Shields, C.R., Ten Eikelder, H.M.M., Janssen-Bienhold, U., Zoidl, G., McMahon, D.G., Kamermans, M., 2011. Synaptic transmission from horizontal cells to cones is impaired by loss of connexin hemichannels. PLoS Biol. 9. doi:10.1371/journal.pbio.1001107

Koike, C., Numata, T., Ueda, H., Mori, Y., Furukawa, T., 2010. TRPM1: A vertebrate TRP channel responsible for retinal ON bipolar function. Cell Calcium 48, 95–101. doi:10.1016/j.ceca.2010.08.004

Kranz, K., Dorgau, B., Pottek, M., Herrling, R., Schultz, K., Bolte, P., Monyer, H., Penuela, S., Laird, D.W., Dedek, K., Weiler, R., Janssen-Bienhold, U., 2013. Expression of Pannexin1 in the outer plexiform layer of the mouse retina and physiological impact of its knockout. J. Comp. Neurol. 521, 1119–1135. doi:10.1002/cne.23223

Kreitzer, M.A., Birnbaum, A.D., Qian, H., Malchow, R.P., 2009. Pharmacological characterization, localization, and regulation of ionotropic glutamate receptors in skate horizontal cells. Vis. Neurosci. 26, 375–387. doi:10.1017/S0952523809990149

Kreitzer, M.A., Collis, L.P., Molina, A.J.A., Smith, P.J.S., Malchow, R.P., 2007. Modulation of extracellular proton fluxes from retinal horizontal cells of the catfish by depolarization and glutamate. J. Gen. Physiol. 130, 169–182. doi:10.1085/jgp.200709737

Kröger, R.H.H., Wagner, H.J., 1996. Horizontal cell spinule dynamics in fish are affected by rearing in monochromatic light. Vision Res. 36, 3879–3889. doi:10.1016/S0042-6989(96)00132-0

Kulkarni, V.A., Firestein, B.L., 2012. The dendritic tree and brain disorders. Mol. Cell. Neurosci. 50, 10–20. doi:10.1016/j.mcn.2012.03.005

Lefebvre, J.L., Sanes, J.R., Kay, J.N., 2015. Development of dendritic form and function. Annu. Rev. Cell Dev. Biol. 31, 741–777. doi:10.1146/annurev-cellbio-100913-013020

Lendvai, B., Stern, E.A., Chen, B., Svoboda, K., 2000. Experience-dependent plasticity of dendritic spines in the developing rat barrel cortex in vivo. Nature 404, 876–881.

Li, B., McKernan, K., Shen, W., 2008. Spatial and temporal distribution patterns of Na-K-2Cl cotransporter in adult and developing mouse retinas. Vis. Neurosci. 25, 109–23. doi:10.1017/S0952523808080164

Lisman, J., Schulman, H., Cline, H., 2002. The molecular basis of CaMKII function in synaptic and behavioural memory. Nat. Rev. Neurosci. 3, 175–190. doi:10.1038/nrn753

Liu, X., Hirano, A. a, Sun, X., Brecha, N.C., Barnes, S., 2013. Calcium channels in rat horizontal cells regulate feedback inhibition of photoreceptors through an unconventional GABA- and pH-sensitive mechanism. J. Physiol. 591, 3309–24. doi:10.1113/jphysiol.2012.248179

Ludwig, M., Pittman, Q.J., 2003. Talking back: Dendritic neurotransmitter release. Trends Neurosci. 26, 255–261. doi:10.1016/S0166-2236(03)00072-9

Lv, T., Gong, H.-Q., Liang, P.-J., 2014. Caffeine-induced Ca2+ oscillations in type I horizontal cells of the carp retina and the contribution of the store-operated Ca2+ entry pathway. PLoS One 9, e100095. doi:10.1371/journal.pone.0100095

Mank, M., Reiff, D.F., Heim, N., Friedrich, M.W., Borst, A., Griesbeck, O., Zellula, A.G., 2006. A FRET-based calcium biosensor with fast signal kinetics and high fluorescence change. Biophys. J. 90, 1790–6. doi:10.1529/biophysj.105.073536

Marvin, J.S., Borghuis, B.G., Tian, L., Cichon, J., Harnett, M.T., Akerboom, J., Gordus, A., Renninger, S.L., Chen, T.-W., Bargmann, C.I., Orger, M.B., Schreiter, E.R., Demb, J.B., Gan, W.-B., Hires, S.A., Looger, L.L., 2013. An optimized fluorescent probe for visualizing

glutamate neurotransmission. Nat. Methods 10, 162–170. doi:10.1038/nmeth.2333

Masu, M., Iwakabe, H., Tagawa, Y., Miyoshi, T., Yamashita, M., Fukuda, Y., Sasaki, H., Hiroi, K., Nakamura, Y., Shigemoto, R., Takada, M., Nakamura, K., Nakao, K., Katsuki, M., Nakanishi, S., 1995. Specific deficit of the ON response in visual transmission by targeted disruption of the mGIuR6 gene. Cell 80, 757–765. doi:10.1016/0092-8674(95)90354-2

Matsuzaki, M., Honkura, N., Ellis-Davis, G.C.R., Kasai, H., 2004. Structural basis of long-term potentiation in single dendritic spines. Nature 429, 761–766. doi:10.1038/nature02594.1.

Mel, B.W., Schiller, J., Poirazi, P., 2017. Synaptic plasticity in dendrites: complications and coping strategies. Curr. Opin. Neurobiol. 43, 177–186. doi:10.1016/j.conb.2017.03.012

Menger, N., Wässle, H., 2000. Morphological and physiological properties of the A17 amacrine cell of the rat retina. Vis Neurosci 17, 769–780.

Miller, R.F., Fagerson, M.H., Staff, N.P., Wolfe, R., Doerr, T., Gottesman, J., Sikora, M.A., Schuneman, R., 2001. Structure and functional connections of presynaptic terminals in the vertebrate retina revealed by activity-dependent dyes and confocal microscopy. J. Comp. Neurol. 437, 129–55.

Molday, R.S., Moritz, O.L., 2015. Photoreceptors at a glance. J. Cell Sci. 128, 4039–4045. doi:10.1242/jcs.175687

Molina, A.J.A., Verzi, M.P., Birnbaum, A.D., Yamoah, E.N., Hammar, K., Smith, P.J.S., Malchow, R.P., 2004. Neurotransmitter modulation of extracellular H+ fluxes from isolated retinal horizontal cells of the skate. J. Physiol. 560, 639–657. doi:10.1113/jphysiol.2004.065425

Neitz, J., Neitz, M., 2011. The genetics of normal and defective color vision. Vision Res. 51, 633–651. doi:10.1016/j.visres.2010.12.002

Nikonov, S.S., Kholodenko, R., Lem, J., Pugh, E.N., 2006. Physiological features of the S- and M-cone photoreceptors of wild-type mice from single-cell recordings. J. Gen. Physiol. 127, 359–374. doi:10.1085/jgp.

Oesch, N., Euler, T., Taylor, W.R., 2005. Direction-selective dendritic action potentials in rabbit retina. Neuron 47, 739–750. doi:10.1016/j.neuron.2005.06.036

Packer, O.S., Verweij, J., Li, P.H., Schnapf, J.L., Dacey, D.M., 2010. Blue-yellow opponency in primate S cone photoreceptors. J. Neurosci. 30, 568–572. doi:10.1523/JNEUROSCI.4738-09.2010

Pang, J.-J., Gao, F., Lem, J., Bramblett, D.E., Paul, D.L., Wu, S.M., 2010. Direct rod input to cone BCs and direct cone input to rod BCs challenge the traditional view of mammalian BC circuitry. Proc. Natl. Acad. Sci. 107, 395–400. doi:10.1073/pnas.0907178107

Peichl, L., González-Soriano, J., 1994. Morphological types of horizontal cell in rodent retinae: a comparison of rat, mouse, gerbil, and guinea pig. Vis. Neurosci. 11, 501–517. doi:10.1017/S095252380000242X

Penzes, P., Cahill, M.E., Jones, K.A., VanLeeuwen, J.-E., Woolfrey, K.M., 2011. Dendritic spine pathology in neuropsychiatric disorders. Nat. Neurosci. 14, 285–293. doi:10.1038/nn.2741

Pottek, M., Schultz, K., Weiler, R., 1997. Effects of nitric oxide on the horizontal cell network and dopamine release in the carp retina. Vision Res. 37, 1091–1102. doi:10.1016/S0042-6989(96)00298-2

Prochnow, N., Hoffmann, S., Vroman, R., Klooster, J., Bunse, S., Kamermans, M., Dermietzel, R., Zoidl, G., 2009. Pannexin1 in the outer retina of zebrafish, danio rerio. Neuroscience 162, 1039–1054. doi:10.1016/j.neuroscience.2009.04.064

Pugh, E.N., Nikonov, S., Lamb, T.D., 1999. Molecular mechanisms of vertebrate photoreceptor light adaptation. Curr. Opin. Neurobiol. 9, 410–418. doi:10.1016/S0959-4388(99)80062-2

Puller, C., Haverkamp, S., Neitz, M., Neitz, J., 2014. Synaptic elements for GABAergic feed-forward signaling between HII horizontal cells and blue cone bipolar cells are enriched beneath primate S-cones. PLoS One 9, 1–11. doi:10.1371/journal.pone.0088963

Purgert, R.J., Lukasiewicz, P.D., 2015. Differential encoding of spatial information among retinal on cone bipolar cells. J. Neurophysiol. 114, 1757–1772. doi:10.1152/jn.00287.2015

Raghuram, V., Sharma, Y., Kreutz, M.R., 2012. Ca2+ sensor proteins in dendritic spines: a race for Ca2+. Front. Mol. Neurosci. 5, 1–12. doi:10.3389/fnmol.2012.00061

Risher, W.C., Ustunkaya, T., Alvarado, J.S., Eroglu, C., 2014. Rapid golgi analysis method for efficient and unbiased classification of dendritic spines. PLoS One 9. doi:10.1371/journal.pone.0107591

Roberts, T.F., Tschida, K.A., Klein, M.E., Mooney, R., 2010. Rapid spine stabilization and synaptic enhancement at the onset of behavioural learning. Nature 463, 948–952. doi:10.1038/nature08759

Rogerson, L.E., Behrens, C., Euler, T., Berens, P., Schubert, T., 2017. Connectomics of synaptic microcircuits: lessons from the outer retina. J. Physiol. 595, 5517–5524. doi:10.1113/JP273671

Röhlich, P., van Veen, T., Szél, A., 1994. Two different visual pigments in one retinal cone cell. Neuron 13, 1159–1166. doi:10.1016/0896-6273(94)90053-1

Rose, G.J., Call, S.J., 1992. Evidence for the role of dendritic spines in the temporal filtering properties of neurons: The decoding problem and beyond. Proc. Natl. Acad. Sci. 89, 9662–9665.

Schmitz, F., 2009. The making of synaptic ribbons: how they are built and what they do. Neurosci. 15, 611–24. doi:10.1177/1073858409340253

Schubert, T., Euler, T., 2010. Retinal processing: Global players like it local. Curr. Biol. 20, R486–R488. doi:10.1016/j.cub.2010.04.034

Schubert, T., Huckfeldt, R.M., Parker, E., Campbell, J.E., Wong, R.O., 2010. Assembly of the outer retina in the absence of GABA synthesis in horizontal cells. Neural Dev 5, 15. doi:10.1186/1749-8104-5-15

Schubert, T., Kerschensteiner, D., Eggers, E.D., Misgeld, T., Kerschensteiner, M., Lichtman, J.W., Lukasiewicz, P.D., Wong, R.O., 2008. Development of presynaptic inhibition onto retinal bipolar cell axon terminals is subclass-specific. J Neurophysiol 100, 304–316. doi:10.1152/jn.90202.2008

Schubert, T., Weiler, R., Feigenspan, A., 2006. Intracellular calcium is regulated by different pathways in horizontal cells of the mouse retina. J. Neurophysiol. 96, 1278–1292. doi:10.1152/jn.00191.2006

Schultz, K., Janssen-bienhold, U., Weiler, R., 2001. Selective synaptic distribution of AMPA and kainate receptor subunits in the outer plexiform layer of the carp retina. J. Comp. Neurol. 435, 433–449.

Shelley, J., Dedek, K., Schubert, T., Feigenspan, A., Schultz, K., Hombach, S., Willecke, K., Weiler, R., 2006. Horizontal cell receptive fields are reduced in connexin57-deficient mice. Eur J Neurosci 23, 3176–3186. doi:10.1111/j.1460-9568.2006.04848.x

Sinha, R., Hoon, M., Baudin, J., Okawa, H., Wong, R.O.L., Rieke, F., 2017. Cellular and circuit mechanisms shaping the perceptual properties of the primate fovea. Cell 168, 413–426.e12. doi:10.1016/j.cell.2017.01.005

Sivyer, B., Williams, S.R., 2013. Direction selectivity is computed by active dendritic integration in retinal ganglion cells. Nat. Neurosci. 16, 1848–56. doi:10.1038/nn.3565

Sjöström, P.J., Rancz, A., Roth, A., Häusser, M., 2008. Dendritic excitability and synaptic plasticity. Physiol. Rev. 88, 769–840. doi:10.1152/physrev.00016.2007.

Spruston, N., 2008. Pyramidal neurons: dendritic structure and synaptic integration. Nat. Rev. Neurosci. 9, 206–221. doi:10.1038/nrn2286

St-Pierre, F., Marshall, J.D., Yang, Y., Gong, Y., Schnitzer, M.J., Lin, M.Z., 2014. High-fidelity optical reporting of neuronal electrical activity with an ultrafast fluorescent voltage sensor. Nat. Neurosci. 17, 884–9. doi:10.1038/nn.3709

Ströh, S., Sonntag, S., Janssen-Bienhold, U., Schultz, K., Cimiotti, K., Weiler, R., Willecke, K., Dedek, K., 2013. Cell-specific Cre recombinase expression allows selective ablation of

glutamate receptors from mouse horizontal cells. PLoS One 8, e83076. doi:10.1371/journal.pone.0083076

Sun, X., Hirano, A.A., Brecha, N.C., Barnes, S., 2017. Calcium-activated BK Ca channels govern dynamic membrane depolarizations of horizontal cells in rodent retina. J. Physiol. 1–39. doi:10.1113/JP274132

Szél, A., Röhlich, P., Caffé, A.R., Juliusson, B., Aguirre, G., Van Veen, T., 1992. Unique topographic separation of two spectral classes of cones in the mouse retina. J. Comp. Neurol. 325, 327–342. doi:10.1002/cne.903250302

Szikra, T., Trenholm, S., Drinnenberg, A., Jüttner, J., Raics, Z., Farrow, K., Biel, M., Awatramani, G., Clark, D.A., Sahel, J.-A., da Silveira, R.A., Roska, B., 2014. Rods in daylight act as relay cells for cone-driven horizontal cell-mediated surround inhibition. Nat. Neurosci. 17, 1728–35. doi:10.1038/nn.3852

Tainaka, K., Sakaguchi, R., Hayashi, H., Nakano, S., Liew, F.F., Morii, T., 2010. Design strategies of fluorescent biosensors based on biological macromolecular receptors. Sensors 10, 1355–1376. doi:10.3390/s100201355

Tatsukawa, T., Hirasawa, H., Kaneko, A., Kaneda, M., 2005. GABA-mediated component in the feedback response of turtle retinal cones. Vis. Neurosci. 22, 317–24. doi:10.1017/S0952523805223076

Thoreson, W.B., Mangel, S.C., 2012. Lateral interactions in the outer retina. Prog. Retin. Eye Res. 31, 407–441. doi:10.1016/j.preteyeres.2012.04.003

Tian, L., Hires, S.A., Mao, T., Huber, D., Chiappe, M.E., Chalasani, S.H., Petreanu, L., Akerboom, J., McKinney, S.A., Schreiter, E.R., Bargmann, C.I., Jayaraman, V., Svoboda, K., Looger, L.L., 2009. Imaging neural activity in worms, flies and mice with improved GCaMP calcium indicators. Nat. Methods 6, 875–881. doi:10.1038/nmeth.1398

Tornqvist, K., Yang, X.-L., Dowling, J.E., 1988. Modulation of cone horizontal cell activity in the teleost fish retina . lll . Effects of prolonged darkness and dopamine on electrical coupling between horizontal cells. J. Neurosci. 8, 2279–2288.

Toyoda, J., Kujiraoka, T., 1982. Analyses of bipolar cell responses elicited by polarization of horizontal cells. J. Gen. Physiol. 79, 131–145.

Trong, T.M.H., Motley, S.E., Wagner, J., Kerr, R.R., Kozloski, J., 2017. Dendritic spines modify action potential back-propagation in a multicompartment neuronal model. IBM J. Res. Dev. 61, 1–13. doi:10.1147/JRD.2017.2679558

Tropea, D., Majewska, A.K., Garcia, R., Sur, M., 2010. Structural dynamics of synapses in vivo correlate with functional changes during experience-dependent plasticity in visual cortex. J. Neurosci. 30, 11086–11095. doi:10.1523/JNEUROSCI.1661-10.2010

Trumpler, J., Dedek, K., Schubert, T., de Sevilla Müller, L.P., Seeliger, M., Humphries, P., Biel, M., Weiler, R., 2008. Rod and cone contributions to horizontal cell light responses in the mouse retina. J. Neurosci. 28, 6818–6825. doi:10.1523/JNEUROSCI.1564-08.2008

Tsay, D., Yuste, R., 2002. Role of dendritic spines in action potential backpropagation: a numerical simulation study. J. Neurophysiol. 88, 2834–2845. doi:10.1152/jn.00781.2001

Tsukamoto, Y., Morigiwa, K., Ueda, M., Sterling, P., 2001. Microcircuits for night vision in mouse retina. J. Neurosci. 21, 8616–23. doi:21/21/8616

VanLeeuwen, M., Fahrenfort, I., Sjoerdsma, T., Numan, R., Kamermans, M., 2009. Lateral gain control in the outer retina leads to potentiation of center responses of retinal neurons. J. Neurosci. 29, 6358–6366. doi:10.1523/JNEUROSCI.5834-08.2009

Vanleeuwen, M.T., Joselevitch, C., Fahrenfort, I., Kamermans, M., 2007. The contribution of the outer retina to color constancy: a general model for color constancy synthesized from primate and fish data. Vis. Neurosci. 24, 277–90. doi:10.1017/S0952523807070058

Vardi, N., Zhang, L.L., Payne, J.A., Sterling, P., 2000. Evidence that different cation chloride cotransporters in retinal neurons allow opposite responses to GABA. J. Neurosci. 20, 7657–7663. doi:20/20/7657

Veruki, M.L., Oltedal, L., Hartveit, E., 2008. Electrical synapses between AII amacrine cells: dynamic range and functional consequences of variation in junctional conductance. J Neurophysiol 100, 3305–3322. doi:10.1152/jn.90957.2008

Verweij, J., Hornstein, E.P., Schnapf, J.L., 2003. Surround antagonism in macaque cone photoreceptors. J. Neurosci. 23, 10249–10257. doi:23/32/10249

Vessey, J.P., 2005. Proton-mediated feedback inhibition of presynaptic calcium channels at the cone photoreceptor synapse. J. Neurosci. 25, 4108–4117. doi:10.1523/JNEUROSCI.5253-04.2005

Villa, K.L., Berry, K.P., Subramanian, J., Cha, J.W., Oh, W.C., Kwon, H.B., Kubota, Y., So, P.T.C., Nedivi, E., 2016. Inhibitory synapses are repeatedly assembled and removed at persistent sites in vivo. Neuron 89, 756–769. doi:10.1016/j.neuron.2016.01.010

Vroman, R., Kamermans, M., 2015. Feedback-induced glutamate spillover enhances negative feedback from horizontal cells to cones. J. Physiol. 593, 2927–2940. doi:10.1113/JP270158

Vroman, R., Klaassen, L.J., Howlett, M.H.C., Cenedese, V., Klooster, J., Sjoerdsma, T., Kamermans, M., 2014. Extracellular ATP hydrolysis inhibits synaptic transmission by increasing pH buffering in the synaptic cleft. PLoS Biol. 12. doi:10.1371/journal.pbio.1001864

Vroman, R., Klaassen, L.J., Kamermans, M., 2013. Ephaptic communication in the vertebrate

retina. Front Hum Neurosci 7, 612. doi:10.3389/fnhum.2013.00612

Wang, S.S., Denk, W., Häusser, M., 2000. Coincidence detection in single dendritic spines mediated by calcium release. Nat. Neurosci. 3, 1266–1273.

Wang, T.-M., Holzhausen, L.C., Kramer, R.H., 2014. Imaging an optogenetic pH sensor reveals that protons mediate lateral inhibition in the retina. Nat. Neurosci. 17, 262–8. doi:10.1038/nn.3627

Warren, T.J., Van Hook, M.J., Supuran, C.T., Thoreson, W.B., 2016a. Sources of protons and a role for bicarbonate in inhibitory feedback from horizontal cells to cones in Ambystoma tigrinum retina. J. Physiol. 594, 6661–6677. doi:10.1113/JP272533

Warren, T.J., Van Hook, M.J., Tranchina, D., Thoreson, W.B., 2016b. Kinetics of inhibitory feedback from horizontal cells to photoreceptors: implications for an ephaptic mechanism. J. Neurosci. 36, 10075–10088. doi:10.1523/JNEUROSCI.1090-16.2016

Wässle, H., 2004. Parallel processing in the mammalian retina. Nat. Rev. Neurosci. 5, 747–57. doi:10.1038/nrn1497

Wässle, H., Puller, C., Müller, F., Haverkamp, S., 2009. Cone contacts, mosaics, and territories of bipolar cells in the mouse retina. J. Neurosci. 29, 106–117. doi:10.1523/JNEUROSCI.4442-08.2009

Wei, T., Schubert, T., Paquet-Durand, F., Tanimoto, N., Chang, L., Koeppen, K., Ott, T., Griesbeck, O., Seeliger, M.W., Euler, T., Wissinger, B., 2012. Light-driven calcium signals in mouse cone photoreceptors. J. Neurosci. 32, 6981–6994. doi:10.1523/JNEUROSCI.6432-11.2012

Werblin, F.S., 1978. Transmission along and between rods in the Tiger Salamander Retina. J. Physiol. 280, 449–470.

Witkovsky, P., 2004. Dopamine and retinal function. Doc. Ophthalmol. 108, 17–40. doi:10.1023/B:DOOP.0000019487.88486.0a

Xin, D., Bloomfield, S.A., 1999. Dark- and light-induced changes in coupling between horizontal cells in mammalian retina. J. Comp. Neurol. 405, 75–87. doi:10.1002/(SICI)1096-9861(19990301)405:1<75::AID-CNE6>3.0.CO;2-D

Xu, T., Yu, X., Perlik, A.J., Tobin, W.F., Zweig, J.A., Tennant, K., Jones, T., 2009. Rapid formation and selective stabilization of synapses for enduring motor memories. Nature 462, 915–919. doi:10.1038/nature08389

Yang, G., Pan, F., Gan, W., 2009. Stably maintained dendritic spines are associated with lifelong memories. Nature 462, 920–924. doi:10.1038/nature08577

Yang, X.L., Fan, T.X., Shen, W., 1994. Effects of prolonged darkness on light responsiveness and spectral sensitivity of cone horizontal cells in carp retina in vivo. J. Neurosci. 14, 326–334.

Yuste, R., Bonhoeffer, T., 2004. Genesis of dendritic spines: insights from ultrastructural and imaging studies. Nat. Rev. Neurosci. 5, 24–34. doi:10.1038/nrn1300

Zariwala, H.A., Borghuis, B.G., Hoogland, T.M., Madisen, L., Tian, L., De Zeeuw, C.I., Zeng, H., Looger, L.L., Svoboda, K., Chen, T.-W., 2012. A Cre-dependent GCaMP3 reporter mouse for neuronal imaging in vivo. J. Neurosci. 32, 3131–3141. doi:10.1523/JNEUROSCI.4469-11.2012